Targeted Delivery of MicroRNAs by Nanoparticles: A Novel Therapeutic Strategy in Acute Myeloid Leukemia

Dissertation

Presented in Partial Fulfillment of the Requirements for the Degree
Doctor of Philosophy in the Graduate School of The Ohio State University

By

Xiaomeng Huang, B.S.

Graduate Program in Molecular, Cellular and Developmental Biology

The Ohio State University

2014

Dissertation Committee:

L. James Lee, PhD, Advisor

Guido Marcucci, MD, Co-advisor

Robert J. Lee, PhD

Natarajan Muthusamy, DVM, PhD

Abstract

Acute myeloid leukemia (AML) is a biologically complex neoplastic disease of the hematopoietic system, characterized by an uncontrolled proliferation of malignant myeloid precursors leading to bone marrow failure at the clinical level. Today, the majority of AML patients fail to achieve long-term survival. Thus, new therapeutic approaches are needed. MicroRNAs (miRs), short noncoding RNAs that regulate the expression of their target mRNA-encoded proteins, are involved in tumorigenesis. We demonstrated that deregulated *miR-29b* and *miR-181a* in AML patients were associated with worse outcome. Moreover, AML patients with a higher pre-treatment level of *miR-29b* respond better to a hypomethylating agent, decitabine; and patients with higher *miR-181a* have longer survival under cytarabine/daunorubicine-based chemotherapy. Thus, increasing the levels of these miRs prior to the respective treatments may be beneficial. However, free synthetic miRs are easily degraded in the bio-fluid and have limited cellular uptake. To overcome this problem and explore miR-based therapy, our research focused on three major aims: (1) to develop a novel nanocarrier suitable for delivering miRs into AML cells; (2) to deliver *miR-29b* and assess the antileukemic activity; and (3) to investigate the role of *miR-181a* in AML, unravel the mechanism, and perform therapeutic evaluation via nanocarrier-delivered

miR-181a. For aim 1, since AML cells overexpress transferrin receptor on their surface, we formulated novel transferrin (Tf) targeted anionic lipid based nanoparticles (NP) encapsulating miR mimic and demonstrated low toxicity and high efficiency. For aim 2, following *miR-29b*-nanoparticle treatment, we showed a significant increase in intracellular *miR-29b* levels and downregulation of its known targets. This resulted in decreased leukemia growth and improved survival in an AML mouse model. Furthermore, we showed that pretreatment with *miR-29b* nanoparticles improved the antileukemic activity of decitabine. For aim 3, we demonstrated that *miR-181a* served as a tumour suppressor in AML, which may be partially attributed to *miR-181a* supressing the oncogenic RAS/MAPK pathway by directly targeting RAS and MAPK1 proteins. We are the first to show that *miR-181a*-nanoparticle treatment leads to RAS/MAPK signaling inhibition and antileukemic activity.

In conclusion, nanoparticle-based miR replacement therapy, particularly when combined with existing chemotherapy regimens, may represent a promising new treatment strategy for AML patients.

This work is dedicated to

My mother for being supportive and caring

My beloved husband Yi Qiao for the love and friendship

And driving thousands of miles to see me

Acknowledgments

I would like to thank my primary advisor, Dr. James Lee, who supported me throughout my entire PhD study; and my co-advisor Dr. Guido Marcucci, who generously made his lab space and resources available to me. I am always inspired by their passion in nanotechnology, curiosity in cancer biology and the spirit of hard-working. I also appreciate the many opportunities to be involved in many projects in both labs, researching applications of novel nanotechnologies in Dr. Lee's lab and microRNA biology in cancer in Dr. Marcucci's lab. Their expertise and interdisciplinary mentorship have been invaluable to my scientific career.

I would like to acknowledge my committee members, Drs. Robert J. Lee and Natarajan Muthusamy for offering helpful advices and insightful comments on my candidacy proposal and manuscripts. I am very grateful to Dr. Robert Lee's initial help and recommendation in introducing me into OSU. I would like to thank Dr. Clara Bloomfield for her support on my projects and my fellowship application.

I would like to thank Dr. Bo Yu and Dr. Sebastian Schwind for their help and tremendous contribution to my project and training. As senior members in the lab, they taught me assays and experiment designs, as well as helped me in abstract and talk preparations. I thank Dr. Santhanam Ramasamy for his assistance with animal studies and other former and current colleagues for their help. Special

gratitude extends to Dr. Ann-Kathrin Eisfeld and Pia Hoellerbauer for their friendship and company through the course of my study. At last, I would like to thank my family and friends who support me, encourage me and love me. Special thank to Dr. Yong Su for inspiring and supporting me to pursue a scientific career in life science, and providing me with many opportunities.

Vita

1987	Born- Lanzhou, China
2004-2008	B.S. Biological Science, Zhejiang University, Hangzhou, China
2009-2010	Research assistant, P.I. Dr. Robert J. Lee, College of Pharmacy, The Ohio State University, Columbus, Ohio
2010 to present	Nanoscale Science and Engineering Center Fellow, Molecular, Cellular Developmental Biology Program, Advisor: Dr. L. James Lee, Chemical and Biomolecular Engineering; Co-advisor: Dr. Guido Marcucci, Internal Medicine, The Ohio State University, Columbus, Ohio

Publications

Huang X, Schwind S, Yu B, Santhanam R, Wang H, Hoellerbauer P, Mims A, Klisovic RB, Walker AR, Chan KK, Blum W, Perrotti D, Byrd JC, Bloomfield CD, Caligiuri MA, Lee RJ, Garzon R, Muthusamy N, Lee LJ and Marcucci G, Targeted

Delivery of microRNA-29b by Transferrin Conjugated Anionic Lipopolyplex Nanoparticles: A Novel Therapeutic Strategy in Acute Myeloid Leukemia, ***Clinical Cancer Research,*** 2013; 19:2355-2367.

Huang X, Caddell R, Yu B, Xu S, Theobald B, Lee LJ, and Lee RJ. Ultrasound-enhanced microfluidic synthesis of liposomes (2010) ***Anticancer Research***, 30 (2): 463-466

Mims A, Walker AR, **Huang X**, Sun J, Wang H, Santhanam R, Dorrance AM, Walker C, Hoellerbauer P, Tarighat SS, Chan KK, Klisovic RB, Perrotti D, Caligiuri MA, Byrd JC, Chen C-S, Lee LJ, Jacob S, Mrózek K, Bloomfield CD, Blum W, Garzon R, Schwind S, and Marcucci G, "Increased Anti-leukemic Activity of Decitabine via AR-42-induced Upregulation of *miR-29b*: A Novel Epigenetic-targeting Approach in Acute Myeloid Leukemia", ***Leukemia***, 2013; 27(4): 871-878.

Yu B, Zhu J, Xue W, Wu Y, **Huang X**, Lee LJ, and Lee RJ. Microfluidic assembly of lipid-based oligonucleotide nanoparticles (2011) ***Anticancer Research***, 31(3): 771-776.

Wu Y, Kwak KJ, Agarwal K, Marras A, Wang C, Mao Y, **Huang X**, Ma J, Yu B, Lee JR, Marcucci G, Byrd J, Muthusamy N, Huang K, Castro CE, Paulaitis M, Nana-Sinkam P, Lee LJ. Detection of extracellular RNAs in cancer and viral infection via tethered cationic lipoplex nanoparticles containing molecular beacons. ***Anal Chem.*** 2013 Dec 3;85(23):11265-74.

Eisfeld A, Schwind S, Hoag K, Walker CJ, Liyanarachchi S, Patel R, **Huang X**, Markowitz J, Duan W, Otterson GA, Carson WE, Marcucci G, Bloomfield CD, de la Chapelle A. Novel NRAS isoforms differentially affect cell proliferation, differentiation and transformation. ***PNAS***. 111 (11), 4179-4184

Alachkar H, Maharry K, Santhanam R, Metzeler KH, **Huang X**, Kohlschmidt J, Mendler JH, Menito JM, Hickey C, Neviani P, Dorrance AM, Khalife J, Volinia S, Whitman SP, Paschka P, Hoellerbauer P, Wu YZ, Han L, Bolon BN, Blum W, Mrózek K, Carroll AJ, Perrotti D, Andreeff M, Caligiuri MA, Konopleva M, Garzon R, Bloomfield CD, Marcucci G. SPARC Activates ILK/AKT/β-catenin and Promotes an Aggressive Phenotype in Acute Myeloid Leukemia. Accepted by ***The Journal of Clinical Investigation.*** 2014; 124(4):1512–1524.

Havelange V, Ranganathan P, Geyer S, Nicolet D, **Huang X**, Yu X, Volinia S, Kornblau SM, Andreeff M, Croce CM, Marcucci G, Bloomfield CD, Garzon R. Implications of the miR-10 family in chemotherapy response of NPM1 mutated AML. ***Blood.*** 2014; 123(15):2412-5.

Eisfeld A, Schwind S, Patel R, **Huang X**, Santhanam R, Walker C, Markovitz, K, Hoag KW, Jarvinen TM, Leffel B, Perrotti D, Carson WE, Marcucci G, Bloomfield C, Chapelle A de la. Intronic miR-3151 hosted by BAALC drives leukemogenesis by direct deregulation of the TP53 pathway. ***Science Signaling***. 2014; 15;7(321) ra36.

Yang Z, Yu B, Zhu J, **Huang X**, Xie J, Xu S, Wang X, Yuang BC, Lee LJ, Lee RJ, Teng L. A microfluidic method for synthesis of transferrin-lipid nanoparticles loaded with siRNA LOR-1284 for therapy of acute myeloid leukemia. ***Nanoscale***. 2014; First published online 03 Jun 2014. DOI: 10.1039/C4NR01510J.

Huang X, Schwind S, Santhanam R, Eisfeld AK, Chiang C, Yu B, Hoellerbauer P, Dorrance A, Yan J, Tarighat SS, Khalife J, Walker A, Chan KK, Caligiuri M, Perrotti D, Muthusamy N, Bloomfield CD, Garzon R, Lee RJ, Lee JL, Marcucci G. Targeting the RAS/MAPK pathway with *miR-181a* in Acute Myeloid Leukemia. Submission.

Dorrance AM, Neviani P, **Huang X**, Nicloet D, Maharry K, Ferenchak G, Ozer HG, Hoellerbauer P, Khalife J, Hill E, Lee RJ, Lee LJ, Croce CM, Garzon R, Caligiuri MA, Bloomfield C, Marcucci G. Targeting Leukemia Stem Cells with AntagomiR-126 Nanoparticles in Acute Myeloid Leukemia. Submission.

Wang H, Santhanam R, Xie Z, **Huang X**, Phelps M, Ellis J, Tarighat SS, Caligiuri MA, Bekaii-Saab T, Walker A, Jacob ST, Garzon R, Croce CM, Lee RJ, Lee JL, Muthusamy N, Chan KK and Marcucci G. Pharmacokinetics, Pharmacodynamics and Therapeutic Activity of a Novel Single-stranded 2'-O-Methyl phosphorothioate miR-29b Mimic in Acute Myeloid Leukemia. Submission.

Gao K, **Huang X**, Wang X, Boukany P, Marcucci G, Lee LJ. Analysis of Mcl-1 siRNA induced apoptosis in wild-type and FLT3-ITD Acute Myeloid Leukemia (AML) cells by nanoelectroporation and single cell qRT-PCR. ***Nanoletter***, Under revision.

Abstract: (*indicates poster presentation, † indicates oral presentation)

Huang X, Schwind S, Yu B, Liu S, Pang J, Santhanam R, Wu YZ, Chan KK, Blum W, Bloomfield CD, Perroti D, Garzon R, Byrd JC, Muthusamy N, Lee RJ, Marcucci G, Lee LJ. A Novel Anionic Nanoparticle Delivery System for Microrna-29b Targets FLT3 and KIT Receptor Tyrosine Kinase Expression in Acute Myeloid Leukemia, (October 2012) *American Institute of Chemical Engineers Annual Meeting, Pittsburgh*, PA, Abs 326a&732f. †

Huang X, Schwind S, Eisfeld AK, Yu B, Santhanam R, Hoellerbauer P, Jin Y, Hickey CJ, Pang J, Chan KK, Perroti D, Muthusamy N, Byrd JC, Blum W, Bloomfield CD, Liu S, Garzon R, Lee RJ, Lee LJ, Marcucci G. Therapeutic Targeting of the RAS-pathway by Synthetic *miR-181a* Nanoparticles in Acute Myeloid Leukemia (AML). (2012) *Blood* 120 (Abstract #2422). *

Huang X, Schwind S, Yu B, Pang J, Santhanam R, Chan K, Garzon R, Blum W, Bloomfield CD, Liu S, Perrotti D, Lee RJ, Byrd JC, Muthusamy N, Lee LJ, Marcucci G. Targeted Delivery of *MicroRNA-29b* by Nanoparticles Provides Antileukemic Activity and Increases Sensitivity to the Hypomethylating Agent Decitabine (DAC) in Acute Myeloid Leukemia (AML). (2011) *Blood* 118:39-39 (Abstract #81). †

Huang X, Schwind S, Eisfeld AK, Yu B, Hickey CJ, Pang J, Santhanam R, Chan K, Perrotti D, Muthusamy N, Byrd JC, Blum W, Bloomfield CD, Liu S, Garzon R, Lee RJ, Lee LJ, Marcucci G. Synthetic *microRNA-181a* nanoparticles (NP) target RAS and sensitize cells to daunorubicin (DNR) in acute myeloid leukemia (AML). In: Proceedings of the 103rd Annual Meeting of the American Association for Cancer Research; 2012 Mar 31-Apr 4; Chicago, IL. Philadelphia (PA): AACR; Cancer Res 2012;72(8 Suppl):Abstract #1111. *

Mims AS, Walker AR, Hoellerbauer P, **Huang X**, Chan KK, Klisovic RB, Perrotti D, Caligiuri MA, Byrd JC, Chen CS, Blum W, Garzon R, Schwind S, Marcucci G: AR42, a Histone Deacetylase Inhibitor (HDACI), increases microRNA (*miR)-29b* and sensitizes cells to decitabine (DAC) treatment: a novel epigenetic-targeting approach in Acute Myeloid Leukemia (AML). In: Proceedings of the 103rd Annual Meeting of the American Association for Cancer Research; 2012 Mar 31-Apr 4; Chicago, IL. Philadelphia (PA): AACR; Cancer Res 2012;72(8 Suppl):Abstract #119.

Zhao X, Wu Y, Wang X, Gallego-Perez D, Boukany PE, **Huang X**, Schwind S, Marcucci G, Lee LJ. CEBPA mutant regulates miR-181a expression in AML cells: A single cell study by nanochannel electroporation. (October 2012) *American Institute of Chemical Engineers Annual Meeting, Pittsburgh*, PA, Abs 662e.

Eisfeld A, Schwind S, Patel R, **Huang X**, Santhanam R, Walker C, Jarvinen T, Leffel B, Perrotti D, Marcucci G, Bloomfield C, Chapelle A de la. Overexpression of intronic *miR-3151* and its host gene BAALC increases leukemogenesis in Acute Myeloid Leukemia (AML) by direct deregulation of TP53 and may be targeted by bortezomib. Haematologica 2013; 98(s1):8. Abstract #020.

Havelange V, Ranganathan P, Geyer S, **Huang X**, Yu X, Fernandez-Cymering C, Volinia S, Andreeff M, Croce CM, Marcucci G, Garzon R. Implications of *miR-10* in chemotherapy response of NPM1 mutated AML. Haematologica 2013;

98(s1): 277. Abstract #658.

Gao K, **Huang X**, Li L, Chang L, Wang X, Marcucci G, Lee JL. Single-cell level study of precise siRNA delivery and dynamic in Acute Myeloid Leukemia cells by nanochannel electroporation system. (November 2013) *American Institute of Chemical Engineers Annual Meeting, San Francisco, CA,* Abs 7e.

Wang H, Santhanam R, Xie Z, **Huang X**, Chiu M, Phelps M, Walker A, Caligiuri MA, Garzon R, Lee JL, Muthusamy N, Chan KK, Marcucci G. A novel therapeutic approach in Acute Myeloid Leukemia (AML): *in vivo* preclinical pharmacokinetic (PK), pharmacodynamic (PD) and antileukemia activities of synthetic 2'-O-Methylphosphorothioate *miR-29b.* (December 2013) *American Society of Hematology Annual Meeting.* Abstract #3933.

Khalife JC, Radomska HS, Saultz J, Santhanam R, **Huang X**, Wang H, Curfman J, Wu YZ, Hoellerbauer P, Alachkar H, Dorrance A, Caligiuri M, Garzon R, Mendler JH, Marcucci G. Targeting *miR-155* via the NEDD8-activating enzyme inhibitor MLN4924: A novel therapeutic approach for Acute Myeloid Leukemia (AML). (December 2013) *American Society of Hematology Annual Meeting.* Abstract #3804.

Fields of Study

Major Field: Molecular Cellular and Developmental Biology

Table of Contents

List of Table

List of Figures

Chapter 1: Introduction and Background

1.1 Acute Myeloid Leukemia

Acute myeloid leukemia (AML) is a complex neoplastic disease of the hematopoietic system resulting in maturation arrest and aberrant proliferation of leukemic cells. Normally, hematopoietic stem cells in bone marrow have the ability to give rise to different types of mature blood cells. The maturation process is under a great precision regulation of a series of growth factors (e.g. stem cell factor SCF, interleukins) and transcriptional factors responding to the environment. However, in AML, progenitor cells (blasts) which lose their ability to differentiate and respond to normal regulator of proliferation (*1*) are accumulated in the bone marrow thus interfering the normal blood cell production and escape into the peripheral blood and infiltrate to other organs including brain and lung (*1*). AML patients typically show symptoms like anemia, bleeding and fever. According to World Health Organization (WHO) criteria, >20% blasts of myeloid lineage in marrow or blood is considered as diagnosis of AML (*2*), though 20% is an arbitrary cutoff and should be combined with other risk considerations to make clinical decisions (*3*). For example, patients with the following cytogenetic abnormalities: t(8;21)(q22;q22), inv(16)(p13q22) or t(16;16)(p13;q22),

t(15;17)(q22;q12) and 11q23 (MLL) should be considered to have AML even when they have less blast percentage (*4*) because they respond so well to AML therapy (*3*). Table 1.1 shows WHO classification of AML. Table 1.2 shows a summery of AML with characteristic genetic abnormalities.

1.2 Prognosis and Survival

With advances in the treatment of AML, approximately 60-70% of adult patients can expect to achieve complete remission status following appropriate induction therapy. More than 25% of adult AML patients can survive 3 or more years and maybe cured. Based on National Cancer Institute information, there are estimated 18,860 new cases of AML and 10,460 deaths in 2014.

To make appropriate treatment decision and better predict the outcome, some prognostic factors are discovered. Grimwade et al. (*5*) did cytogenetic analysis of 1,612 AML patients and defined three prognostic groups on the basis of response to induction treatment, relapse risk and overall survival. Three groups included the favorable outcome (inv(16), t(8;21) or t(15;17)), adverse risk (a complex karyotype, -5, del(5q), -7, or abnormalities of 3q) and intermediate prognosis (11q23 abnormalities, +8 (trisomy 8), +21, +22, del(9q), del(7q) or other miscellaneous structural or numerical defects). Some recent studies added more insight to the prognositic impact of these cytogenetic markers. Becker et al. (*6*) reported that among younger adults, comparing to patients with t(9;11), sole +8 patients had shorter disease free survival (DFS) and overall survival (OS) whereas comparing to other Intermediate-II patients, complete remission (CR)

rate is also low and OS is shorter. Among +8 patients, high *BAALC* expression and *FLT3*-ITD associated with worse outcomes in younger population and *TET2* mutations and wild-type *RAS* among older (*6*). Schwind et al. (*7*) reported that the presence of a *KIT* mutation confers worse outcome in inv(16)/t(16;16).

Besides these chromosomal translocations, 40-50% of AMLs are cytogenetic normal (CN-AML) (*8*). In this group, molecular markers such as mutations in *FLT3* (*9, 10*), *NPM1* (*8, 11-14*), *CEBPA* (*15-19*), *RUNX1* (*20, 21*), *MLL* (*22, 23*), *IDH1*/*IDH2* (*24-27*) as well as high expression of *BAALC* (*28, 29*) and ERG (*30*) have been found to predict outcome. Most studies were focused on the mutational status of *FLT3-ITD*, *NPM1* and *CEBPA* (*31*).

Mutation on FMS-like tyrosine kinase-3 (*FLT3*) including internal tandem duplications in the juxtamemberane domain (ITD) and mutations in the second tyrosine kinase domain (TKD) have been found in 30-45% of CN-AML (*32*). Both types of mutations can cause constitutively activation of FLT3 resulting in triggering downstream oncogenic signaling pathways including RAS-MAP/AKT kinases and signal transducer and activator of transcription-5 (STAT5) (*33*). *FLT3-ITD* was observed in 28-34% of CN-AML and has been associated with worse OS, relapse-free survival (RFS) whereas the prognostic impact of *FLT3-TKD* in younger patients was uncertain (*10, 31, 34*).

NPM1 gene encodes nucleophosmin which a ubiquitously expressed nuclear protein that shuttles between the nucleus and cytoplasm, and is implicated in multiple functions such as biogenesis of ribosome and regulating p53 and ARF pathways (*35*). Mutation of nucleophosmin (*NPM1*) gene that results in the

relocalization of *NPM1* from the nucleus into the cytoplasm represents the most common genetic alteration in CN-AML (50-60%) (*11*). *NPM1* mutation was associated with favorable outcome in the absence of *FLT3-ITD* (*36*) and higher CR and longer 3-year DFS and 3-year OS in older AML patients (age ≥ 60) (*14*). Patients with *FLT3*-ITD and wild-type *NPM1* constituted a high-risk group and had a worse outcome than the low-risk group of which patients without *FLT3*-ITD but *NPM1* mutation (*37*). Thus patients in this low-risk group may not be considered candidates for allogeneic hematopoietic stem-cell transplantation (HSCT) in first CR (*38*).

CCAAT enhancer-binding protein alpha encoded by *CEBPA* is an important regulatory transcription factor in hematopoiesis. Loss function of CEBPA resulted in the block of maturation of granulocytes (*39*). Mutations on CEBPA were detected in 10-18% CN-AML patients and predicted better event-free survival (EFS), DFS, and OS independently of other molecular and clinical prognosticators (*15-17, 31*). In most cases, *CEBPA*-mutation had an N-terminal frameshift mutation on one allele and a C-terminal in-frame mutation on the other allele (*40*). Recent studies (*18, 19*) showed that only biallelic mutations (bi*CEBPA*), but not monoallelic mutation (mo*CEBPA*) (either C- or N- terminal mutation on both allele) predicted favorable outcome compared with wild type CEBPA.

Based on the 2008 revision of the WHO classification of myeloid neoplasms and acute leukemia, an international expert group, on behalf of the European

LeukemiaNet (ELN), proposed a standardized system for correlation of cytogenetic and molecular genetic data with clinical data (Table 1.3) (*41*). In practice, it is difficult for clinician to summarize and interpret the prognostic information provided by the large panel of individual risk markers. Recently, Pastore et al. (*42*) developed an easy prognostic indices for CN-AML based on routinely available information such as age and white blood count, Eastern Cooperative Oncology Group (ECOG) performance status, and well-established molecular characteristics such as mutation status on *NPM1*, *FLT3*-ITD and bi*CEBPA*. Such tool can be used to stratify therapy in the future.

All other gene mutations identified in AML (summarized in Table 1.4) have not been employed into clinical practice and remain under close investigation (*38*). In addition to structural genetic aberrations, changes in expression of specific genes could also impact prognosis in AML. For example, a high expression level of *BAALC* (brain and acute leukemia, cytoplasmic) or a high blood *ERG* (v-ets erythroblastosis virus E26 oncogene homolog) level is a poor prognostic factors in CN-AML (*28*-*30*).

1.3 MicroRNA in AML

1.3.1 microRNA biogenesis

RNA interference (RNAi) is a biological response to double strand RNA (dsRNA) which results in sequence specific gene silencing. This phenomenon is very conservative and important in post-transcriptional gene regulation (*43*). RNAi

machinery has several conserved factors with the roles in recognizing, processing, transporting and conducting response to dsRNA.

MicroRNAs (miRNAs or miRs) are a growing family of small non-coding RNAs found in many eukaryotic organisms. MiRNAs are processed by RNAi machinery and have been shown to regulate genes expression. MiRNA genes are often located in clusters that may be transcribed as polycistrons, e.g. *miR-17-92* cluster (*44*) and their transcription is under strict development stage- and tissue-specific control (*45*). Transcribed pri-miRNAs size ranging from several hundred nucleotides (nt) to several kilobases (*46*) are folded into stem-loop structure (*45*). Then these are recognized and cleaved into precursor miRNA (pre-miRNA) in the nucleus by an RNase III enzyme Drosha with possible other partners i.e. Pasha (*46*). Pre-miRNA are short, hairpin RNAs of approximately 70 nt having the characteristic 2 nt 3′ overhang end structure left by the staggered cut of RNase III enzymes. Then the pre-miRNAs are exported to the cytoplasm by a RanGTP/exportin 5-dependent mechanism (*47-49*). It has been mentioned that a 2-3 nt overhang may be required for Exportin-5 recognition (*48*). Once in the cytoplasm, pre-miRNAs are recognized and processed into their mature form, 22-mer miRNAs, by Dicer. Dicer is a predominantly cytoplasmic enzyme and can also cleave dsRNA into 22-mer siRNAs (*50, 51*). It was thought that miRNA or siRNA released from Dicer are incorporated into a RNA-induced silencing complex (RISC). Chendrimada et al. (*52*), from human cells, isolated a Dicer-containing complex containing TRBP (the human immunodeficiency virus transactivating response RNA-binding protein) which was demonstrated to be

required for the recruitment of Ago2, a member of *Argonaute* gene family and the catalytic engine of RISC. This indicates the role of Dicer-TRBP complex not only in miRNA processing but also in RISC assembly. MiRNAs/siRNAs enter RISC in an asymmetric fashion that only one strand is assembled into RISC and mediates target RNA cleavage (*53*). Very interestingly, Schwarz et al. (*53*) showed that small changes in siRNA sequence have profound and predictable effects on the extent to which individual strands of an siRNA duplex enter the RNAi pathway. The choice was governed by an enzyme and always was the one whose 5′ end was less tightly paired to its complement. The biogenesis and process of miRNA is shown in Figure 1.1.

1.3.2 miRNA expression signature associated with cytogenetic abnormalities

Due to RNAi mechanism, miRNA are crucial regulators of many physiological processes such as differentiation, proliferation, apoptosis and development. Aberrant expressions of miRNAs have been found in many types of cancer, where they can function as both oncogenes and tumor suppressor genes (*54-56*). In AML, distinct miRNA profiles have been identified corresponding to specific cytogenetic subtypes, mutations, and to be associated with certain genetic abnormities and clinical outcome of AML patients.

By using genome-wide bead-based miRNA-expression analysis (*56*) and RT-PCR, distinct miRNA expression pattern for t(15;17) translocations, *MLL* translocations, as well as CBF fusion t(8;21) and inv(16) were observed (*57-62*).

Li et al. (*57*) reported that expression signatures of a minimum of two (*miR-126/126**), three (*miR-224, miR-368, and miR-382*), and seven in *miR-17-92* cluster miRNAs could accurately discriminate CBF, t(15;17), and MLL-rearrangement AMLs, respectively. A signature in Acute promyelocytic leukemia (APL) patients with t(15;17) comprised 7 upregulated miRNAs (*miR-127, miR-154, miR-154*, miR-299, miR-323, miR-368* and *miR-370*) and 9 downregulated miRNAs (*miR-17-3p, miR-185, miR-187, miR-194, miR-200a, miR-200b, miR-200c, miR-330, and miR-339*) (*60*). Garzon et al. (*61*) identified 8 miRNAs upregulated (*miR-326, miR-219, miR-194, miR-301, miR-324, miR-339, miR-99b,* and *miR-328*) and 14 downregulated (*miR-34b, miR-15a, miR-29a, miR-29c, miR-372, miR-30a, miR-29b, miR-30e, miR-196a, let-7f, miR-102, miR-331, miR-299,* and *miR-193*) in patients with t(11q23)/MLL versus all other AML patients.

Diaz-Beya et al. (*63*) observed a specific miRNA signature for t(8;16) in AML characterized by 90 downregulated including *let-7* family, *miR-34a*, *miR-15a, miR-26a/b* and *miR-125b* and 4 upregulated miRNAs compared with the remaining AML subtypes.

Though no correlation between an additional +8 and miRNA expression (*60*), two studies, when looking at patients with isolated +8, two signatures of miRNA were described by, one composed of 42 upregulated and no downregulated miRNA (*61*) and the other with a relatively large patient cohort composed of 5 upregulated (*miR-34b, miR-107, miR-370, miR-342-3p* and *miR-96*) and 2 downregulated (*miR-496* and *miR-493*) miRNAs (*6*).

A recent study showed a miRNA expression profile in complex karyotype AML with (CK-AML) with *TP53* alteration and identified *miR-34a* and *miR-100* as the most significantly down- and upregulated miRNA, respectively (*64*). Clinically, low *miR-34a* expression and *TP53* alterations predicted for chemotherapy resistance and inferior outcome.

1.3.3 miRNA expression signature associated with molecular markers

Several of recurrent mutations in CN-AML have also been correlated with miRNA expression signatures. Mutations in the *NPM1* gene have been linked to a signature including upregulation of *miR-10a/b and miR-196a/b* both of which are embedded in the *HOX* clusters (*14, 58*), as well as several tumor suppressors including *miR-15a*/*miR-16-1*, *miR-29*s (a/b/c), and the *let-7* (*let-7a*, *let-7b*, and *let-7f*), which is consistent with clinical observation that NPM1 mutation/FLT3 wt is a good prognosis marker (*8, 14*). The signature also contains the donwregulated miRNAs including *miR-130a, miR-486-5p, miR-451, miR-126, miR-450a, miR-424* (*14, 65*), *miR-204* and *miR-128,* the latter two of which target the *HOX* gene (*8*).

In AML with *FLT3*-ITD, Garzon et al. (*61*) found 3 upregulated miRNAs, *miR-155, miR-10a* and *miR-10b.* Significantly overexpressed *miR-155* in *FLT3*-ITD patients was confirmed by other studies (*8, 58*). In addition, 32 differentially expressed miRNAs with upregulated miRNAs, such as *miR-125b-2** and downregulated miRNAs, such as *miR-144* and *miR-451*, were shown in the signature of *FLT3*-

ITD in primarily older CN-AML patients (age ≥ 60) (*10*).

CEBPA mutations have been associated with a miRNA expression pattern including 15 upregulated miRNAs, 8 of which corresponding to the *miR-181* family, and 2 downregulated miRNAs, *miR-194* and *miR-34a* (*17, 58*). Recently, our group showed that a higher level of *miR-181a* in CN-AML patients is predominately presented in patients harboring *CEBPA* N-terminal mutations, but not in those having single C-terminal mutation or wt *CEBPA*, possibly due to CEBPα-p30 (protein product of N-terminal mutated *CEBPA*) modulated *miR-181a* expression (*66*). In another study, a decreased expression of *miR-196b* was associated with biCEBPA mutations (*67*).

Marcucci et al. (*68*) reported that a signature consisting of 12 miRNAs (4 upregulated and 8 downregualted) was associated with *DNMT3A* mutation in older AML patients whereas no signature in the younger group and a signature consisting of 24 miRNAs (13 upregulated e.g. *miR-1* and *miR-133* and 11 downregulated) was associated with *IDH2* R172 mutation (*24*). Mendler et al. (*21*) showed that 8 microRNAs (2 in *let-7* family, *miR-223, miR-99a, miR-100, miR-211, miR-220* and *miR-595*) were downregulated in *RUNX1*-mutated patients compared to *RUNX1* wild-type patients. Metzeler et al. (*69*) identified distinct microRNA-expression signatures in favorable-risk and intermediate-I–risk patients with TET-2 mutation. In the favorable-risk group, the signature of TET2-mutated patients compared with TET2-wt patients was composed of 5 upregulated (e.g. *miR-148a, miR-24*) and 2 downregulated miRNAs (e.g. *miR-135a*). In intermediate-I–risk group, the signature of TET2-mutated patients

compared with TET2-wt patients, showed 6 upregulated (e.g. *miR-204*) and 7 downregulated (e.g. *miR-126*) microRNAs.

Schwind et al. (*70*) for the first time derived microRNA signatures for low *ERG* (11 miRNAs: 5 up- and 6 down- regulated) and low *BAALC* (18 miRNAs: 10 up- and 5 down- regualted) in older CN-AML patients. Another study showed that there was no miRNA expression signature that differentiated between the low and high *BAALC* expressers in younger CN-AML patients by microarray profiling method. However there was a striking inverse correlation between *miR-148a* and *BAALC* expression (*28*). Two studies identified miRNA expression patterns associated with low *MN1* expression in younger and older AML patients respectively (*71, 72*). In younger AML patients with low *MN1*, 8 miRNAs were downregulated (e.g. *miR-126*) and 7 miRNAs were upregulated (e.g. *miR-424, miR-16, miR-19a*) compared with the high *MN1* group (*71*). In older AML patients with low *MN1*, 9 downregulated (e.g. *miR-126, miR-146a, miR-30b*) and 7 upregualted miRNAs (e.g. *miR-10a, miR-10b, let-7b, miR-449a*) were in the signature compared with the high *MN1* group (*72*).

Bulk AML blasts are hypothesized to be originated and maintained by a distinct population of leukemia-initiating cells or leukemic stem cells (LSCs) which are defined by their unique capability of self-renewal and long-term engraftment in immunodeficient mice (*73, 74*). A recent study derived a “core enriched” (CE) LSC-related gene expression signature (GES) comprising of 44 genes from comparing LSC GES with a signature from normal hematopoietic stem cells (*75*). Metzeler et al. (*76*) studied CE GES on 364 well-characterized CN-AML patients

and identified a miRNA expression signature (15 upregulated miRNAs, e.g.*miR-99, miR125a/b, miR-126* and *miR-155*) in high CE score patients comparing with low CE score patients.

1.3.4 miRNA expression and clinical outcome

From prognostic standpoint, miRNA expression is associated with clinical outcome. Three different studies, which included heterogeneous cytogenetic AML cohorts, identified that patients with a higher level of *miR-191* (*61*), *miR-199a* (*61*)*, miR-196b* (*77*) or *miR-212* (*78*) had significantly worse overall survival comparing to those with a lower level of corresponding miRNAs. A Cancer and Leukemia Group B (CALGB) study (*37*) identified a miRNA-expression signature composed of 12 miRNA probes, which was associated with event-free survival in CN-AML patients with high-risk molecular features: *FLT3*-ITD, *NPM1* wt, or both. In this signature, an increased expression of 5 miRNA probes representing *miR-181* family was associated with decreased risk and an increased expression of *miR-124, miR-128-1, miR-194, miR-219-5p, miR-220a* and *miR-320* (two probes) were associated with increased risk. Later, the same group confirmed the individual prognostic value of *miR-181a* that a higher *miR-181a* expression was associated with a higher CR, longer OS and a trend for longer DFS (*79*). They also identified another miRNA, *miR-155*, as an individual prognostic marker that a higher level of *miR-155* was associated with lower CR and shorter DFS and OS in a cohort of CN-AML patients (*80*). An intronic miRNA, *miR-3151,* has been demonstrated to interplay with its host gene *BAALC* and independently affects

the outcome of older CN-AML patients. A higher expression of *miR-3151* was associated with shorter DFS and OS (*81*). In addition, a recent study showed that higher levels of *miR-196b* and *miR-644* were independently associated with shorter OS, and lower levels of *miR-135a* and *miR-409-3p* with a higher risk of relapse in intermediate-risk cytogenetic AML (IR-AML) patients (*67*).

Previously, our group reported that older AML patients with a higher *miR-29b* level responded better to a demethylating drug, decitabine, in a Phase II clinical trial with single-agent decitabine (*82*). Those patients were not candidates for or refused intensive chemotherapy. Recently, we reported that a higher baseline *miR-10* family including *miR-10a-5p* and *miR-10b-5p* in cytogenetically heterogeneous AML patients was associated with achieving CR after chemotherapy (i.e. idarubicin and cytarabine) (*83*).

1.4 Objectives and Overview of this thesis

By using high-throughput genome-scale technologies, we have learnt more about the complexity and biological heterogeneity of AML. The importance of miRNA increases not only our basic knowledge about the pathology of leukemias but also their therapeutic potentials. Some pitfalls could be encountered in clinical translation include dosage, efficacy, functionality, delivery, nonspecific toxicity and immune activation (*84, 85*).

To overcome some of above mentioned difficulties regarding clinical application of miRNAs, development of targeted nanoparticle-based delivery system for miRNA replacement therapy is the goal of this thesis. The research we present in

the following chapters focused on three major aims: to develop a targeted novel nanocarrier suitable for delivering miRs into AML cells; to deliver *miR-29b* and assess the antileukemic activity; and to investigate the role of *miR-181a* in AML, unravel the mechanism, and perform therapeutic evaluation via nanocarrier-delivered *miR-181a*.

In Chapter 2, the main focus is to design and synthesize novel anionic-lipid based lipopolyplex nanoparticles. Several parameters such as particle size, surface charge and entrapment efficiency are investigated. The delivery efficacy and *in vivo* toxicity of transferrin (Tf) targeting or antibody targeting nanoparticle (Tf-NP or antibody-NP) are also assessed.

In Chapter 3, we implement Tf-NP delivery system in *miR-29b* replacement therapy. The intracellular *miR-29b* level and protein level of its target genes are measured after the treatment of Tf-NP encapsulating *miR-29b* mimic molecules (Tf-NP-*miR-29b*) in AML cell lines and patient blasts. Anti-leukemic activity of Tf-NP-*miR-29b* are investigated both *in vitro* and *in vivo*. Furthermore, the idea that priming AML cells with *miR-29b* mimic could sensitize them to decitabine treatment is explored.

In Chapter 4, we first investigate the role of *miR-181a* as a tumor suppressor in AML. We propose that *miR-181a* would suppress the oncogenic RAS/MAPK pathway by directly targeting *RAS* and *MAPK1*. Then by using above-mentioned Tf-NP system, *miR-181a* mimic molecules are able to be delivered and have anti-leukemic activity.

In conclusion, nanoparticle-based miR replacement therapy, particularly when

combined with existing chemotherapy regimens, may represent a promising new treatment strategy for AML patients.

1.5 Tables and Figures

Table 1. 1 WHO classification of Acute Myeloid Leukemia

Acute myeloid leukemia and related neoplasms
Acute myeloid leukemia with recurrent genetic abnormalities
AML with t(8;21)(q22;q22); *RUNX1-RUNX1T1*
AML with inv(16)(p13.1q22) or t(16;16)(p13.1;q22); *CBFB-MYH11*
APL with t(15;17)(q22;q12); *PML-RARA*
AML with t(9;11)(p22;q23); *MLLT3-MLL*
AML with t(6;9)(p23;q34); *DEK-NUP214*
AML with inv(3)(q21q26.2) or t(3;3)(q21;q26.2); *RPN1-EVI1*
AML (megakaryoblastic) with t(1;22)(p13;q13); *RBM15-MKL1*
Provisional entity: AML with mutated NPM1
Provisional entity: AML with mutated CEBPA
Acute myeloid leukemia with myelodysplasia-related changes
Therapy-related myeloid neoplasms
Acute myeloid leukemia, not otherwise specified
AML with minimal differentiation
AML without maturation
AML with maturation
Acute myelomonocytic leukemia
Acute monoblastic/monocytic leukemia
Acute erythroid leukemia
Pure erythroid leukemia
Erythroleukemia, erythroid/myeloid
Acute megakaryoblastic leukemia
Acute basophilic leukemia
Acute panmyelosis with myelofibrosis

	Genetic Abnormalities	FAB	% in AML	Fusion gene	Respond to Chemo
AML	t(8;21)(q22;22)	M2	5%-12%	*AML1/ ETO*	Good to high dose cytarabine
AML	inv(16)(p13;q22) or t(16;16)(p13;q22)	M4	10%-12%	*CBFβ/ MYH11*	Higher CR when treated with high-dose cytarabine in post-remission phase
APL	t(15;17)(q22;q12)	M3	5%-8%	*PML/ RARA*	Specific sensitive to all-trans retinoic acid (ATRA)
AML	11q23 (MLL)	M4, M5a and M5b	5%-6%	*MLL* rearrang -ement	Difficult to determine

Table 1. 2 AML with characteristic genetic abnormalities

Table 1. 3 European LeukemiaNet standardized reporting system for correlation of cytogenetic and molecular genetic data in AML with clinical data (*41*)

Genetic Group	Subsets
Favorable	t(8;21)(q22;q22); *RUNX1-RUX1T1* inv(16)(p13.1q22) or t(16;16)(p13.1;q22); *CBFB-MYH11* Mutated *NPM1* without *FLT3*-ITD (normal karyotype) Mutated *CEBPA* (normal karyotype)
Intermediate-I	Mutated *NPM1* and *FLT3*-ITD (normal karyotype) Wild-type *NPM1* and *FLT3*-ITD (normal karyotype) Wild-type *NPM1* without *FLT3*-ITD (normal karyotype)
Intermediate-II	t(9;11)(p22;q23); *MLL3-MLL* Cytogenetic abnormalities not classified as favorable or adverse
Adverse	inv(3)(q21q26.2) or t(3;3)(q21;q26.2); *RPN1-EVI1* t(6;9)(p23;q34); *DEK-NUP214* t(v;11)(v;q23); *MLL* rearranged -5 or del(5q); -7; abnl(17p); complex karyotype

Table 1. 4 Recurrent molecular genetic abnormalities in adult AML, their biology features and clinical relevance.

Gene	Biology features	Prognosis impact
CEBPA	Regulatory transcription factor in hematopoiesis	biCEBPA: favorable
FLT3	Member of the class III receptor tyrosine kinase family; Mutations cause constitutively activation of FLT3	FLT3-ITD: unfavorable FLT3-TKD: controversial
NPM1	Nuclear-cytoplasmic shuttling phosphoprotein with pleiotropic functions; Mutations lead to abnormal cytoplasmic localization of the protein	NPM1 mutation without FLT3: favorable
KIT	Member of the class III receptor tyrosine kinase family	KIT mutation in CBF-AML: unfavorable
WT1	Transcription factor implicated in regulation of apoptosis, proliferation, and differentiation of hematopoietic progenitor cells	Controversial
MLL	DNA binding protein that regulates gene expression in hematopoiesis possibly through epigenetic mechanisms	MLL-PTD: unfavorable
RAS	Membrane-associated proteins regulating mechanism of proliferation, differentiation, and apoptosis	Controversial
RUNX1	Transcription factor required for definitive hematopoiesis	Mutation: unfavorable

Continued

Table 1. 4: Continued

Gene	Biology features	Prognosis impact
IDH1/IDH2	Cytosolic (IDH1) and mitochondrial (IDH2) metabolic enzymes catalyzing oxidative decarboxylation of isocitrate to α-ketoglutarate; involved in cellular defense of oxidative damage	IDH1 R132 and IDH2 R140: favorable IDH2 R172 mutation: unfavorable IDH1 SNP rs11554137: unfavorable
TET2	Catalyzing the conversion of the modified DNA base methylcytosine to 5-hydroxymethylcytosine	Mutation: unfavorable
ASXL	Member of the Polycomb group of proteins	Mutation: unfavorable
JAK2	Non-receptor tyrosine kinase	Mutation: unfavorable
TP53	Tumor suppressor	Mutation: unfavorable
DNMT3A	Member of DNA methyltransferase; Catalyzing the transfer of methyl groups to specific CpG structures in DNA	Mutation: unfavorable
BAALC	Function unknown	High expression: unfavorable
ERG	Member of the ETS family of transcription factors	High expression: unfavorable
MN1	Transcription coregulator	High expression: unfavorable
EVI1	Dynamic modulator of transcription and chromatin remodeling	Aberrant expression: unfavorable

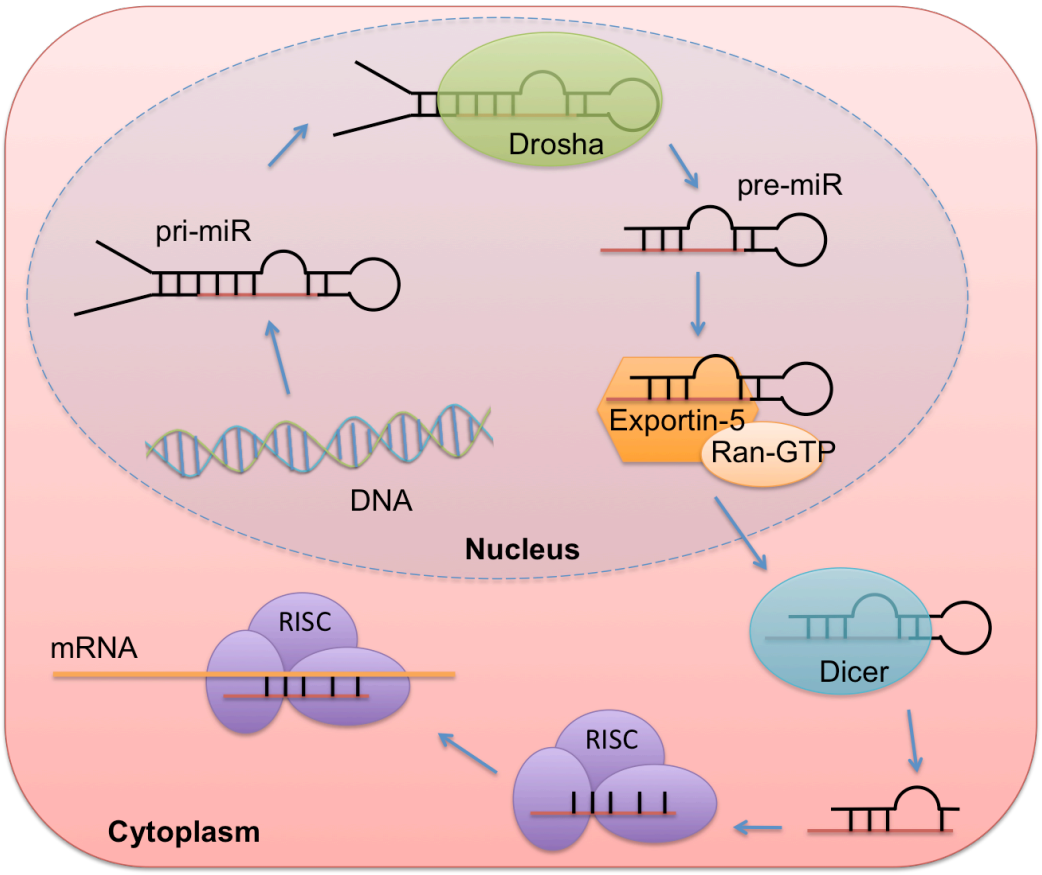

Figure 1. 1 Schematic diagram of a model of miRNA biogenesis, trafficking and assembly to RISC.

miRNAs are transcribed in the nucleus and pri-miRNAs are cleaved by Drosha into pre-miRNAs. Pre-miRNAs are exported into cytoplasm by Exportin-5, a Ran-GTP dependent nuclear export factor. Then pre-miRNAs are cleaved by Dicer and released as ~22 nt miRNA. miRNA duplex enters RISC in asymmetric manner. Only one of strand is assembled into RISC serving as a guide to substrate mRNA selection. Once target mRNA is loaded into RISC, translation repression or mRNA degradation occurs.

Chapter 2. Targeted Anionic-lipid Based Lipopolyplex for Oligonucleotides Delivery

2.1 Introduction

Cancer refers to diseases in which abnormal cells proliferate without control and have ability to invade other organs. Mutations on DNA or certain environmental stimuli (e.g. bacteria) cause aberrant expression of oncogenes and tumor suppressors or constitutive signals in the cells, which can make them escaping suicide and apoptosis. Despite the uniqueness of each cancer type, chemotherapy is one of comment treatment methods due to highly proliferative property of tumorous cells. Nanotechnology has been embedded with drug development to overcome the pharmaceutical drawbacks of drugs such as poor aqueous solubility, poor stability, insufficient bioavailability and unwanted cytotoxicity (*86*). Nanocarriers can be loaded with a large amount of drug molecules, either hydrophobic or hydrophilic. The coating on the nanocarrier (e.g. polyethylene glycol) can delay the clearance by the reticuloendothelial system (RES), increase the particle half-life in the blood circulation, prevent opsonization by avoiding protein binding (*87, 88*). Typically, the majority of opsonized particles are cleared by a receptor-mediated mechanism by phagocytic cells in the liver

and spleen. The nanoscale size of those drug loaded particles also enable the increase of drug payload to the tumor owing to the enhanced permeability and retention effect (*89*) which is considered as passive targeting to the tumors. Active targeted delivery can be achieved by functionalizing the surface of nanoparticles with ligands (peptides, nucleic acids or small molecules) that are specifically recognized by certain receptors on targeted cell surface while reducing nonspecific distribution (*90*), thus lowering the exposure of healthy tissue to toxic side effects (*90, 91*). When the carrier particle degrades, the drug molecules are released and the degradation rate of carrier particles can even be controlled.

Besides the successful delivery of small molecular drugs [e.g. doxorubicin (Doxil), paclitaxel (Abraxane)], the nanoparticle system has a more important role in delivery of a new class of macromolecules, nucleic acid, which has been found to be able to modulate gene expression and have anti-cancer potential (*92-94*). Unlike most currently marketed small molecule drugs which usually target proteins such as enzymes and receptors, nucleic acids can modulate the expression of genes by targeting mRNA that has been proven to be effective for targets that are not treatable by current drugs (*94*). The most common approaches involving oligonucleotide therapy includes: RNA interference (RNAi), antisense oligonucleotides (ASO) and steric-blocking oligonucleotides (*94*). RNAi technologies use natural cellular machinery to induce silencing when introduced exogenous small interfering RNA (siRNA) or microRNA paired with its mRNA target. The mechanism that mediated gene silencing involves double –strands

RNA (dsRNA) interacting with a multiprotien RNA-induced silencing complex (RISC) (more details see 1.3 in Chapter 1). ASO is typically ~20 nucleotides long and has a phosphorothioate linkage between the nucleotides that form the backbone. Other modifications including five nucleotides at each flank protect the ASO from exonucleases for high stablity *in vivo* (*94*). The 10-nucleotide gap in between flank regions allows the binding with the target and cleavage of targeted mRNA by ribonuclease H (RNase H) (*95*). Unlike the previous discussed oligonucleotides, another type of oligonucleotides as developed, that modulate the RNA function by blocking the access of cellular machinery to RNA and do not necessarily involve enzymatic RNA degradation system (i.e. RISC and RNase H). This difference leads to outcomes such as repairing defective RNA and restore the production of desirable proteins (*94*). In addition, because RNA-blocking oligonulceotides do not need cellular enzymes for their activity, they can be subjected to more extensive chemical modifications, e.g. peptide nucleic acids (PNAs), alternating locked nucleic acids (LNAs), deoxynucleotide oligonucleotides, fully modified 2′-substituted oligonucleotides and phosphorodiamidate morpholino oligomers (PMOs) (*94, 96-98*).

The poor intracellular uptake of these oligonucleotides due to their large size, negative charge and hydrophilicity impeds their use as therapeutics (*94*). Thus a safe, effective and cancer cell specific delivery system is needed for successful clinic application of oligonucleotide therapy (*99, 100*).

2.1.1 Delivery system for oligonucleotides

Oligonucleotides delivery strategies include viral and non-viral systems. Many delivery systems based on virus to deliver shRNAs or artificial miRNAs have been developed and optimized depending on the research aims and cell types, such as retroviral vector, lentiviral vector, adenoviral vector and adenovirus associated vector (AAVs) (Table 2.1). Two important features of viral vectors over synthetic siRNA/miRNA are their highly effective and stabilized transfection, which make them more suitable to treat certain diseases such as neurodegenerative disease and cardiovascular disease (*101*) when one wants to save the cell with RNAi (*93*). For example, Huntington's disease is known to be caused by mutated hutingtin (HTT) gene that contains a polyglutamine expansion which can be translated into an elongated protein. Then the protein is cut into smaller, toxic fragments that accumulated in neurons. Several studies have utilized AAV vectors to express anti-huntingtin (HTT) shRNAs to reduce the level of HTT mRNA and protein, which results in behavioral improvements in mouse models (*102-104*). Lentiviral vector and AAV were mostly used because they have the best safety records (*101*). The major difference between these two systems is that lentiviral vector requires integration into cell genome while AAV can remain episomal that avoiding possible insertional mutagenesis (*93*). In terms of anti-cancer therapeutics, AAV8 vector was successfully used to express *miR-26a* to treat hepatocellular carcinoma (HCC) in mouse model (*105*). So far, there are currently no AAV mediated RNAi vectors in clinical trial. ShRNA delivered by viral vectors can bypass Drosha processing and is exported out to

nucleus by Exportin 5 followed by Dicer cleavase to generate siRNA. Observed toxicity of shRNA molecules such as sever liver injury and even fatality of mice when injected with a high dose of shRNA may be explained by the high level of shRNA competing with endogenous miRNAs for intracellular processing and saturation of RNAi machinery including Exportin 5 and argonaute 2 (*106-108*). Thus, alternatively, synthetic siRNA or miRNA mimics that bypass the process of siRNA/miRNA maturation are widely used.

Many non-viral delivery methods have been developed around such synthetic siRNAs or miRNA mimics. Among the most common ones are lipid-based or polymer-based carriers and cholesterol conjugates to sense strand of the duplex. Cholesterol-conjugated siRNA can be efficiently delivered to liver that express low-density lipoprotein (LDL) (*109, 110*). Polymers such as poly-L-lysine (PLL), polyethyleneimine (PEI) (*111*), chitosan (*112-116*), cyclodextrin (*117, 118*) and polyamidoamine dendrimer (*119-122*) are biodegradable, biocompatible and non-toxic, which are desirable properties for *in vivo* delivery system (*111*). Low functionalization, toxicity and batch-to-batch reproducibility are still the potential problems that will be solved in the future with the most advanced polymers, chitosans, dextrins and PEI derivatives (*123*). Cationic lipids such as dioleoyl trimethylammonium propane (DOTAP), 3b[N-(N′,N′-dimethylaminoethane)-carbamoyl) cholesterol (DC-Chol) and N-[1-(2,3-dioleoyloxy) propyl]-N,N,N-trimethylammonium chloride (DOTMA) are usually used for lipid-based carriers because they are the simplest and the fastest way to bind nucleic acids and to enhance cellular uptake, taking advantage of the electrostatic interactions. (*92,*

123-125). Solid lipid nanoparticles (SLNP) have emerged as alternatives to liposomes. The formulation is usually composed of cationic lipids that interact with nucleic acids to form a tight complex, fusogenic lipids and PEG derivatives (*123*). In general, the role of PEGylated lipids includes regulating fusogenicity, shielding surface charge, reducing the particle size, avoiding aggregation during storage, and improving the plasma stability (*126*). The cationic lipids forming SLNPs often have ionizable amine headgroups and a double-hyphocarbonated alkyl chain. Some SLNPs in RNAi or anti-sense technology have been reported in clinical trials for cancer treatment (*123, 127*). For example, TKM-080301 targets PLK1 to treat advanced solid tumor supported by Tekmira Pharmaceutics (NCT01262235); Atu027 targets PKN3 to treat metastatic pancreatic cancer supported by Silence Therapeutics (NCT01808638); ALN-VSP comprising two siRNAs against vascular endothelial growth factor (VEGF) and kinesin spindle protein (KSP) is used to treat solid tumors supported by Alnylam Therapeuticals (NCT01158079) (*128*).

2.1.2 Targeted delivery

Complexing siRNA with carriers provides opportunities for targeting specific tissue or cell type, which also allows for enhanced circulation time and cellular uptake and decrease systemic toxicity. The commonly used targeting molecules include peptides, antibodies and small molecules. To date, there are thirteen ligand-targeted nanomedicines that have been progressed in clinical trial (*129*). Twelve of them are developed for cancer treatment. With the complexity of RNAi

and nanocarrier chemistry, only one nanomedicine involves siRNA and targeting delivery (CALAA-01).

Transferrin (Tf) whose primary function of serum iron transportation when binding to ferric iron has high affinity to transferrin receptor (TfR) (*130-132*). In early studies, it has been shown that TfR expressed at a greater level on the cells with a high proliferation rate. The reason may be cancer cells require more iron for the iron-dependent enzyme, ribonucleotide reductase, which regulates the total rate of DNA synthesis (*133*). Other studies showed an upregulation of TfR on many cancer types (*134*). Thus, the ability to successfully deliver chemotherapeutic compounds or oligonucleotides via targeting TfR either through Tf-mediated endocytosis or antibody-antigen interaction would lead to cancer cell death. MBP-426 is a Tf-conjugated liposome loaded with oxaliplatin (L-OHP) for the treatment of second line gastric, gastroesophageal or esophagieal adenocarcinomas in combination with leucovorin and fluorouracil (NCT00355888). CALAA-01 is also a Tf-conjugated nanomedicine of which nanocarrier contains cyclodextrin polymer and encapsulates siRNA for solid tumor treatment (NCT00689065) (*135*). This siRNA can knockdown the M2 subunit of ribboneotide reductase (RRM2) that catalyzes the reduction of ribonucleotides into deoxytibonucleotides for DNA synthesis (*136, 137*). SGT-53 (NCT00470613) and SGT-94 (NCT01517464) are TfR targeting nanoparticles with cationic lipids complexing with plasmid DNA encoding tumor suppressor wild-type p53 (*138*) and RB94 (*139*) respectively. Similar idea of targeting tumor specific marker has been extended to other surface proteins such as HER2 (*140*),

epithelial growth factor receptor (EGFR) (*141, 142*) and prostate-specific membrane antigen (PSMA) etc. Recently, Zhang et al. (*143*) developed a DOTAP-based cationic liposomes attached to a six repetitive sequence peptide, $(AspSerSer)_6$, which can deliver an osteogenic siRNA which targets casein kinase-2 interacting protein-1 (*Plekho1*) specifically to bone-formation surface. An aptamer or small molecule, S,S-2-[3-[5-amino-1-carboxypentyl]-ureido]-pentanedioic acid (ACUPA), which can specifically bind to PSMA has been reported to deliver DNA-activated protein kinase (DNAPK) shRNA (*144*) and a polymeric nanoparticle encapsulating docetaxel (DTXL) (BIND-014, NCT01812746, (*145*)) respectively to prostate cancer.

2.2 Materials and Methods

2.2.1 Materials

The synthetic scramble control labeled with the fluorescent dye FAM (FAM-miR) were purchased from Ambion (Austin, TX). FAM/Cy3/Cy5 labeled oligonucleotide DNA (ODN) was purchased from Alpha DNA. Polyethylenimine (MW, ~2000, PEI), linoleic acid and human holo-tranferrin (Tf) were purchased from Sigma-Aldrich. 1,2-dioleoyl-sn-glycero-3-phosphoethanolamine (DOPE) was purchased from Avanti Polar Lipids. 1,2-dimyristoyl-sn-glycerol, methoxypolyethylene glycol (MW~2000; DMG-PEG) was purchased from NOF America Corporation. Traut's reagent (2-Iminothiolane•HCl) was purchased from Thermo Scientific.

2.2.2 Preparation of anionic lipid based nanoparticles

As shown in Figure 2.1, mimic miRs were mixed with PEI at room temperature (Step 1). The N/P ratio (the ratio of moles of the amine group of PEI to those of the phosphate groups of RNA) was 10:1. The lipid mix consists of DOPE, linoleic acid and DMG-PEG as the ratio of 50/48/2. To form empty nanoparticles, lipid ethanol solvent was injected into 20 mmol/L HEPES buffer, pH= 7.4 (Step 2). The percentage of ethanol was less than 5%. The pre-made empty nanoparticles in step 2 were then added to PEI/miR polyplex (Step 3). The mass ratio of lipid to miR was 10:1. Using vortexing and sonication, lipopolyplex nanoparticle-containing the mimic miRs were produced.

2.2.3 Preparation of Transferrin-PEG-DSPE

A post-insertion method was adopted to incorporate Tf ligand onto the miR-loaded nanoparticles (*146*). Tf was reacted with Traut's reagent at a molar ratio of 1:10 in PBS buffer (pH=8) for 2 hours at room temperature to yield Tf-SH. Extra Traut's reagent was removed by PD10 column (GE Healthcare). Tf-SH was then reacted with Mal-PEG-DSPE in PBS buffer (pH=6.5) at a molar ratio of 1:10 for overnight at room temperature to yield micelles of Tf-PEG-DSPE which then stored at 4°C.

2.2.4 Preparation of anti-CD56/CD45.2 antibody-PEG-DSPE

Anti-CD56 or anti-CD45.2 antibody was reacted with Traut's reagent in PBS buffer (pH=8) for 2 hours at room temperature to yield anti-CD56 or CD45.2

antibody-SH. The Extra Traut's reagent was removed by Microcon-10KDa Centrifugal Filter Unit (Millipore). Anti-CD56 or CD45.2 antibody-SH was then reacted with Mal-PEG-DSPE in PBS buffer (pH=6.5) at a molar ratio of 1:10 for 2 hours at room temperature to yield micelles of antibody-PEG-DSPE which then stored at 4°C.

2.2.5 Preparation of Tf or antibody conjugated NP-miR

We prepared the transferrin-conjugated NP as shown in Figure 2.1. MiR-loaded NP was mixed with Tf-PEG-DSPE at ratio of lipid:Tf=2000:1 and was incubated at 37°C for 1 hour (Step 4). miR-loaded NP was mixed with antibody-PEG-DSPE at various ratios.

2.2.6 Characterization of Nanoparticles

The size of NP was analyzed using a NICOMP Particle Sizer Model 370 (Particle Sizing Systems, Santa Barbara, CA). The zeta potential was determined using a ZetaPALS, Zeta Potential Analyzer (Brookhaven Instruments Corp., Worcestershire, NY).

The miR entrapment efficiency was assessed by gel electrophoresis. 0.5% sodium dodecyl sulfate (SDS) was used to dissolve the NP. The amount of miR in solution was compared before and after dissolution by SDS by agarose gel electrophoresis of RNA using empty NP and free miR as controls.

2.2.7 Cell lines and cell culture

Kasumi-1, MV4-11, THP-1, KG1, and KG1a cells were obtained from the American Type Culture Collection (ATCC; Manassas, VA); OCI-AML3 cells were obtained from DSMZ (Braunschweig, Germany). AML patient blasts were obtained from the Ohio State University (OSU) Leukemia Tissue Bank. All patients provided written informed consent in accordance with the Declaration of Helsinki under an Institutional Review Board- approved protocol for discovery studies according to OSU institutional guidelines for tissue collection and the use of the tissue in research.

2.2.8 Laser-scanning confocal microscopy

Cells were incubated with Tf-NP-FAM-miR or NP-FAM-miR at a final concentration of 100 nmol/L for 4 hours at 37°C and washed twice with PBS followed by fixation with 4% paraformaldehyde. Nuclei were stained with 5 mg/mL of Hoechst (Biostatus Limited) for 5 minutes at room temperature. The cells were attached to a poly-D-lysine–coated cover glass slide (Sigma-Aldrich). Green fluorescence of FAM-miR and blue fluorescence of Hoechst were acquired by confocal microscopy (Olympus FV1000).

2.2.9 Flow cytometry

The transferrin receptor cell surface expression was detected using antibodies from BD Bioscience. Flow cytometry was carried out on a FACSCalibur (BD

Biosciences). A minimum of 10,000 events were collected and analyzed using Flow Jo software (Tree Star Inc).

2.2.10 Nanoparticle toxicity profiling

Immunocompetent B6.SJL-Ptprc^{a}Pepc^{b} mice (BoyJ; The Jackson Laboratory) were used for *in vivo* nanoparticles toxicity studies. In the first group, 7-week-old male mice were injected with saline, empty nanoparticles (15 mg/kg/d of lipids), or Tf-NP-*miR-29b* (1.5 mg/kg/d of miR). Blood was collected 24 hours after the injection. The serum levels of alanine aminotransferase (ALT), aspartate aminotransfer- ase (AST), alkaline phosphatase (ALP), g-glutamic transfer- ase (GGT), blood urea nitrogen (BUN), and creatinine were assessed by the Clinical Pathology Services at OSU. A second group of mice were treated with either saline or Tf-NP (1.5 mg/kg/d of miR) with 3 doses, every other day. During the treatment, body weight was monitored every other day and for 1 additional week after the treatment. Blood counts were assessed weekly.

2.2.11 In vivo biodistribution study of NP

NOD scid gamma (NSG; Jackson Lab) were engrafted with MV4-11 cells. Tf conjugated NP or NP without Tf encapsulating Cy5-labeled oligodeoxynucleotide at 1.5 mg/kg were given to the mice through tail vain injection 15 days after engraftment. After 24 hours, mice were euthanized and tissue were collected and fixed in 10% formalin for 12 hours. The tissue were then soaked in 30 wt % sucrose solution for another 12 hours. The fluorescence signals of Cy5 emitted

by the whole tissue were measured using Xenogen IVIS-200 Optical In Vivo Imaging System (Caliper Life Science).

2.2.12 Colony-forming cell and replating colony assays

$2x10^4$ CD34+ AML cells treated with Tf-NP-anti-126 or Tf-NP-anti-sc were plated into growth factor-containing Methocult H4034 Optimum or GF M3434 (StemCell Technologies), respectively. Colonies were scored after 12-14 days. For serial replating assays, whole plates were harvested and 10^4 recovered cells were replated in the same conditions at 12-14 day intervals.

2.2.13 CD45.2 antibody conjugated NP-anti-126 in vivo study

To test the anti-leukemic activity of CD45.2-NP-miR-126, we used our previously established *Mll* PTD *Flt3* ITD mouse model (*147*). In primary transplant, lethally irradiated (10Gy) 8-10 week old BoyJ (C57Bl/6J-CD45.1) (Jackson Laboratory) were intravenously injected through tail vein with $5.0x10^6$ leukemic *Mll* PTD *Flt3* ITD BM cells along with $1.0x10^6$ BM from BoyJ (C57Bl/6J-CD45.1). NP treatment started 5-weeks post-BMT. Mice were treated with, CD45.2-NP-scramble (n=3), and CD45.2-NP-miR-126 (n=3); 1 mg/kg/d of miR molecule injected I.V. on Monday, Wednesday, and Friday, and 2 mg/kg/d of miR molecules injected I.P. on Tuesday/Thursday. Alternating i.v. and i.p. administration was required to avoid the technical challenge of daily i.v. tail injection.

2.3 Results

2.3.1 Preparation and characterization of Tf-conjugated microRNA loaded anionic-lipid based lipopolyplex

A high transferrin receptor surface expression was observed in Kasumi-1, OCI-AML3, and MV4-11 cells and in AML patient blasts (Figure 2.2). Thus, to facilitate an efficient, targeted delivery, we conjugated the nanoparticles with transferrin (Tf-NP).

Particle size and z-potential values are presented in Table 2.2. The average size and – ζ potential of empty nanoparticles were 129.6 ± 1.0 nm (±SD) and -9.8 ± 1.5 mV (±SD) and NP-miR were 137.6 ± 1.0 nm and 22.5 ± 1.4 mV, respectively. After the transferrin conjugation, the size of the miR-loaded Tf-NP was increased to 147.3 ± 4.7 nm and the ζ-potential was 5.8 ± 1.9 mV. The achieved size and charge of the nanoparticles has been previously shown to be optimal for a long-lasting in vivo circulation time (*87, 148*). The mimic miR-29b entrapment efficiency of nanoparticles was evaluated by agarose gel electrophoresis. Analysis of the Tf-NP encapsulating miR before the SDS treatment showed no visible band, whereas a clear band comparable with the size and intensity of free miR was observed after dissolving the Tf-NP and releasing the entrapped miR molecules, thereby supporting a high miR entrapment efficiency (Figure 2.3).

2.3.2 Transferrin targeted delivery to Acute Myeloid Leukemia cells

To assess the efficiency of cellular uptake of the miR molecules, we treated 3 AML cell lines, Kasumi-1, OCI-AML3, and MV4-11 with free FAM-labeled miR (FAM-miR), non–transferrin-conjugated FAM-miR-loaded nanoparticles (NP-FAM-miR), or transferrin-conjugated FAM-miR-loaded nanoparticles (Tf-NP-FAM-miR). Four hours after the treatment, the FAM-label fluorescence was measured by flow cytometry. The mean fluorescence intensity (MFI) levels for Tf-NP–treated Kasumi-1, OCI-AML3, and MV4-11 were, 2.5-, 7.4-, and 4.7-fold higher than the non-transferrin–conjugated nanoparticle-treated cells, whereas free FAM-labeled-miR was barely detectable in the cells (Figure 2.4A). This indicated an enhancement of miR uptake using Tf-NP. The qualitative intracellular FAM-miR uptake by AML cells following Tf-NP treatment was confirmed by confocal microscopy that showed an accumulation of FAM-miR mostly in the cytoplasm (Figure 2.4B).

2.3.3 Cytotoxicity of transferrin conjugated nanoparticles *in vivo*

To assess the safety profile of systemic nanoparticle treatment, we evaluated basic hepatic and renal functions in immunocompetent mice after saline, empty nanoparticles, or Tf-NP-*miR-29b* treatment. We examined serum level of alanine aminotransferase (ALT), aspartate aminotransferase (AST), alkaline phosphatase (ALP), blood urea nitrogen (BUN), creatinine and gamma-glutamyl

transferase (GGT). No significant organ impairment was observed (Figure 2.5B). Moreover, Tf-NP treatment did not result in body weight changes (Figure 2.5C) or significant changes in hemoglobin (Hb) level, white blood count (WBC), or platelet (PLT) count (Figure 2.5D), which indicated that our Tf-NP system would not affect the normal bone marrow function.

2.3.4 Biodistribution of nanoparticles *in Vivo*

To evaluate the biodistribution of Tf-NP *in vivo*, we injected Tf-NP-Cy5-ODN or NP-Cy5-ODN to MV4-11 engrafted NSG mice. Major organs including heart, lung, sternum, spleen, kidney, liver, and bone were harvested 24 hours later. The fluorescence signals of Cy5 were analyzed and compared with PBS treated ones. As shown in Figure 2.6, in general, both Tf-NP and NP did not accumulate in specific organs. However, some signals were observed in kidney and liver inevitably. ,

2.3.5 Transferrin targeted delivery to Acute Myeloid Leukemia stem cells

Subclonal cell populations are found in AML patients. A small population of quiescent stem cells recognized by their surface proteins, CD34 and CD123 lose their stem cell properties and give arise to highly proliferative leukemic cells (*149*). However, some of those cells (leukemic stem cell, LSC) have acquired the abnormal self-renewal ability and act as a reservoir maintaining the great bulk AML population. Though chemotherapy e.g. cytarabine (ara-C) can help patient

achieve remission due to reduction of this bulk population, the high frequency of relapse indicates the requirement of leukemic stem cells compartment management (*3*). *miR-126* was found to be expressed in hematopoietic stem cells (HSCs) and early hematopoietic progenitor cells (HPCs) and to regulate normal hematopoiesis by activating HSC (*150*). de Leeuwet et al. (*151*) recently reported that *miR-126* was expressed in HSCs and increased in LSCs compared to leukemic progenitors (LPs), respectively. Furthermore, Eppert et al. (*75*) reported that high expression of *miR-126* was found in AML cell samples characterized by a LSC-gene expression signature. These data support a role of *miR-126* in myeloid leukemogenesis and suggest this miR as a potentially novel therapeutic target for AML LSCs.

We tested whether our Tf-NP delivery system can be applied to LSCs. Figure 2.6 shows that CD34+ blasts sorted from primary AML patients expressed high level of transferrin receptor on their surface. Then we formulated antigo*miR-126* into Tf-NP (Tf-NP-anti-126) and treated selected CD34+ cells at a concentration of 200 nM. Tf-NP-antagomiR-scramble (Tf-NP-anti-sc) treatment was used as control. 48 hours later, *miR-126* expression was measured by qRT-PCR in treated CD34+ cells. Levels of *miR-126* were approximately 80% decreased in Tf-NP-anti-126 treated CD34+ blasts compared to Tf-NP-anti-sc treated controls ($P<0.01$; Figure 2.7). Tf-NP-anti-126 and Tf-NP-anti-sc treated CD34+ blasts were used in colony-forming cell (CFC) assays to assess the impact of miR-126 downregulation on LP activity. We found no significant differences in the number of CFC in Tf-NP-anti-126 treated cells compared to Tf-NP-anti-sc treated controls

scored after 14 days in culture (Figure 2.8 upper). To determine if *miR-126* knock-down impacted on LSC self-renewal capacity, we then harvested primary CFCs and replated them in methylcellulose for an additional 14-days in culture. We found significant decreases in the number of CFC in the secondary colonies from Tf-NP-anti-126 treated CD34+ blasts compared with Tf-NP-anti-sc treated controls (Figure 2.8 bottom). These results demonstrate a role for *miR-126* in LSC self-renewal while having little effect on the survival/proliferation of the more differentiated LP.

2.3.6 CD45.2 antibody targeted delivery to mouse cells

Since *in vitro* targeting of *miR-126* in LSC resulted in reduced LSC frequency and the number of quiescent CD34+ LSCs, next we sought to determine whether nanoparticle delivering antagomiR-126 could effectively target the LSCs *in vivo*. For these experiments, we used our previously established *Mll*$^{PTD/WT}$ *Flt3*$^{ITD/ITD}$ double knock-in (dKI) mouse model, which develops an aggressive AML that recapitulates important clinical, cytogenetic and molecular features of the human disease (*147*).

We used nanoparticles conjugated to antibody against CD45.2 which is expressed exclusively on the *Mll*$^{PTD/WT}$ *Flt3*$^{ITD/ITD}$ AML mouse cells to deliver antogomiR-126 specifically in those leukemia cells. To optimize the lipid to antibody ratio in nanoparticle formulation, we prepared anti-CD45.2-NP-Cy3-ODN at various molar ratios of lipid to antibody from 200:1 to 2000:1 in the first trial and from 2000:1 to 50000:1 in the second trial to treat CD45.2 leukemic cells

isolated from dKI mice for 24 hours. The percentages of Cy3 positive cells are given in Figure 2.9. We found that when lipid to antibody ratio is 10000:1, the cellular uptake was the highest.

We transplanted bone marrow (BM) cells from primary dKI AML (CD45.2+) mixed with BM from WT-BoyJ (CD45.1+) donors into lethally irradiated WT-BoyJ (CD45.1+) recipients. Five weeks post-BM transplantation (BMT), mice were treated once daily for five consecutive days with anti-CD45.2-NP-anti-126 or anti-CD45.2-NP-anti-sc control (Figure 2.10A). Forty-eight hours after the last dose, BM was harvested from the treated mice. We confirmed successful targeting of *miR-126 in vivo,* by demonstrating ~50% decrease in *miR-126* expression in BM and spleen from mice treated with anti-CD45.2-NP-anti-126 compared with controls treated with anti-CD45.2-NP-anti-sc (Figure 2.10B). Following these mice longitudinally, we showed that mice transplanted with 10^6 and 10^5 cells from CD45.2-NP-anti-126 treated primary recipients had respectively a median survival of 46 and 60 days compared with 31 and 35 days of those transplanted with cells from the anti-CD45.2-NP-anti-sc treated primary recipients (Figure 2.10C, $P<0.01$ for both cell doses). These data demonstrate that *in vivo* knock-down of *miR-126* leads to a decrease in functional LSCs.

2.4 Discussion

Currently, the miR-delivery for potential cancer therapy is based on viral (*105, 152-154*) and non-viral (*155-169*) systems. Among the reported viral-based systems, the adeno-associated virus (AAV)-based approaches appear promising

as supported by significant therapeutic effects in a murine liver cancer models (*105*). Non-viral cationic polymer or cationic lipid carrier systems have also been used to deliver miR-expressing plasmids to solid tumors (*155-167*). However, the miR-expressing vectors and the AAV approach share some drawbacks including limited efficiencies for hematopoietic cells, need for nuclear translocation of large DNA vectors, and limitations in expression of the mature miRs (*170*). With regard to hematopoietic cells, the shortcomings for both viral and non-viral approaches could be bypassed by engineering a targeting delivery system for mature miRs or miR mimic molecules (*93*). Most delivery-systems for solid tumors use cationic or neutral lipid particles to deliver miR molecules due to their tendency of organ accumulation (*160-166, 169*). Thus, we developed a novel anionic lipopolyplex nanocarrier system with desirable features for miR delivery to AML cells, which minimize organ accumulation. And we demonstrated that we were able to attach different targeting molecules for enhanced and specific delivery.

The NP presented here had several remarkable differences from the conventional cationic lipid NP used in solid tumors, which have the tendency to accumulate preferentially in lungs, kidney and liver due to their charge property (*171*). The neutral and anionic lipid formulation of our NP was designed to avoid the non-specific immune response caused by cationic lipids through activation of TLR4 and NF-κB pathways and in turn pro-inflammatory cytokine production (*172, 173*). Moreover, the overall neutral surface charge results in a reduce plasma protein binding and low rate of non-specific cellular uptake (*87*). Low-molecular-weight polyethylenimine was chosen as a core to condense miR

molecules because it is known to be relatively biocompatible and to provide a positive charge, which allows for easy capture of the negatively charged miR molecules, and in turn high entrapment efficiency. The lipid-based carrier was made of DOPE, linoleic acid and DMG-PEG. The low binding affinity between linoleic acid and small RNA may also enhance the dissociation of miRs from the lipopolyplex after endocytosis to facilitate target gene down-regulation (*174*). Furthermore, the NPs are protected from reticuloendothelial system clearance by 2% (molar ratio) of DMG-PEG to achieve long circulation times (*148*) and in turn more efficient delivery in hemtopoietic organs, including bone marrow. To increase the specific effect on tumor cells, NP may be conjugated with molecules that enhance their targeting specificity (*161*).

Tf was conjugated into this delivery system to increase leukemia cell uptake. The methods we used to attach Tf or antibody to nanoparticle was post-insertion. Tf and antibody were first thiolated by Traut's reagent to regenerate the terminal free sulfhydryl group which then couple with Mal-PEG-DSPE to form thioether bonds between proteins and PEG-DSPE. PEG-DSPE served as a spacer arm between liposome and conjugated antibody/protein. During the Incubation of the particles in a micelle solution of PEG lipids, a temperature-induced transfer occurs between phospholipids located in liposomal system and lipid-conjugated polymers (*175*). Post-insertion method is a simple and efficient way to link targeting molecule to nanoparticles. Because synthesis of ligand-PEG-DSPE is independent to nanoparticles, a library of different ligand-PEG-DSPE can be

created and incorporated to nanoparticles to select best targeting ligand or even combining two targeting molecules to further increase specificity and efficiency.

We found that Tf targeting did not only enhance the microRNA delivery to bulk leukemia population, but also be able to target leukemic progenitors and stem cells. Although LSCs only comprise a very small population within AML, they most likely have a profound impact on the clinical presentation and biology of the disease and the current view is that they need to be eradicated in order to achieve cure in AML patients. However, efficient targeting of the small LSC subpopulation in vivo may be challenging. We showed that TfR expressed on CD34+ cells and by using Tf targeting antagomiR-126 were successfully delivered into CD34+ cells and knock down the endogenous *miR-126* resulting in decrease of self-renewal. Further, to determine whether antagomiR-126 could have effect in the LSCs *in vivo,* we used nanoparticles conjugated to antibody against CD45.2 which is expressed exclusively on the $Mll^{PTD/WT}Flt3^{ITD/ITD}$ AML mouse cells to deliver antogomiR-126 specifically in those leukemia cells. We demonstrate the possibility of overcoming the limitation of small LSC subpopulation by using antibody-conjugated nanoparticles. Collectively these data suggests that Tf or antibody conjugated nanoparticle is able to deliver anti-cancer oligonucleotides to both bulk leukemia and small stem cell population which share the same surface marker with bulk population.

2.5 Tables and Figures

Table 2. 1 Viral based RNAi delivery systems. (Modified from (*93*) and (*92*))

	Retrovirus vector	Lentivirus vector	Adenovirus vector	AAV
Packaging capacity	8kb	Up to 13.5kb, ususally ~8kb	Up to ~35kb usually ~7.5kb	~4.5kb
Vector state in cell	Integration into cell genome	Integration into cell genome	Episomal	Episomal
Gene expression	Stable	Stable	Transient	Stable in non-dividing cell
Cell status	Dividing	Dividing and non-dividing	Dividing and non-dividing	Dividing and non-dividing
Immune stimulation	Moderate	Low	High	Very Low
Advantages	Persistent gene transfection in dividing cells	Persistent gene transfection in most tissues	Large packaging capacity; efficient transfection	Non-inflammatory; non-pathogenic;
Side effect	Only transduce dividing cells; may cause mutation when integrating into cell genome	may cause mutation when integrating into cell genome	Cause strong immune and inflammatory responses at high dose	Small packaging capacity; capsid pseudotyping/ engineering facilitates specific cell-targeting

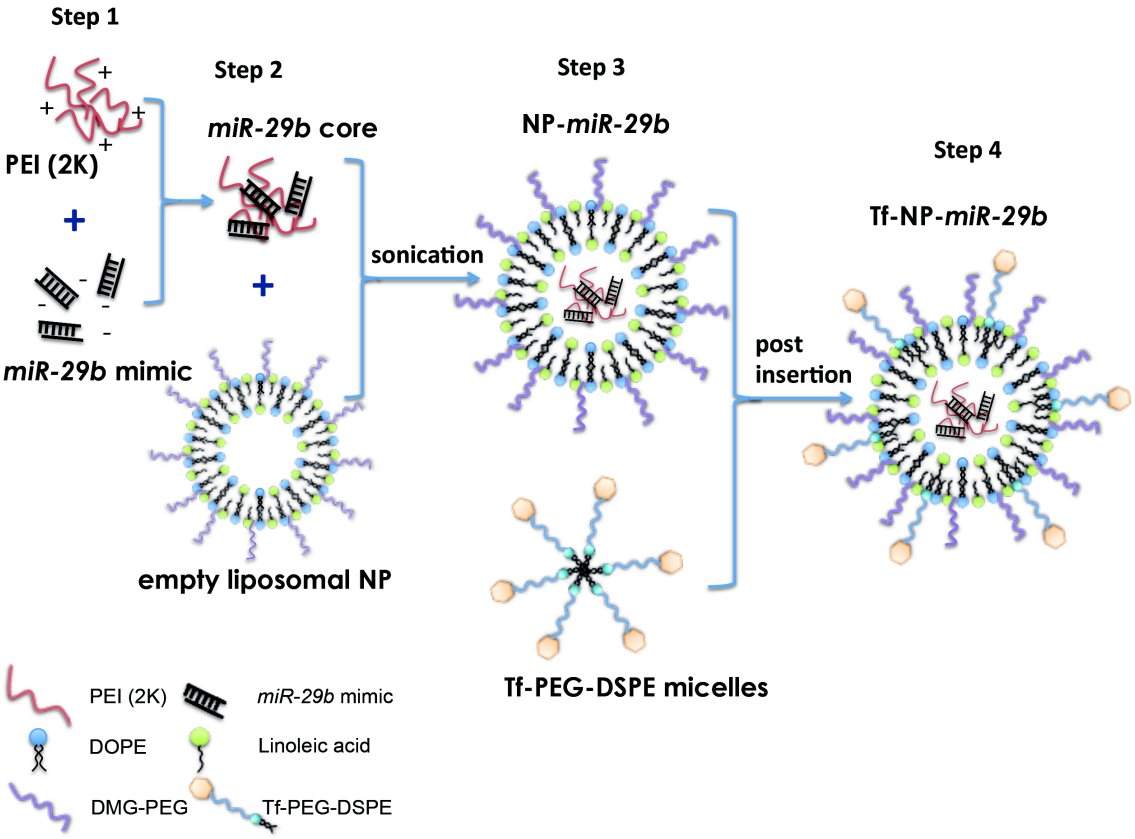

Figure 2. 1 Preparation of miR-loaded transferrin-conjugated-nanoparticles (Tf-NP-miR).

The preparation of Tf-NP-miR is schematically illustrated. Step 1: negatively charged miR molecules were mixed with positively charged polyethylenimine (PEI) to form a miR-PEI core structure. Step 2: empty NP were formed by injection of a lipid ethanol solvent into 20 mM HEPES buffer. Step 3: the miR-PEI were mixed with the empty NP and sonicated to load the miR PEI core into the NP. Step 4: NP-miR were modified to incorporate Tf-PEG-DSPE micelles to form the Tf-NP-miRs.

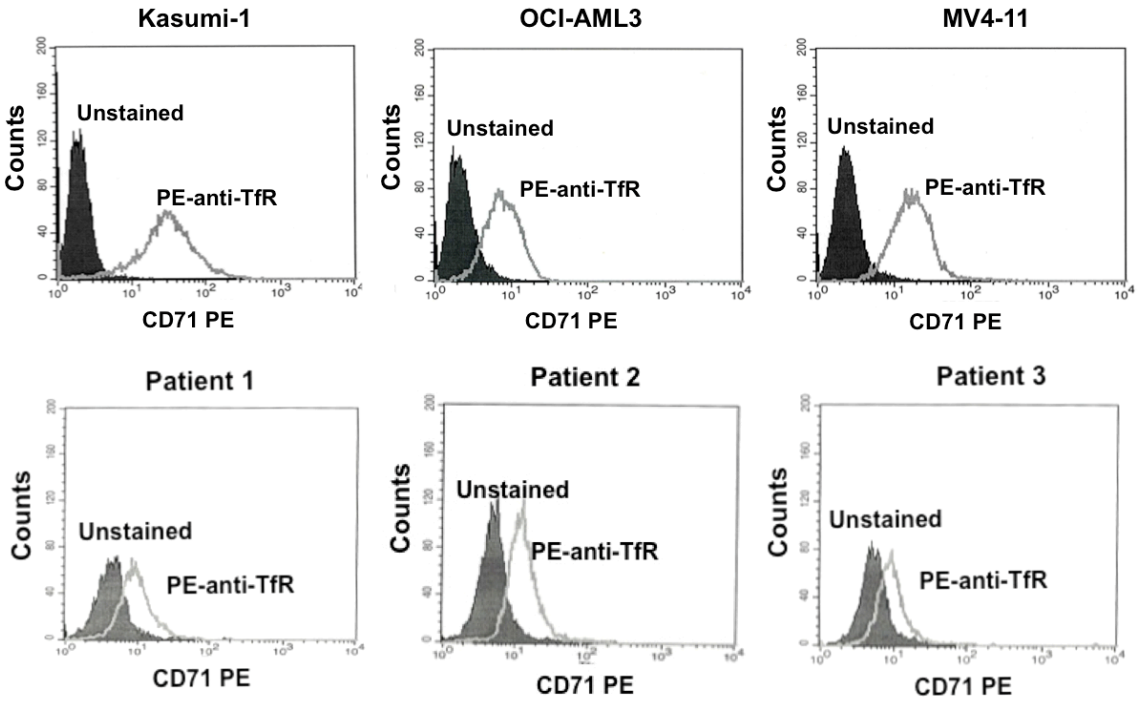

Figure 2. 2 Surface transferrin receptor (CD71) expression on AML cells.

Anti-CD71 antibody conjugated with PE was used to stain Kasumi-1, OCI-AML3 and MV4-11 cells and blasts from three AML patients. Unstained cells are shown as control.

Table 2. 2 Particle size distribution and Zeta potential

	Particle size (nm)	*Zeta potential (mV)*
Empty nanoparticle	129.6 ± 1.02	-9.82 ± 1.53
NP-miR	137.6 ± 0.96	22.48 ± 1.44
Tf-NP-miR	147.3 ± 4.74	5.82 ± 1.87

[a] Data represent the mean ± SD (n=3).

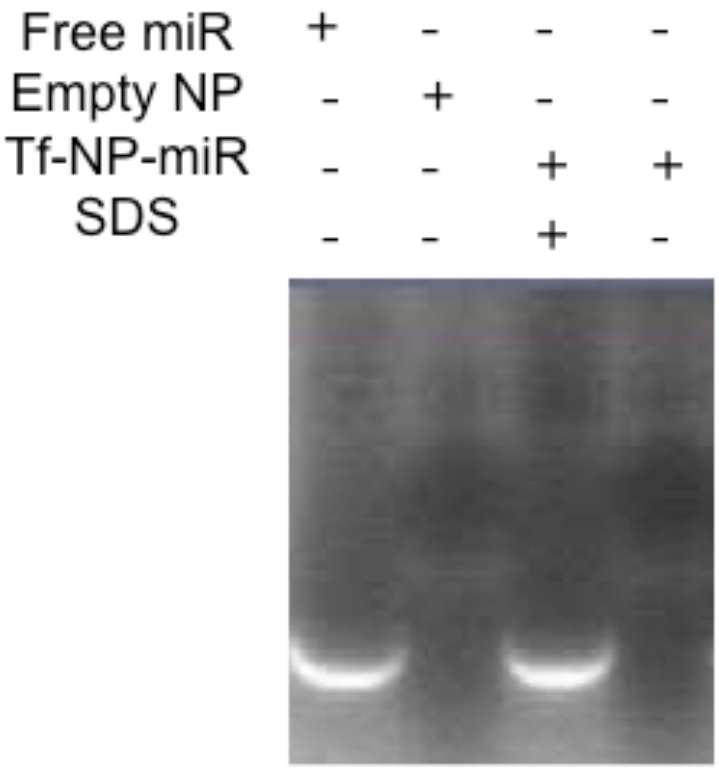

Figure 2. 3 miR entrapment efficiency**.**

0.5% sodium dodecyl sulfate (SDS) was used to dissolve the nanoparticles. The samples were compared before and after dissolution by SDS by agarose gel electrophoresis of RNA. Free miR and SDS treated empty nanoparticles are shown as controls.

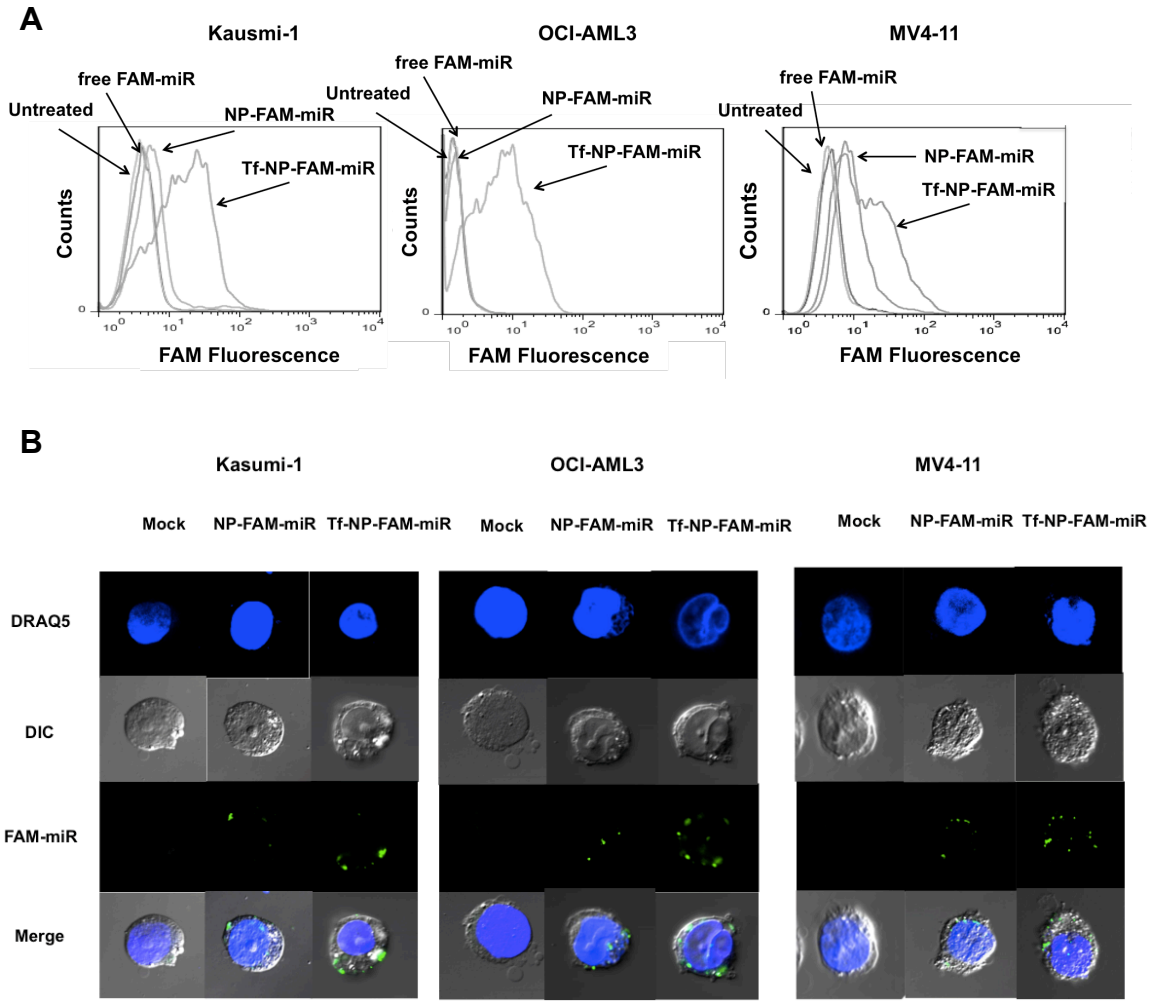

Figure 2. 4 Transferrin targeting enhanced cellular uptake of nanoparticels.

(A) FAM-labeled miR uptake of Kasumi-1, OCI-AML3 and MV4-11 cells. (B) Confocal microscopy study of Kasumi-1, OCI-AML3 and MV4-11 cells treated with Tf-NP-FAM-miR, NP-FAM-miR or mock; FAM-labeled miR: green; nucleus: blue.

Figure 2. 5 Safety profile of Tf-NPs treatment in immune competent mice.

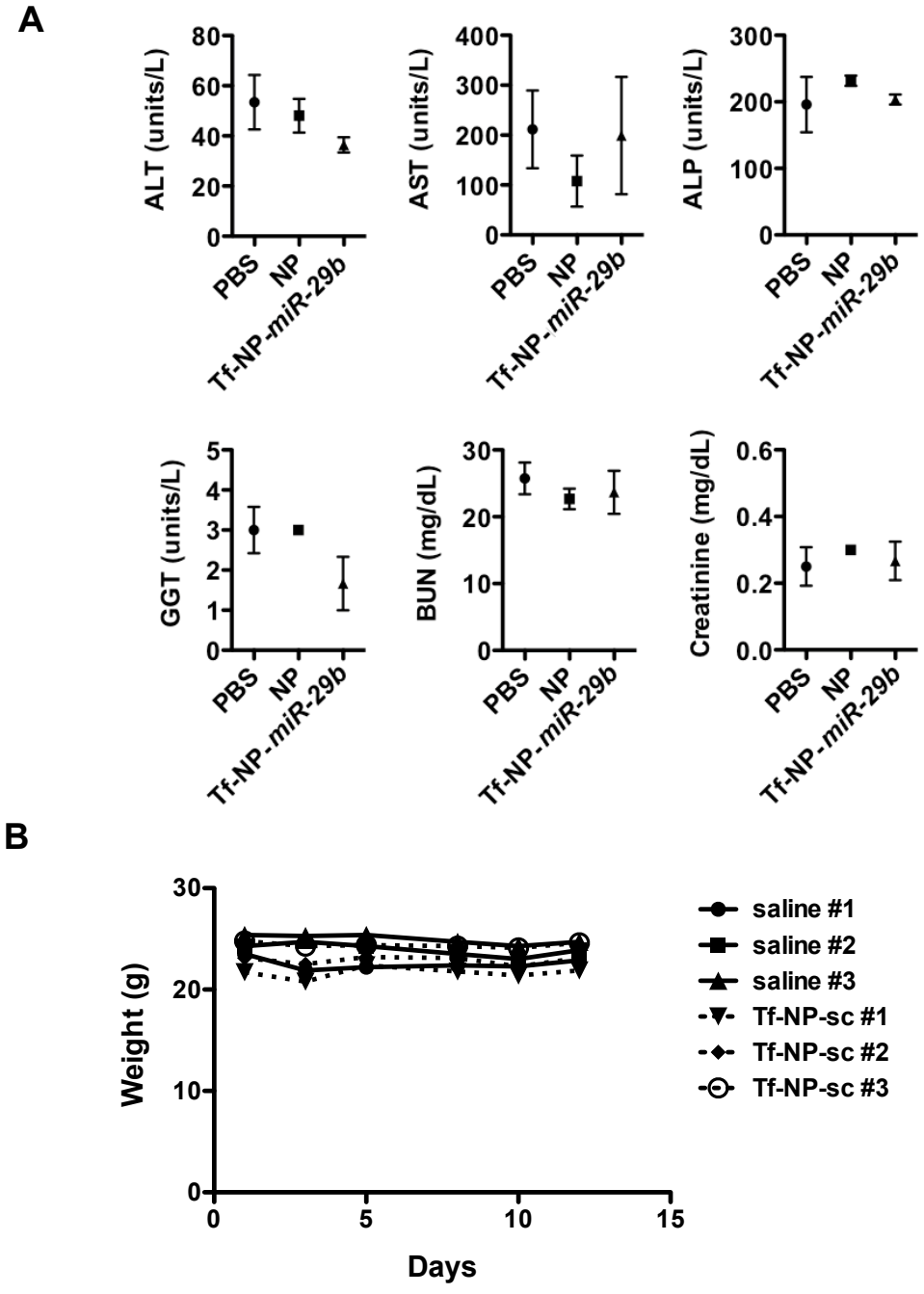

Continued

Figure 2. 5 : Continued

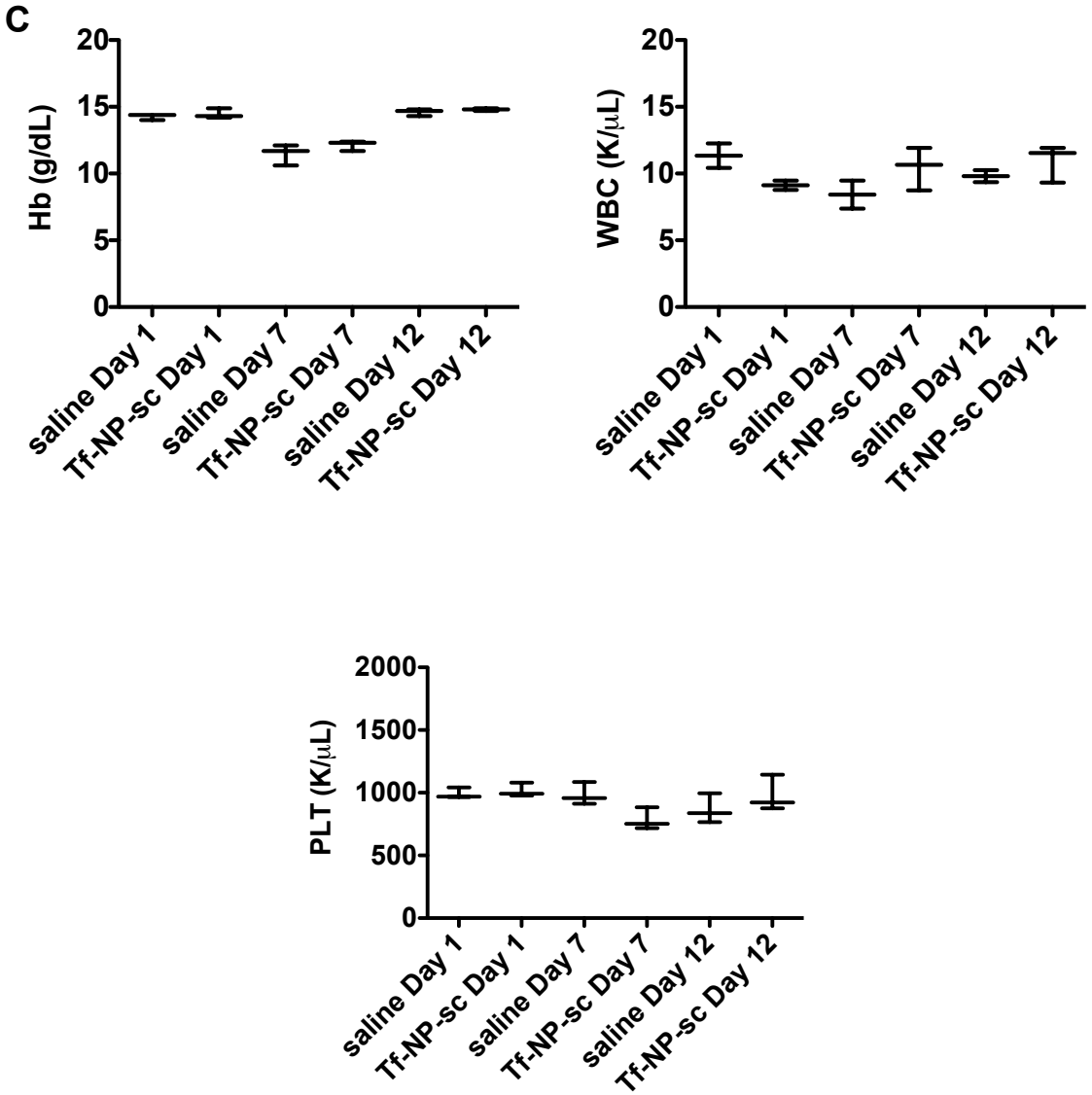

Continued

Figure 2. 5 : Continued

(A) Blood chemistries in response to systemic treatment with empty NP or Tf-NP-miR-29b. Serum levels of alanine aminotransferase (ALT), aspartate aminotransferase (AST), alkaline phosphatase (ALP), gamma-glutamyl transferase (GGT), blood urea nitrogen (BUN) and creatinine of the mice were measured 24 hours after the i.v. injection. Values presented are mean ± SD of at least three mice per group. (B) Body weights were monitored during and after the Tf-NP treatment (3 doses). (C) White blood cell counts (WBC), hemoglobin (Hb) levels and platelet counts(PLT) were also measured before the treatment (Day 1), 2 days after (Day 7) and one week (Day 12) after the last dose of Tf-NP i.v. injection. Bars represent mean and whiskers represent minimum and maximum values.

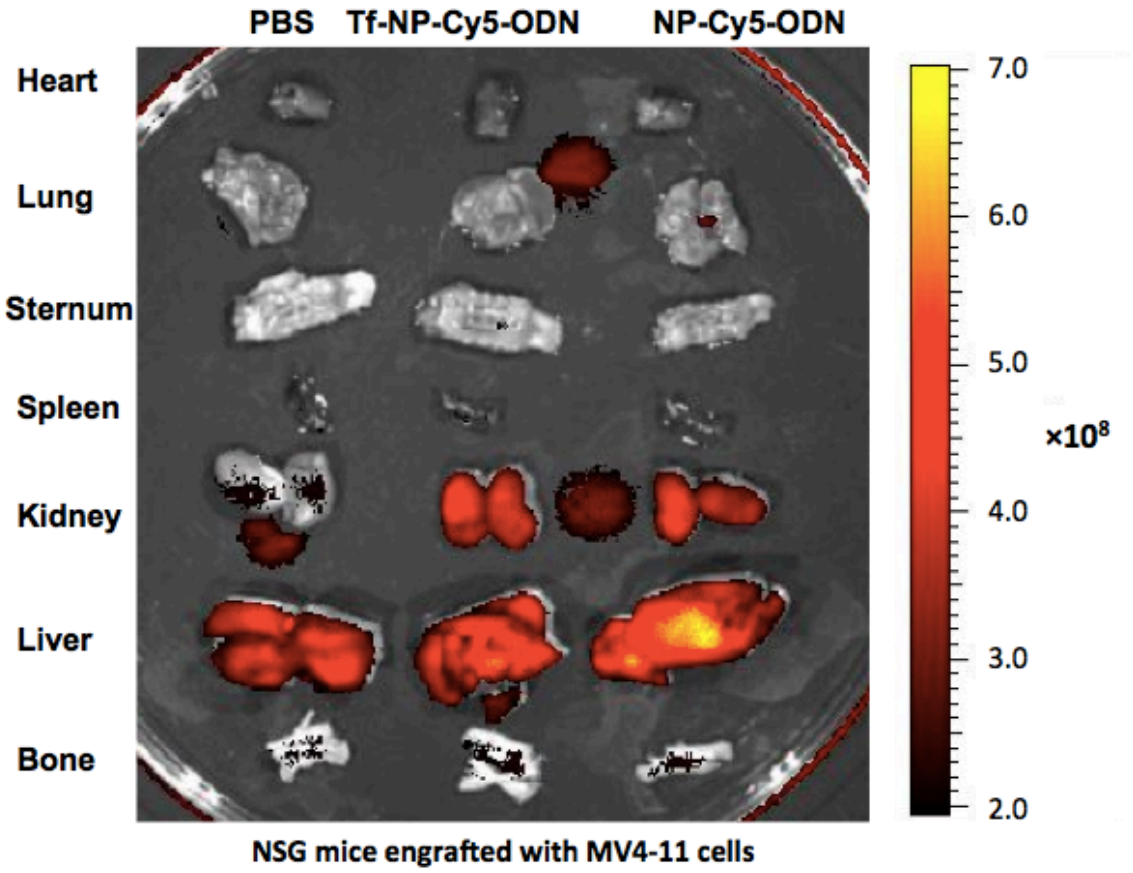

Figure 2. 6 Biodistribution of Tf-NP-Cy5-ODN *in vivo*.

PBS, NP-Cy5.5-ODN and Tf-NP-Cy5.5-ODN were injected by i.v. into NSG mice engrafted with MV4-11 cells respectively. Cy5 signal were measured in major organs 24 hours after the injection.

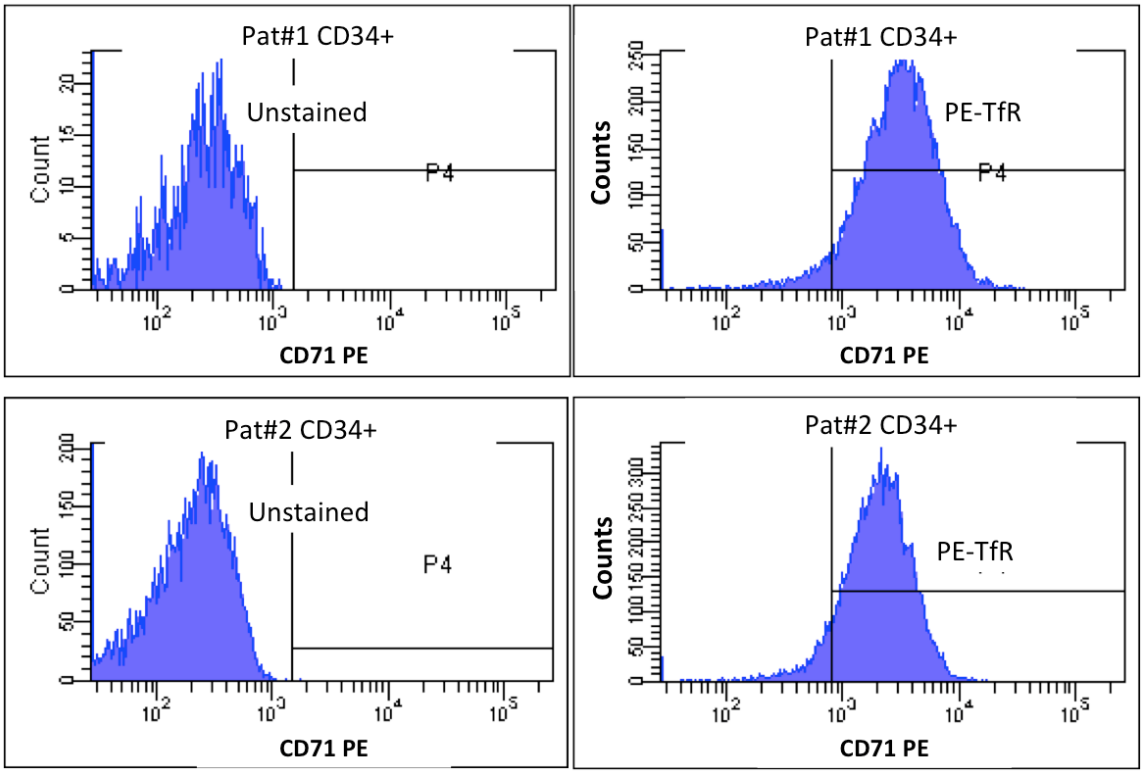

Figure 2. 7 Surface transferrin receptor (CD71) expression on CD34+ patient blasts cells.

Anti-CD71 antibody conjugated with PE was used to stain CD34+ patient blasts cells. Unstained cells are shown as control on the left.

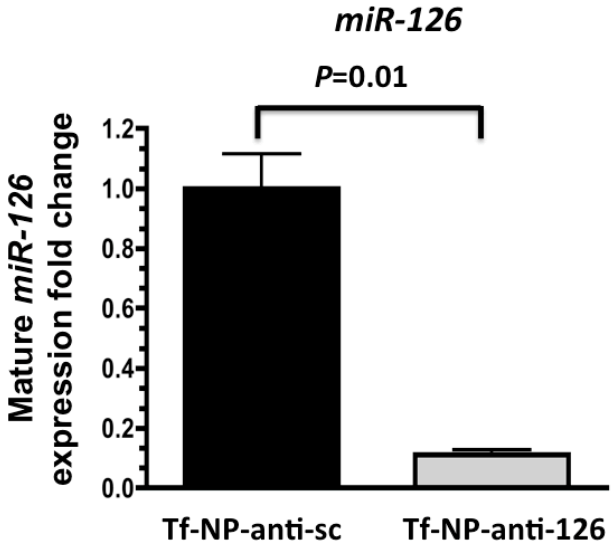

Figure 2. 8 Tf-NP-anti-126 decreased *miR-126* level in CD34+ cells.

miR-126 expression in CD34+ cells from AML patient samples at 48 hours after treatment with Tf-NP-anti-sc or Tf-NP-anti-126.

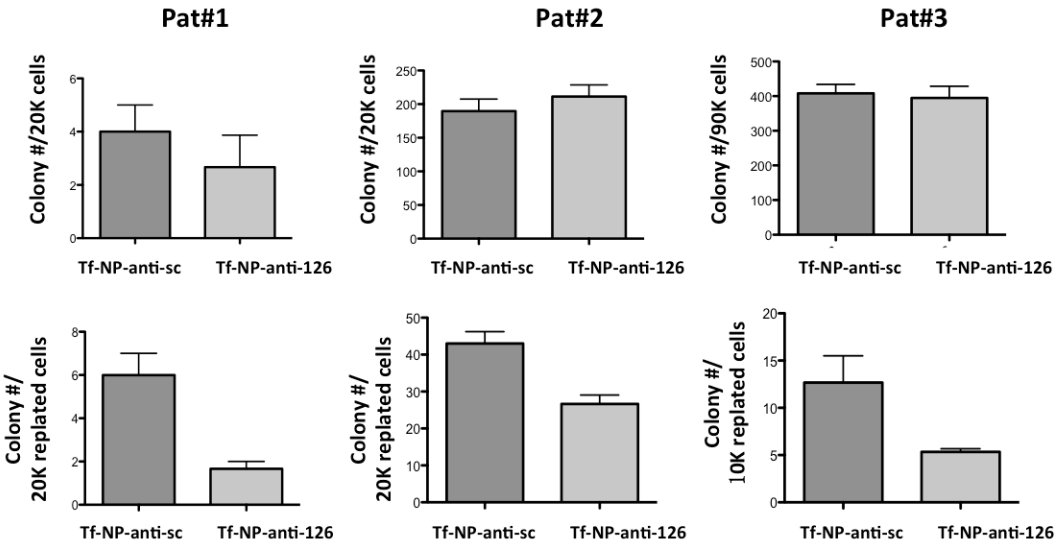

Figure 2. 9 Effect of *miR-126* knock-down by Tf-NP-anti-126 on LSC self-renewal.

Primary colony formation assays of CD34+ cells from AML patient samples (n=3) pre-treated with Tf-NP-anti-sc or Tf-NP-anti-126 for 24 hours (upper). Replating colony assays of cells harvested from the primary colony assays (bottom).

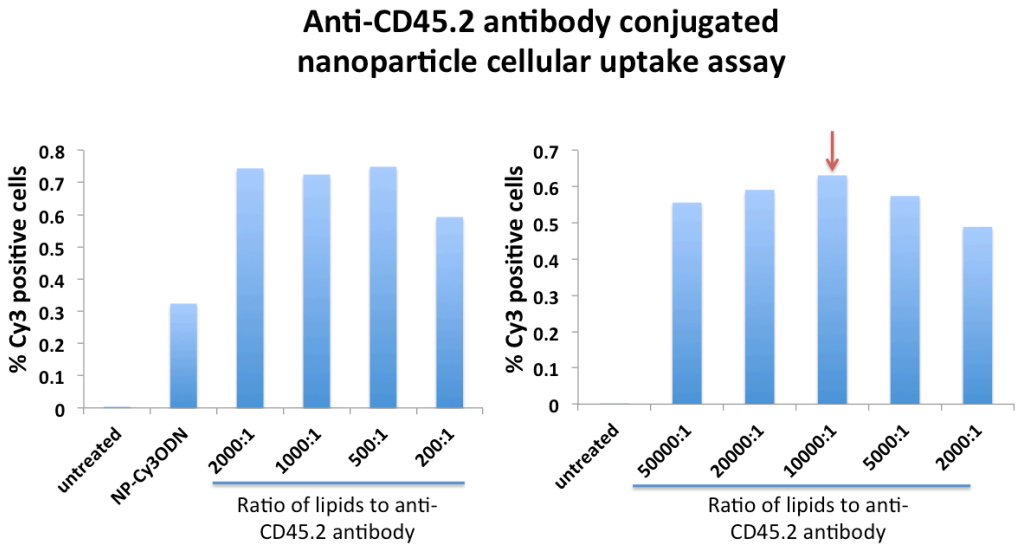

Figure 2. 10 Optimization of lipid to antibody of CD45.2 ratio.

Anti-CD45.2-NP-Cy3-ODN were prepared at various molar ratios of lipid to antibody from 200:1 to 2000:1 in the first trial (A) and from 2000:1 to 50000:1 in the second trial (B) to treat CD45.2 leukemic cells isolated from dKI mice for 24 hours. Then Cy3 positive cells were recognized by flow cytometry.

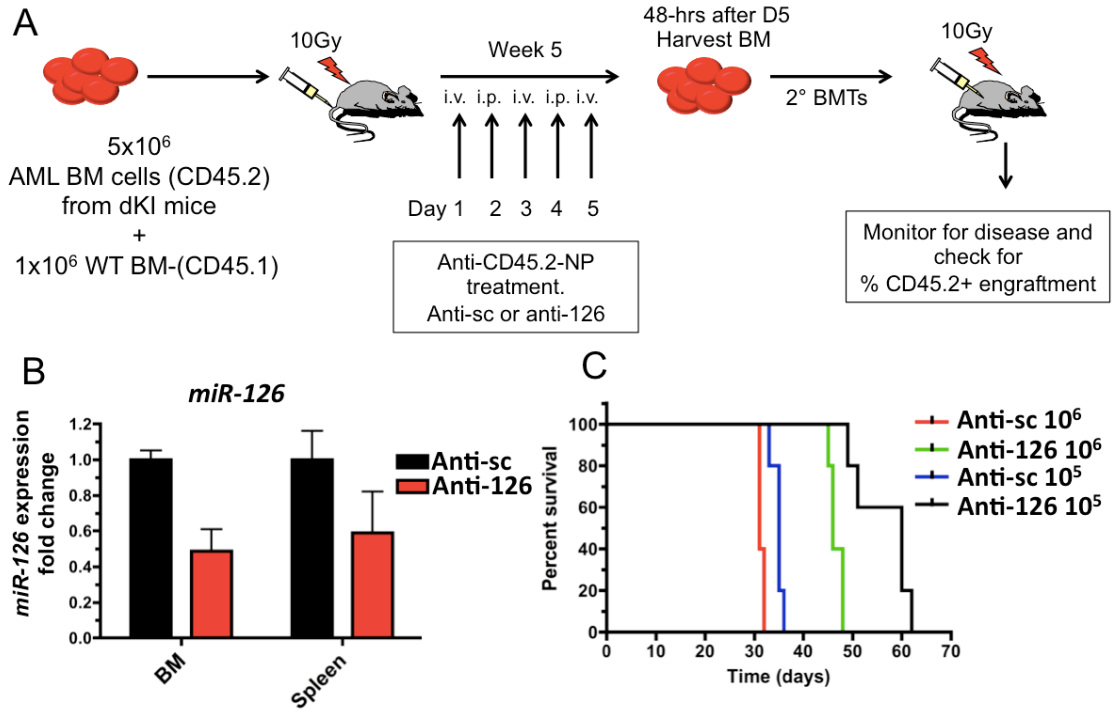

Figure 2. 11 Anti-CD45.2-NP delivery of antigomiR-126 *in vivo*.

(A). Schematic representation of the experimental design. (B). *miR-126* level in sorted CD45.2+ donor leukemia cells 48 hours after final in vivo treatment with anti-CD45.2-NP-anti-sc or anti-CD45.2-NP-anti-126. C. Survival of secondary recipients receiving either 10^5 or 10^6 cells from anti-CD45.2-NP-anti-sc or anti-CD45.2-NP-anti-126 treated primary transplanted mice, co-transplanted with $5x10^5$ (CD45.1) normal BM (n=5 mice per group, $P<0.01$ for both cell doses tested).

Chapter 3. MicroRNA-29b-based Novel Therapeutic Strategy in Acute Myeloid Leukemia

3.1 Introduction

Mature *miR-29* family consists of three members, *miR-29a, miR-29b and miR-29c* which are encoded in two clusters on two chromosomes: *pri-miR-29a/b1* and *pri-miR-29b2/c* from chromosome 7q32.3 and 1q32.2 respectively. The *miR-29* family has been shown involving many functions including modulation of extracellular matrix (*176-179*), regulation of cell proliferation, differentiation and apoptosis, as well as DNA methylation.

miR-29b has been shown to be downregulated in many types of cancer e.g. ovarian cancer (*180, 181*), hepatocellular carcinoma (HCC) (*182*), lung cancer (*183*), mantle cell lymphoma (*184*) and AML (8). And low miR-29b is associated with shorter disease-free survival in ovarian cancer (*180, 181*), HCC (*182*), mantle cell lymphoma (*184*) and AML (*62, 185*). In addition, Amodio et al. reported that miR-29b sensitized multiple myeloma (MM) cells to bortezomib-induced apoptosis (*186*). Our clinical data also showed that higher endogenous *miR-29b* pretreatment levels is associated with improved response to decitabine

(*82*). These data suggests that therapeutic restoration of miR-29b could be beneficial to cancer patient.

Several studies have shown that increasing miR-29b can lead to apoptosis (*181, 186, 187*), inhibition of cancer cell growth (*188*) and metastasis (*189*) as well as block epithelial-mesenchymal transition (EMT) (*190-192*). The anti-tumor activity of miR-29b may be mediated by targeting many oncogenes such as Mcl-1 (*182, 187, 193, 194*) which is an antiapoptotic protein, CDK6 (*184, 194*) which is required for cell cycle to progress into S-phase, and SPARC (*191, 195*) which encodes a matricellular protein that participates in cancer cell invasion and promotes leukemogenesis (*195*). Other mechanisms possibly underlying the tumor-suppressive effect of miR-29b include inducing hypomethylation of DNA by targeting DNA methyltransferases (DNMTs) (*196-199*), promotion of proper myogenic differentiation through NF-kB–YY1–miR-29 circuitry (*200*), and modulation of immunomodulatory glycoprotein B7-H3 to suppress the immune escape by solid tumors (*201*). Furthermore, we recently demonstrated that increasing *miR-29b* levels resulted in decreased expression of the receptor tyrosine kinases (RTKs) FLT3 and KIT, which are frequently mutated and aberrantly activated in AML, via disruption of a NF-κB/SP1 transactivating complex, by targeting the transcription factor SP1 (*10, 202-205*). Thus increasing *miR-29b* levels in AML blasts may represent a promising novel treatment strategy for AML patients with otherwise aberrantly low expression of this miR.

However, synthetic miRs are easily degraded in bio-fluids and have limited cellular uptake, rendering the clinical development of miR-based therapies

relatively difficult. To overcome these limitations, we encapsulated synthetic miR-29b mimic molecules into previous mentioned transferrin-conjugated anionic lipopolyplex nanoparticles and tested them *in vitro* and *in vivo*.

3.2 Materials and Methods

3.2.1 Cell lines, AML patient samples and cell culture

Kasumi-1 and MV4-11 cells were purchased from ATCC and NB4 and OCI-AML3 cells were purchased DSMZ. AML patient blasts were obtained from the OSU Leukemia Tissue Bank. All patients provided written informed consent in accordance with the Declaration of Helsinki under an Institutional Review Board approved protocol for discovery studies according to OSU institutional guidelines for tissue collection and the use of the tissue in research.

3.2.2 RNA extraction and quantitative RT-PCR (qRT-PCR)

Total RNA extraction was performed as previously described by using Trizol (Invitrogen, Carlsbad, CA) (*202*). Total RNA from leukemic mice was isolated using the MirVana^{TM} miRNA Isolation kit (Ambion) according to the Instruction Manual. Then cDNA was synthesized utilizing Superscript III (Invitrogen) or the Taqman miR Reverse Transcription kit (Applied Biosystems, Foster City, CA) for *miR-29b, miR-140* and *U44.* And qRT-PCR was performed with Taqman gene expression assays (Applied Biosystems) following the manufacturer's protocols. Expression of *pri-miR-29b-1*, *pri-miR-29b-2, DNMT1, DNMT3A, DNMT3B, SP1, CDK6, FLT3* and *KIT* was normalized to *18S*. *miR-29b* and *miR-140* expression

was normalized to *U44*. The comparative cycle threshold (C_T) method was used for relative quantification of gene expression as previously described (8).

3.2.3 Western blot analysis

Western blot was performed as previously described (*202, 206*). Anti-DNMT1 (ab87656), and -DNMT3B (52A1018) antibodies were from Abcam (Cambridge, MA). Anti-KIT (SC-17806) and -DNMT3A (SC-20703) antibodies were from Santa Cruz Biotechnology (Santa Cruz, CA). Anti-SP1 (CS200631) antibodies were from Millipore (Billerica, MA). Anti-CDK6 (DCS83) and -FLT3 (8F2) antibodies were from Cell Signaling Technology (Danvers, MA). Anti-Acetylated histone H3 (06-599) and anti-Acetylated histone H4 (06-866) were purchased from Upstate. Equivalent loading was confirmed by Actin (SC-1616; Santa Cruz). The intensity of the resulting bands was measured by ImageJ 1.45s (http://imagej.nih.gov/ij). The intensity ratio of each band respective to the corresponding actin intensity was used for relative quantification and is displayed in the figures.

3.2.4 Growth Analysis

OCI-AML3, Kasumi-1 and MV4-11 cells (3×10^5/mL) and AML patient blasts were treated as described above. For cell lines, cells were counted at 24-hour intervals using a ViCell counter (Beckman Coulter, Miami, FL). Growth curves were generated by MATLAB 7.9.0.529 (R2009b; The Mathworks, Inc., MA). For patient blasts, after 96 hours incubation, cell viability was measured by MTS assay.

CellTiter 96® AQueous One Solution Reagent (Promega, Madison, WI) was used according to the manufacturer's recommendations. Absorbance was read in a microplate reader Germini XS (Molecular devices, Sunnyvale, CA). Each sample was run in triplicates.

3.2.5 Decitabine and AR42 treatment and cytotoxicity studies by MTS assay

In Tf-NP-*miR-29b* and decitabine combination treatment study, Kasumi-1, MV4-11 and OCI-AML3 cells were pretreated with Tf-NP-*miR-29b,* Tf-NP-scramble or mock (buffer only) 48 hours before decitabine exposure. The decitabine doses were based on our previous studies (*207*). After 48 hours incubation, cell viability was measured by MTS assay.

In AR42 and decitabine combination treatment study, Kasumi-1 and NB4 cells were seeded in 96-well plates and were treated for 72 hours with vehicle, AR-42 (0.3 μM) alone, AR-42 (0.3 μM) followed by decitabine (0.5 μM) after 24 hours [AR-42→decitabine], decitabine (0.5 μM) followed by AR-42 (0.3 μM) after 24 hours [decitabine→AR-42] or decitabine (0.5 μM) alone. After 72 hours, cell viability was measured by MTS assay.

In AR42 and VPA cytotoxicity study, Kasumi-1, NB4 and patient primary blasts were seeded in 96-well plates and were treated for 48 hours with vehicle, AR-42 (3 nM, 10 nM, 30 nM, 100 nM, 300 nM or 1 μM) or valproic acid (VPA); 600 μM or 2400 μM). After 48 hours, MTS reagent was added to each well.

Briefly, 20 µl MTS reagent [3-(4,5-dimethylthiazol-2-yl)-5-(3-carboxymethoxyphenyl)-2(4-sulfophenyl)-2H-tetrazolium, inner salt; Promega] was added to each well. Plates were incubated according to the manufacturer's protocol. The absorbance at 495 nM was measured in a Multiskan Spectrum plate reader (Thermo Electron Corporation, Vantaa, Finland). After adjustment for background interference by accounting for wavelength variation secondary to media, data in triplicate from three independent experiments were normalized to the readings from untreated cells.

3.2.6 Colony Formation Assays

Methylcellulose colony formation assays were carried out as previously described (*208*) and counted after 14 days.

3.2.7 *In vivo* studies

To test the anti-leukemic activity of Tf-NP-*miR-29b* or Tf-NP-2'MeOPSmiR-29b we utilized a leukemic NOD/SCID gamma (NSG) mouse model. Six-week-old male NSG mice (The Jackson Laboratory) were intravenously injected through a tail vein with MV4-11 cells ($0.3x10^6$) as described previously (*209*). The treatment started ten days after the engraftment. In the first trial, mice were treated with *miR-29b* mimic (n=3), Tf-NP-scramble (n=6) and Tf-NP-*miR-29b* (n=6, 1 mg/kg/d of miR molecule intravenously on Monday, Wednesday and Friday for two weeks). Mice survival was monitored and recorded. Spleens from the same mice were weighed. In the second trial, mice were treated with saline (n=5), Tf-NP-

scramble alone (n=7; 1.5 mg/kg/d miR intravenously), Tf-NP-*miR-29b* alone (n=7), decitabine alone (n=7; 0.4 mg/kg/d, intraperitoneally), Tf-NP-scramble followed by (→) decitabine and Tf-NP-*miR-29b*→decitabine as depicted in Figure 6B. At day 24, blood was collected for gene expression analysis. In the third trial, mice were treated with saline (n=7), empty NP (n=12), free 2′-MeOPSmiR-29b (2.4 mg/kg; n=4), free 2′-MeOPSsc (24 mg/kg; n=6), free 2′-MeOPSmiR-29b (24 mg/kg; n=6), Tf-NP-2′-MeOPSsc (2.4 mg/kg; n=8) or Tf-NP-2′-MeOPSmiR-29b (2.4 mg/kg; n=8). These studies were performed in accordance with OSU institutional guidelines for animal care and under protocols approved by the OSU Institutional Animal Care and Use Committee.

3.2.8 Statistical analysis

Data were represented as mean ± standard deviation (SD) of at least three independent experiments and analyzed by the 2-tailed Student's t-test. The mean and SD were calculated and displayed in bar graphs as the height and the corresponding error bar, respectively. Mouse survival was calculated using the Kaplan-Meier method, and survival curves were compared by log-rank test. A $P<0.05$ was considered statistically significant.

3.3 Results

3.3.1 Intracellular increase of mature *miR-29b* after synthetic *miR-29b* mimic delivery

The *miR-29b* level was relatively lower in AML cell lines and patient blasts compared with normal bone marrow samples (Figure 3.1). Thus, we hypothesized that increasing *miR-29b* level would have anti-leukemic activity. In this study, we delivered *miR-29b* mimic by Tf-NP to three AML cell lines. The delivery efficiency of the Tf-NP was tested by measuring intracellular levels of mature *miR-29b* (Figure 3.2A). Treatment with NP-*miR-29b* and Tf-NP-*miR-29b*, , increased levels of mature *miR-29b* approximately 240- versus 420-fold (P = 0.009) in Kasumi-1, 130- versus 240-fold (*P* = 0.008) in OCI-AML3, and 150- versus 220-fold (*P* = 0.01) in MV4-11 respectively compared with mock treatment. Thus, Tf-NP was approximately 2 times more efficient than unconjugated nanoparticles in increasing the *miR-29b* levels. These results also indicated an efficient processing of the delivered *miR-29b* mimic molecules into mature *miR-29b*. No significant change of the expression of an unrelated miR, that is, *miR-140*, was observed (Fig. 3.2B), thereby supporting the specificity of our delivery system and the lack of interference with the expression of other endogenous miRs in the targeted cells.

3.3.2 Downregulation of miR-29b target genes by Tf-NP-miR-29b in AML cell

Next, we tested the *miR-29b* targeting activity. We previously reported that *miR-29b* directly downregulates the DNA methyltransferases DNMT3A and DNMT3B and indirectly downregulates DNMT1 by targeting the transcription factor *SP1* that drives *DNMT1* expression (*198*). Furthermore, *miR-29b* has been shown to target the cell cycle regulator *CDK6* (*194*). Indeed, we observed a marked downregulation of DNMT1 by 18.5-, 2.5- and 5.1-fold, DNMT3A by 4.8-, 15.7- and 3.4-fold, DNMT3B by 3.6-, 3.5- and 3.4-fold, SP1 by 4.5-, 3.9- and 3.3-fold and CDK6 by 3.9-, 3.5- and 9.6-fold respectively in Kasumi-1, OCI-AML3 and MV4-11 cells following the treatment with our *miR-29b*-loaded Tf-NP compared to scramble-loaded Tf-NP (Figure 3.2A). Thus the delivered *miR-29b* fulfilled the expected function of the endogenous miR in AML cells.

We recently demonstrated that *miR-29b* also indirectly targets the expression of RTKs FLT3 and KIT in AML (*202, 203*). Aberrant activation - by activating mutations and/or overexpression - of these two RTKs is frequently found in AML (*10, 204, 205*). The downregulation of these RTKs following *miR-29b* increase is likely mediated by the disruption of a transactivation complex comprised of SP1 and NF-κB, by targeting *SP1* (*202, 203*). Since we observed a significant downregulation of SP1 upon Tf-NP-*miR-29b* treatment (Figure 3.3A), we analyzed the FLT3 and KIT expression in Tf-NP-*miR-29b* treated cells. We observed a downregulation of FLT3 by 3.3-, 2.8- and 1.9-fold respectively, as

well as a downregulation of KIT by 7.8- 2.5- and 1.4-fold respectively in Kasumi-1, OCI-AML3 and MV4-11 cells (Figure 3.3B).

3.3.3 Intracellular increase of the endogenous *miR-29b* primary transcripts following Tf-NP-*miR-29b* treatment

The endogenous mature *miR-29b* stems from two precursors (*pri-miR-29b-1* and *pri-miR-29b-2*) encoded by two genes located on human chromosomes 7q32 and 1q23, respectively. We previously reported that an SP1 containing transcription repressor complex downregulated *miR-29b* in AML cells (*202*). Here we show that Tf-NP-*miR-29b* reduced SP1 expression, therefore we hypothesized that Tf-NP-*miR-29b* may increase the endogenous *miR-29b* expression. We found 1.7-, 2.0- and 2.3-fold increase in endogenous *pri-miR-29b-1* and of 2.1-, 1.8- and 2.5-fold increase of *pri-miR-29b-2* levels in Kasumi-1, OCI-AML3 and MV4-11 cells respectively following treatment with the *miR-29b*-loaded Tf-NP (Figure 3.4).

3.3.4 Tf-NP-miR-29b inhibits cell proliferation and colony formation in AML cells

We evaluated the anti-leukemic effects of Tf-NP-*miR-29b* treatment by performing growth curves and analyzing the colony forming ability. The Tf-NP-*miR-29b* treatment reduced the growth rate from 32.2% (Tf-NP-scramble) to 25.3% (Tf-NP-*miR-29b*) in Kasumi-1 cells, from 70.9% (Tf-NP-scramble) to 57.3% (Tf-NP-*miR-29b*) in OCI-AML3 and from 53.0% (Tf-NP-scramble) to 43.9% (Tf-NP-*miR-29b*) in MV4-11 cells (Figure 3.5) compared to the Tf-NP-

scramble treatment. At the last day, the Tf-NP-*miR-29b* treatment was associated with a significantly lower cell counts than in the Tf-NP-scramble or mock (buffer only) treatment for Kasumi-1 (P=0.01 and P=0.01, respectively), OCI-AML3 (P=0.026 and P=0.01, respectively) and MV4-11 (P=0.007 and P=0.002, respectively; Figure 3E) cells. We also observed an approximately 50% reduction in colonies following the Tf-NP-*miR-29b* treatment (Figure 3.6). The average number of colonies (±SD) formed by mock (buffer only), Tf-NP-scramble and Tf-NP-*miR-29b* treated cells were respectively 161±9, 143±9 and 65±6 (P<0.001 for each comparison) for Kasumi-1 cells, 289±11, 269±13 and 156±10 (P<0.001 for each comparison) for OCI-AML3 cells and 234±11, 213±7 and 80±5 (P<0.001 for each comparison) for MV4-11 cells, respectively.

3.3.5 Validation in AML patient blasts

The anti-leukemic activity of Tf-NP-*miR-29b* was further validated in primary blasts from three newly diagnosed AML patients. Patient 1 had a secondary AML with unknown karyotype (standard cytogenetic analysis failed in this patient). Patients 2 and 3 had a *de novo* cytogenetically normal AML. After Tf-NP-*miR-29b* treatment, we observed an approximate 860-, 400- and 750-fold increase in *miR-29b* levels, compared to Tf-NP-scramble after 24 hours in all three patients' blasts samples (Figure 3.7A). No significant change of the expression of an unrelated miR (i.e. *miR-140*) was observed (Figure 3.7B). We also observed 2.2-, 2.1- and 1.9-fold increase in endogenous *pri-miR-29b-1* and 1.6-, 1.4- and 2-fold increase in endogenous *pri-miR-29b-2* compared to controls

following Tf-NP-*miR-29b* treatment in the blasts from all three patients (Figure 3.8).

After 48 hours Tf-NP-*miR-29b* treatment, 1.3-, 2.9- and 6.6-fold DNMT1 downregulation was observed in all three patients' blast samples, as well as 3.5-, 4.4- and 6.4-fold DNMT3A, 6.9-, 9.7- and 6.7-fold DNMT3B, 7.6-, 5.3- and 6-fold SP1, and 8.1-, 4.9- and 2.8-fold CDK6 downregulation, compared to Tf-NP-scramble treatment (Figure 3.9 A). In addition, 1.9- and 2.1-fold FLT3 decrease in patient 1 and patient 2 and 1.9- and 3.3-fold decrease KIT in patient 1 and patient 3 was observed (Figure 3.9B). Tf-NP-*miR-29b* decreased cell viability respectively by approximately 19% (P=0.03), 15% (P=0.017) and 21% (P=0.001) respectively, compared to Tf-NP-scramble in all three AML patients' blasts (Figure 3.10).

3.3.6 *In vivo* evaluation of Tf-NP-*miR-29b* in preclinical models

Next we evaluated the *in vivo* therapeutic efficacy of Tf-NP-*miR-29b*. In a first trial the MV4-11 engrafted mice were treated with free *miR-29b* (n=3; 1 mg/kg/d miR intravenously), Tf-NP-scramble (n=6) or Tf-NP-*miR-29b* (n=6) starting at day 10 after cell injection. The median survival time was 27, 28 and 32.5 days for free *miR-29b,* Tf-NP-scramble and Tf-NP-*miR-29b* treated mice, respectively. The survival in the Tf-NP-*miR-29b* treated group was significantly longer compared to free *miR-29b* treated group (P=0.003, log-rank test), as well as compared to the Tf-NP-scramble treated group (P=0.015, Figure 3.11A). Consistent with the

longer survival the spleen sizes in the Tf-NP-*miR-29b* treated group were significantly smaller than in the free *miR-29b* treated mice (*P*=0.033) or in the Tf-NP-scramble treated group (*P*=0.049). The mean spleen weight was 29.3±4.1 mg, 26.6±1.6 mg and 19.3±3.4 mg for the free *miR-29b*, Tf-NP-scramble and Tf-NP-*miR-29b* treated mice, respectively (Figure 3.11B). To validate these results we conducted a second independent trial, testing a slightly different schedule and dosing (see methods). The engrafted mice were treated with saline (n=5), Tf-NP-scramble (n=7; 1.5 mg miR/kg/d intravenously) or Tf-NP-*miR-29b* (n=7) starting at day 10 after cell injection. The median survival time in this trial was 26, 27 and 34 days for saline, Tf-NP-scramble and Tf-NP-*miR-29b* treated mice, respectively. Similar to the first trial, the Tf-NP-*miR-29b* treatment prolonged the survival of the leukemic mice compared to the Tf-NP-scramble treated group (*P*=0.01, Figure 3.12A).

Blood samples at day 24 (after 6 doses) (second trial) demonstrated a 20-fold increase in intracellular *miR-29b* levels in the Tf-NP-*miR-29b* treated mice compared to the Tf-NP-scramble treated group (*P*=0.003, Figure 3.12B). Furthermore, we observed a decreased expression of the *miR-29b* targets, *DNMT1* by 1.9-fold (*P*=0.028)*, DNMT3A* by 2.9-fold (*P*=0.02)*, DNMT3B* by 4-fold (*P*=0.002), *SP1* by 2.9-fold (*P*=0.039), *CDK6* by 1.6-fold (*P*=0.015), *KIT* by 3.6-fold (*P*=0.018) and *FLT3* by 1.5-fold (*P*=0.029) compared to the Tf-NP-scramble treated group *in vivo* (Figure 3.12B). These findings indicate that the *miR-29b* mimic molecules were successfully delivered to the leukemic cells and decreased *miR-29b* targets *in vivo*.

3.3.7 Antileukemic activity of Tf-NP-*miR-29b* priming followed by decitabine

Since we demonstrated that higher pretreatment *miR-29b* levels associated with improved clinical response to decitabine (*82*), we tested here whether Tf-NP-*miR-29b* treatment would improve the anti-leukemic activity of decitabine in AML cells. Since we observed a *miR-29b* target downregulation at 48 hours, we pretreated AML cell lines and primary blasts with Tf-NP-scramble or Tf-NP-*miR-29b* for 48 hours before exposing them to decitabine.

Pretreatment with Tf-NP-*miR-29b* decreased the cell viability by approximately 40% (P=0.001) compared to Tf-NP-scramble pretreatment after treatment with 0.5 μM decitabine in Kasumi-1, approximately 20% (P<0.001) after treatment with 2.5 μM decitabine in OCI-AML3 cells and approximately 18% (P<0.001) after treatment with 2.5 μM decitabine in MV4-11 cells (Figure 3.13A).

Next we evaluated the *in vivo* Tf-NP-*miR-29b* priming activity. We engrafted NGS mice with MV4-11 cells and treated them with decitabine alone (n=7; 0.4 mg/kg/d intraperitoneally), or Tf-NP-scramble (n=9) or Tf-NP-*miR-29b*→decitabine (n=9). The median survival time was 27, 28 and 37 days for the decitabine alone, Tf-NP-scramble→decitabine and Tf-NP-*miR-29b*→decitabine, respectively (Figure 3.13B). The combination treatment of Tf-NP-*miR-29*→decitabine significantly prolonged the survival of the leukemic mice compared to decitabine alone (P=0.001) and compared to the combination treatment of Tf-NP-

scramble→decitabine (*P*=0.001) and by trend also compared to Tf-NP-*miR-29b* alone (*P*=0.06).

3.3.8 Improvement of the potency of synthetic single-stranded 2′-O-Methylphophorothioate *miR-29b* (2′-MeOPSmiR-29b) by transferrin conjugated nanoparticle

In the above proof-of-concept study, we showed that delivered *miR-29b* duplex mimic by Tf-NP in AML cells could effectively donwregulate its targets and had anti-leukemic activity. However, these oligos are too costly to apply in clinic. A more affordable material, 2′-O-Methylphophorothioate miR which meets current Good Manufacturing Practice (cGMP) standards could be produced in a large scale. Though the naked 2′-MeOPSmiR-29b showed some level of anti-leukemic activity, to further minimize the potential toxicity, increase selectivity and reduce the cost, we formulated 2′-MeOPSmiR-29b into our Tf-NP delivery system. Daily administration of 2.4 mg/kg Tf-NP-2'MeOPSmiR-29b by i.p. for four consecutive days per week for 8 weeks (Figure 3.14 upper) significantly prolonged the survival of the MV4-11 engrafted leukemic mice (median survival=43 days) compared with Tf-NP-2′-MeOPSmiR-sc-treated mice (median survival = 30 days, P<0.001) or the naked 2′-MeOPSmiR-29b at the same dose (median survival = 31 days, P<0.001). The therapeutic efficacy of the 2.4 mg/kg Tf-NP-2′-MeOPSmiR-29b was similar to that of naked 2′-MeOPSmiR-29b given at a 10-fold higher dose (i.e. 24 mg/kg), indicating the formulation significantly improved the 2′-MeOPSmiR-29b potency (Figure 3.14 lower).

3.3.9 Increased leukemic activity of decitabine via AR-42-induced upregulation of *miR-29b*

Previously our group showed that the expression of *miR-29b* is repressed by an SP1/NFκB/HDAC complex, which binds to a *miR-29b* enhancer region. Here we hypothesize that a new HDAC inhibitor, AR-42, could increase *miR-29b* level by disrupt this binding complex and sensitize AML cells to decitabine. Figure 3.15 shows that concentrations of AR-42 as low as 30 nM induced acytylation of histone 3 and 4 (H3 and H4) in Kasumi-1 and NB4 cells at 48 hours. In primary patient samples (n=4, Figure 3.16), we observed acetylation of H3 and H4 histone increased in a similar dose dependent fashion. We used a known HDACI, VPA (*210*) at 600 μM and 2400 μM as a positive control in AML cell lines and patient blasts (Figure 3.15 and 3.16). Interestingly, similar to Stapnes et al (*210*) we observed an anti-proliferative effect of the HDACIs at higher concentrations (i.e., >100 nM AR-42 and 2400 μM VPA), and a more heterogenous response at lower concentrations (i.e., <100 nM AR-42 and 600 μM VPA; Figure 3.17).

We next treated Kasumi-1, NB4 and primary patient blasts (n=4). Compared with vehicle-treated control cells, *miR-29b* expression was found to be upregulated 4±0.93-fold ($P<0.01$) in Kasumi-1 cells, 5±1.18-fold ($P<0.05$) in NB4 cells (Figure 3.18), 1.8±0.18-fold in Pat#4, 3.6±0.4-fold in Pat#5, 2.4±0.16-fold in Pat#6 and 3±0.4-fold in Pat#7 (Figure 3.19). *miR-29b* upregulation was also observed with 2400 μM VPA both in Kasumi-1 and NB4 cell lines as well as in primary patient

blasts (Figure 3.18 and 3.19). VPA-induced increased in miR-29b was similar to that observed with AR-42.

We then compared the anti-leukemic activity of AR-42 followed by decitabine with that of both AR-42 and decitabine as single agents, and decitabine followed by AR-42 in Kasumi-1 and NB4 cells. The cells were treated for 72 hours with vehicle, AR-42 (0.3 μM) alone, AR-42 (0.3 μM) followed by decitabine (0.5 μM) after 24 hours [AR-42→decitabine], decitabine (0.5 μM) followed by AR-42 (0.3 μM) after 24 hours [decitabine→AR-42] or decitabine (0.5 μM) alone. The lowest cell viability was observed in AR-42→decitabine group in all three cell lines (Figure 4a). Kasumi-1 cells treated with AR-42→decitabine were significantly less viable than those treated with decitabine alone (17% vs 91%; $P<0.01$), AR-42 alone (17% vs 40%; $P<0.01$), and decitabine→AR-42 (17% vs 34%; $P<0.01$; Figure 3.20). Similar observations were made for NB4 cells [AR-42→decitabine vs decitabine alone: 59% vs 99% ($P<0.01$); AR-42→decitabine vs AR-42 alone: 59% vs 87% ($P<0.05$); and AR-42→decitabine vs decitabine→AR-42: 59% vs 75% ($P<0.05$)].

3.4 Discussion

We demonstrated that our Tf-NPs were able to efficiently deliver *miR-29b* mimics, increase mature *miR-29b* levels and effectively target a panel of AML-relevant genes and mechanisms involved in epigenetics, cell cycle control and kinase-signaling pathways. Unlike the delivery of siRNA or shRNAs that are usually designed to target single genes, miRs can concurrently target multiple

genes and pathways involved in leukemia， which could potentially result in a better anti-leukemic activity and reduced emergence of resistance mechanisms. Indeed, we showed that Tf-NP-*miR-29b* treatment resulted in an *in vitro* growth inhibition and a reduction of colony formation in AML cells and in a significant therapeutic activity and prolonged survival in two independent AML *in vivo* trials. Interestingly, about 80% of the mice treated with Tf-NP-*miR-29b* were still alive at the time when the control treated mice (i.e. saline, free *miR-29b* or Tf-NP-scramble) had died. Although, several studies investigating miR-anti-sense/plasmid/mimic delivery-approaches were shown to reduce tumor burden *in vivo* (*155-169*), only a few of them were able to show that miR-based therapies (i.e. *miR-145, miR-34a, miR-107*) prolonged survival in mice with an aggressive cancer (*157, 158, 162, 165*).

Finally, in this study we also showed that priming AML cells with Tf-NP-*miR-29b* led to an improved anti-leukemic activity of decitabine *in vitro* and *in vivo*, thereby also supporting our previous finding that higher endogenous *miR-29b* pretreatment levels associate with improved response to decitabine (*82*). We now demonstrated that *miR-29b* expression may not only be a predictor of treatment response to decitabine, but *miR-29b* priming may indeed be integral to decitabine-based regimens, especially for those AML patients with downregulated endogenous *miR-29b*.

In conclusion we developed a novel Tf-conjugated NP system to efficiently deliver synthesized miR mimics to AML blasts. Tf-NP-*miR-29b* treatment increased mature *miR-29b* levels, downregulated known *miR-29b* targets and

showed anti-leukemic activity by improving survival in *in vivo* AML models. Our NP-delivery approach is a promising new anti-leukemic strategy that may be rapidly translated into the clinic.

3.5 Figures

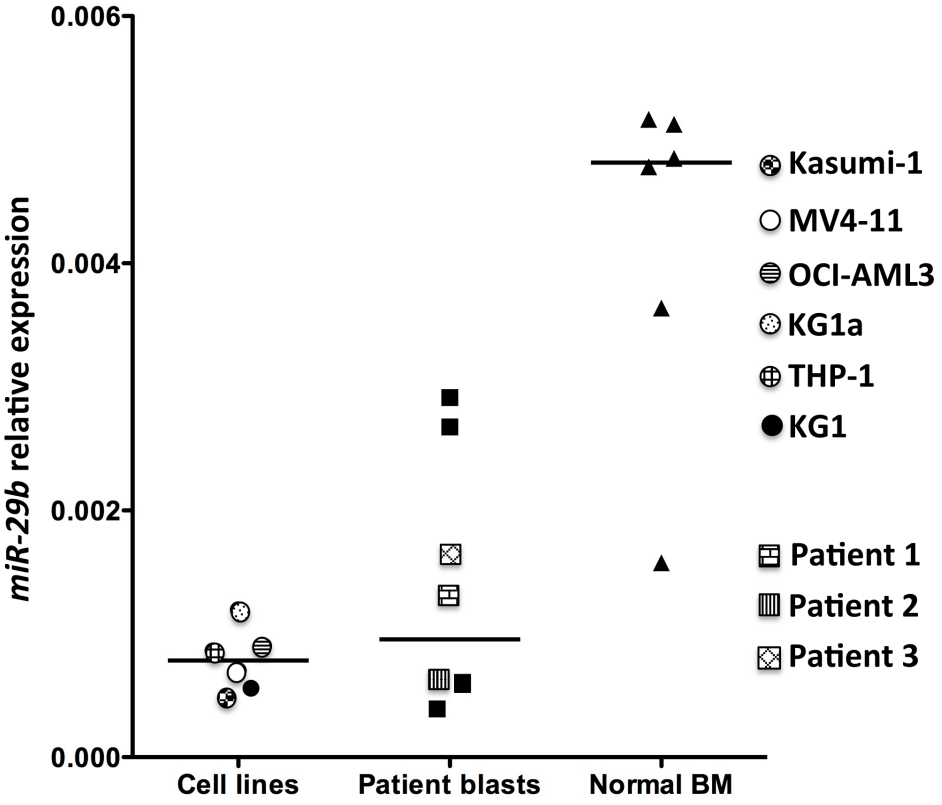

Figure 3. 1 Relative expression of *miR-29b* in AML cell lines, patient blasts and bone marrow samples from healthy donors.

Quantitative RT-PCR of mature miR-29b levels in 6 AML cell lines (THP-1, KG1, KG1a, MV4-11, Kasumi-1, OCI-AML3), 7 patient blasts and 6 bone marrow samples from healthy donors. The results are normalized to U44 expression.

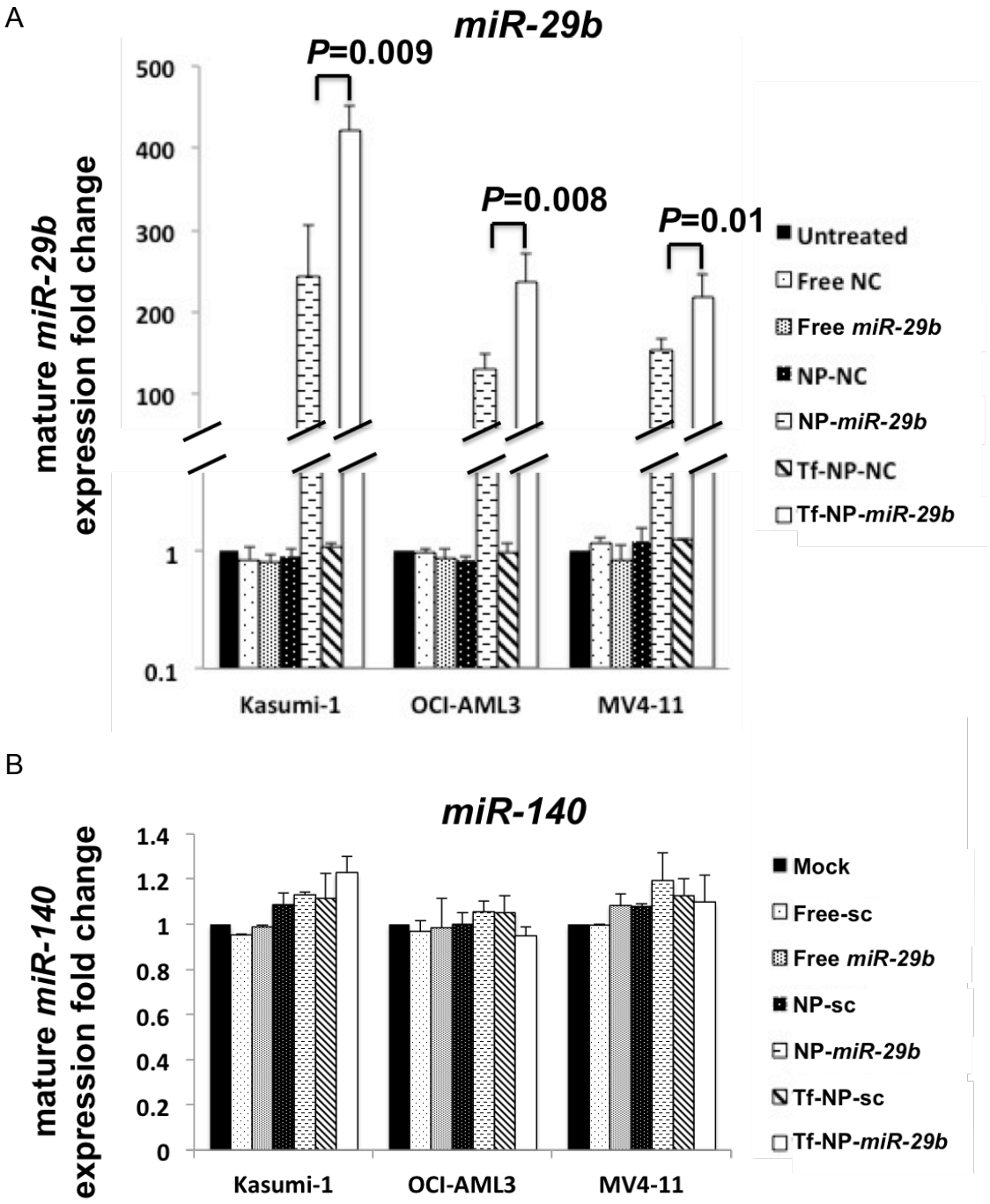

Figure 3. 2 Tf-NP-*miR-29b* treatment increased mature *miR-29b* level.

Mature *miR-29b* expression levels (A) and *miR-140* expression (B) in Kasumi-1, OCI-AML3 and MV4-11 cells.

Figure 3. 3 Tf-NP-*miR-29b* treatment down-regulated its targets in AML cell lines.

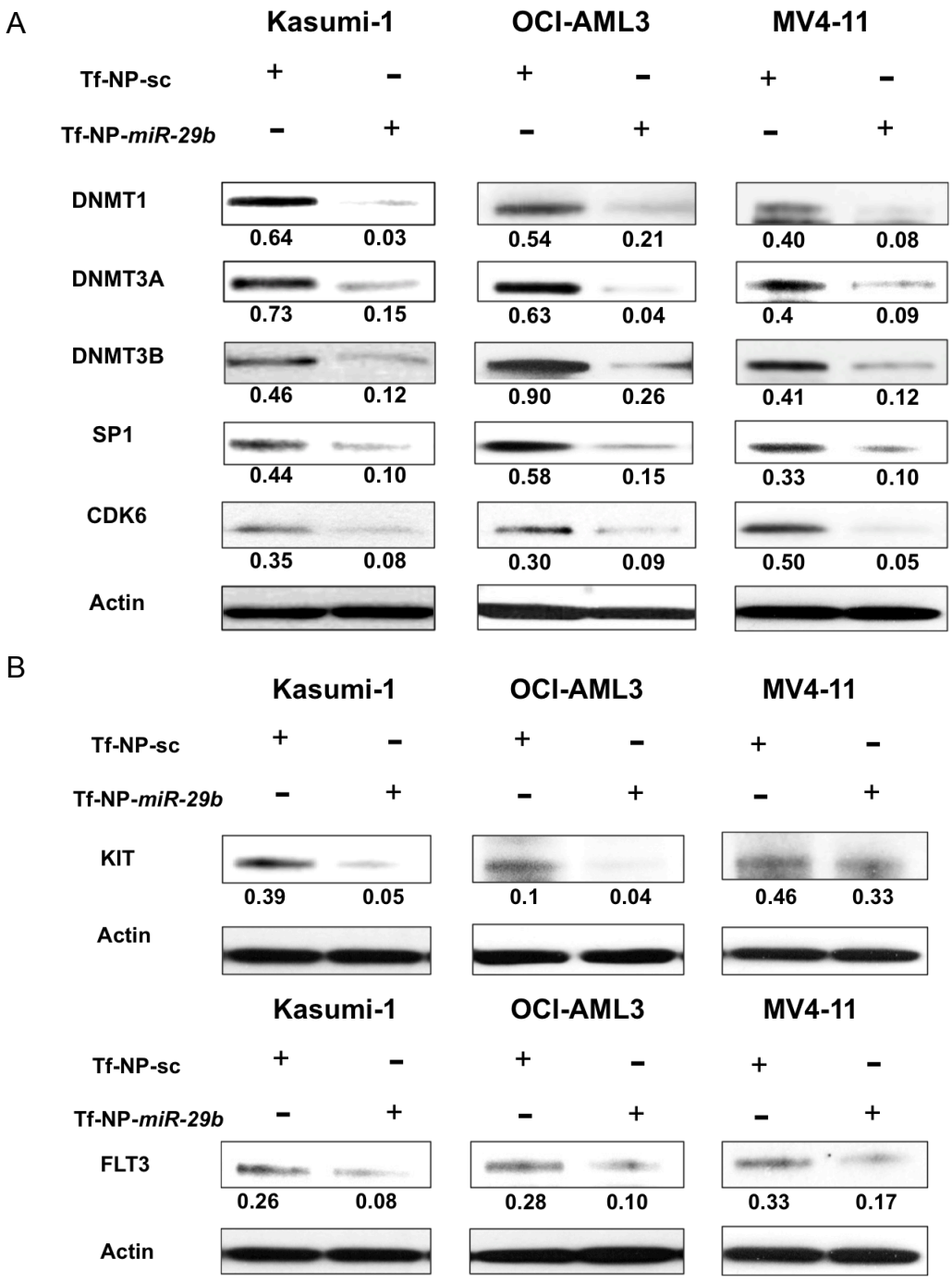

Continued

Figure 3. 3 : Continued

Tf-NP-*miR-29b* treatment down-regulated DNMT1, DNMT3A, DNMT3B, SP1, CDK6, FLT3 and KIT. DNMT1, DNMT3A, DNMT3B, SP1 and CDK6 expression (A) and FLT3 and KIT expression (B) in Kasumi-1, OCI-AML3 and MV4-11 after treatment with Tf-NP-*miR-29b* compared to Tf-NP-sc treatment. The number below each band represents the ratio of the band's intensity to actin used as a loading control.

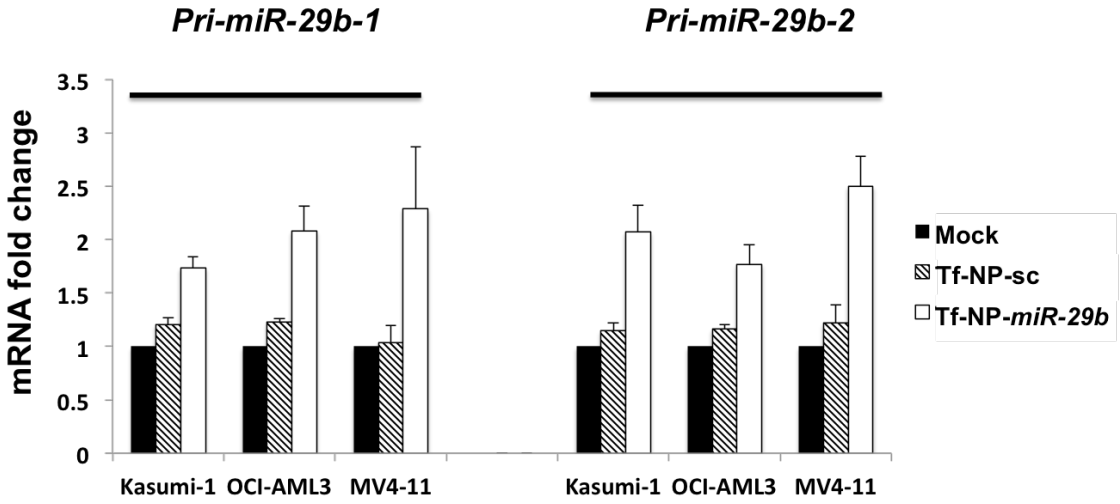

Figure 3. 4 Expression of *pri-miR-29b-1* and *pri-miR-29b-2* in AML cell lines following Tf-NP-*miR-29b* treatment.

Quantitative RT-PCR of *pri-miR-29b-1* and *pri-miR-29b-2* in three AML cell lines 48 hours after treatment with Tf-NP-scramble control and Tf-NP-*miR-29b* or mock (buffer only). The results are shown as mRNA expression level, normalized to *18S* expression.

Figure 3. 5 Cell growth curve of Kasumi-1, OCI-AML3 and MV4-11 cells treated Tf-NP-*miR-29b*, Tf-NP-sc or mock.

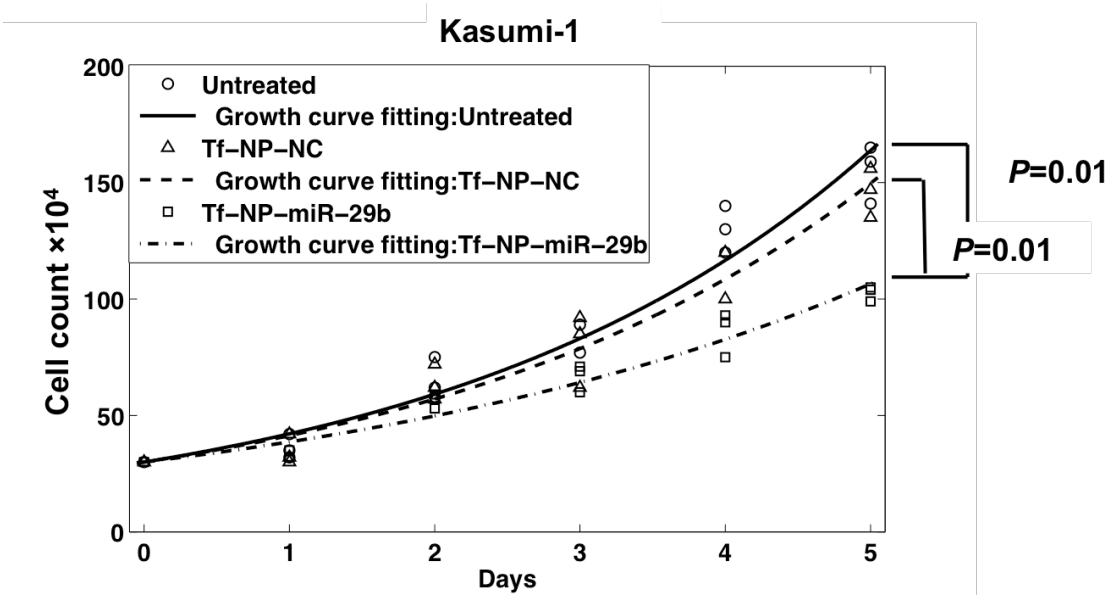

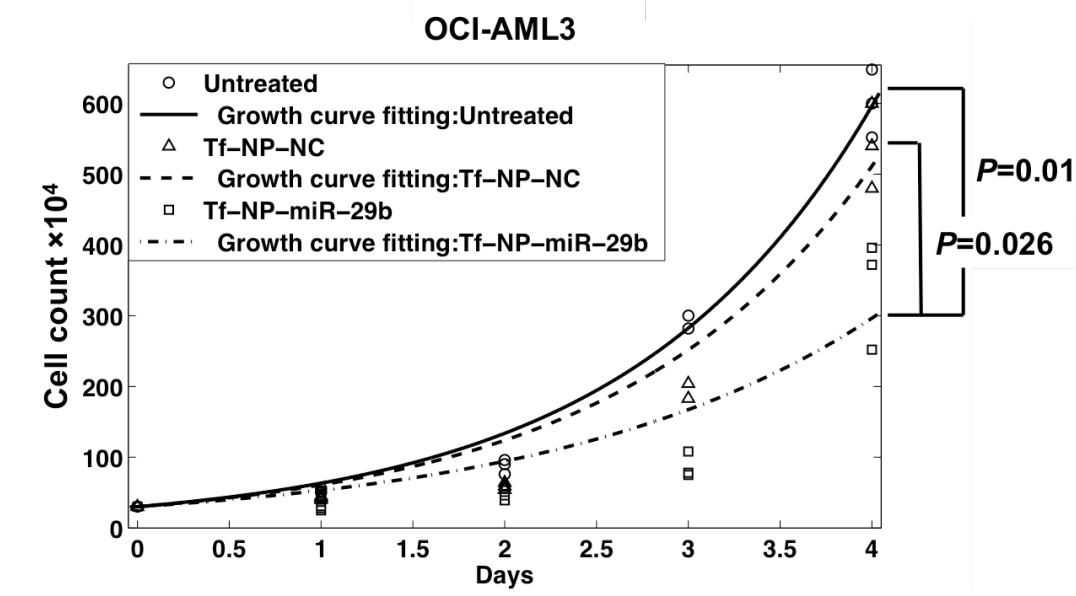

Continued

Figure 3. 5 : Continued

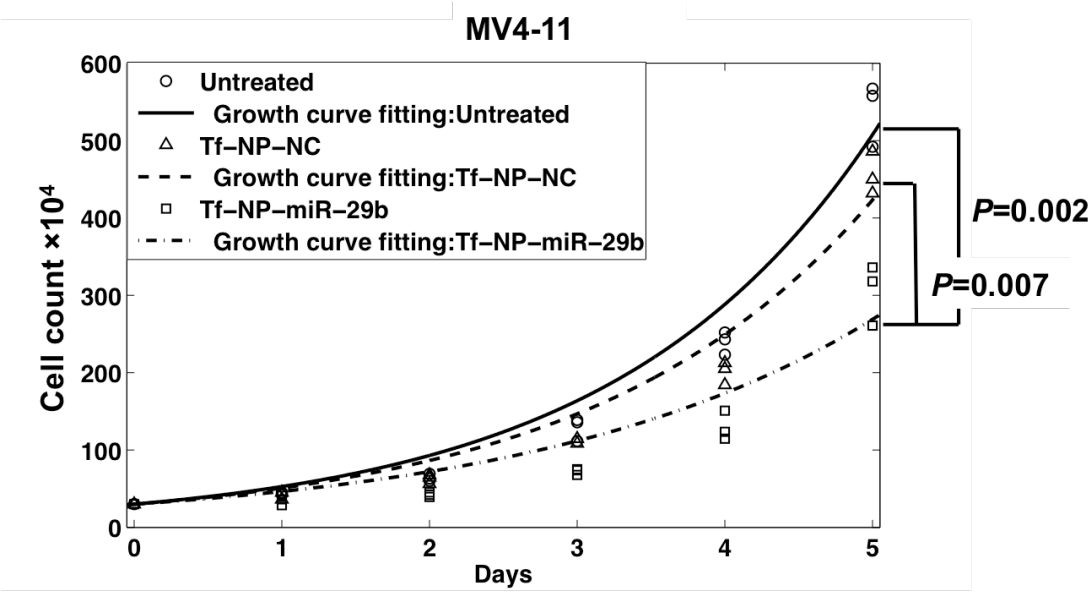

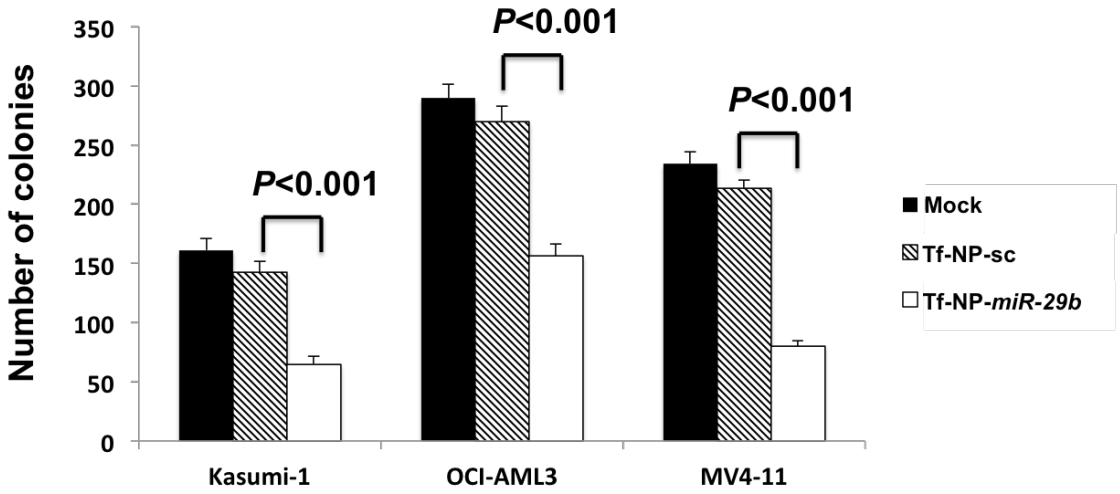

Figure 3. 6 Colony formation assays in Kasumi-1, OCI-AML3 and MV4-11 cells treated with either Tf-NP-*miR-29b*, or Tf-NP-sc or mock.

A

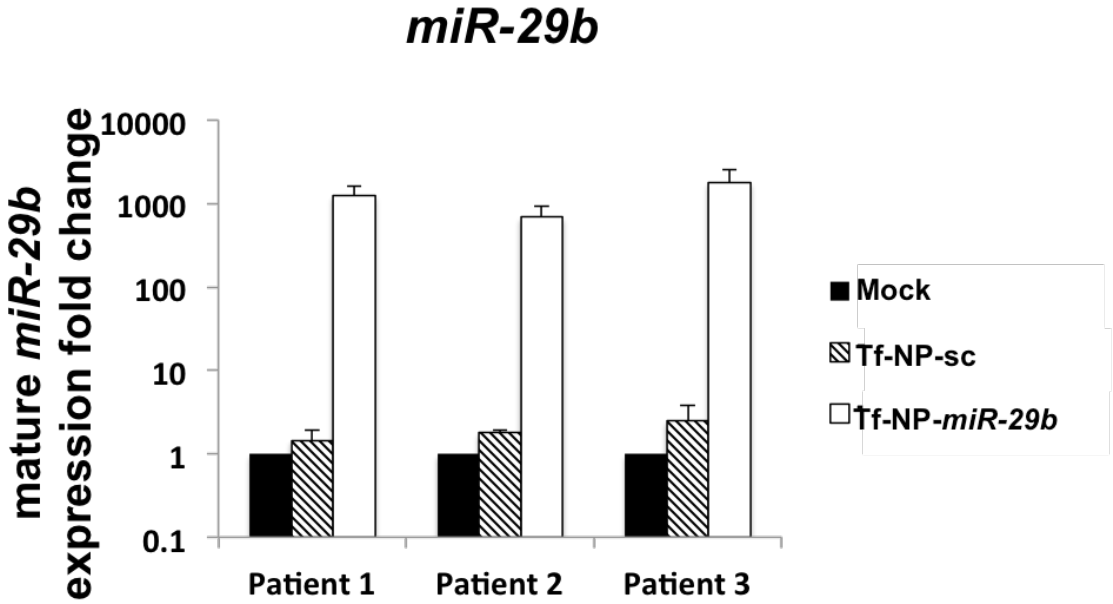

B

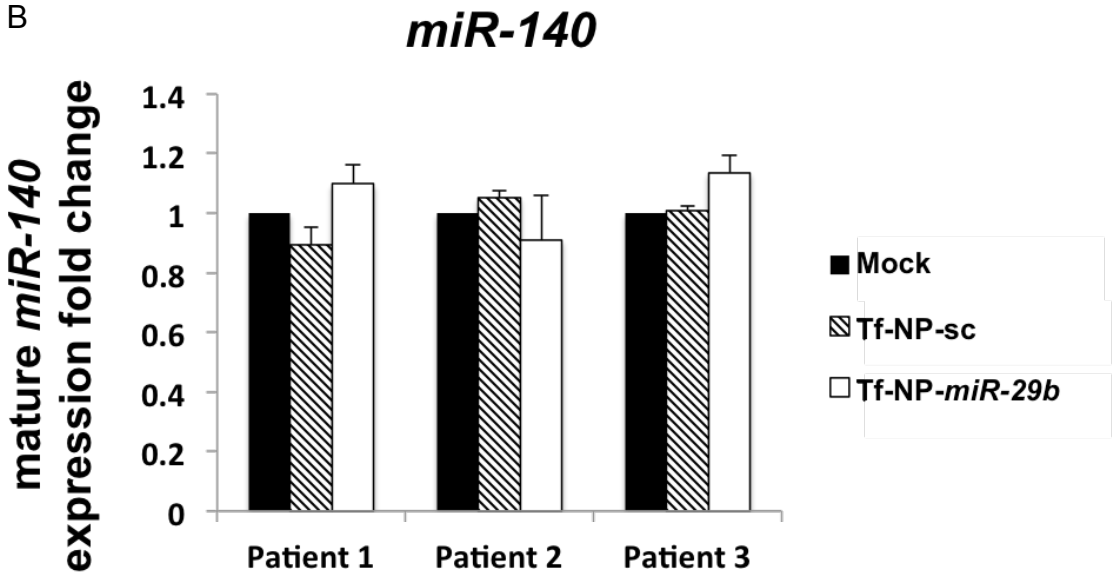

Figure 3. 7 Tf-NP-*miR-29b* treatment increased mature *miR-29b* level.

Mature *miR-29b* expression levels (A) and *miR-140* expression (B) in AML blasts from three patients.

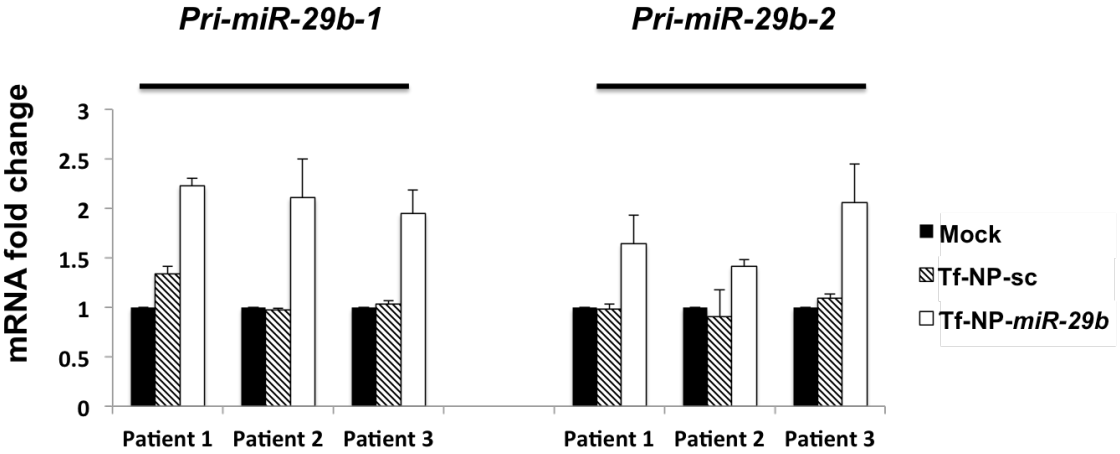

Figure 3. 8 *pri-miR-29b-1* and *pri-miR-29b-2* level in AML blasts followed by Tf-NP-*miR-29b* treatment.

Quantitative RT-PCR of *pri-miR-29b-1* and *pri-miR-29b-2* in three AML blasts from three patients lines 48 hours after treatment with Tf-NP-scramble control and Tf-NP-*miR-29b* or mock (buffer only). The results are shown as mRNA expression level, normalized to *18S* expression.

Figure 3. 9 Tf-NP-*miR-29b* treatment down-regulated its targets in AML patient blasts.

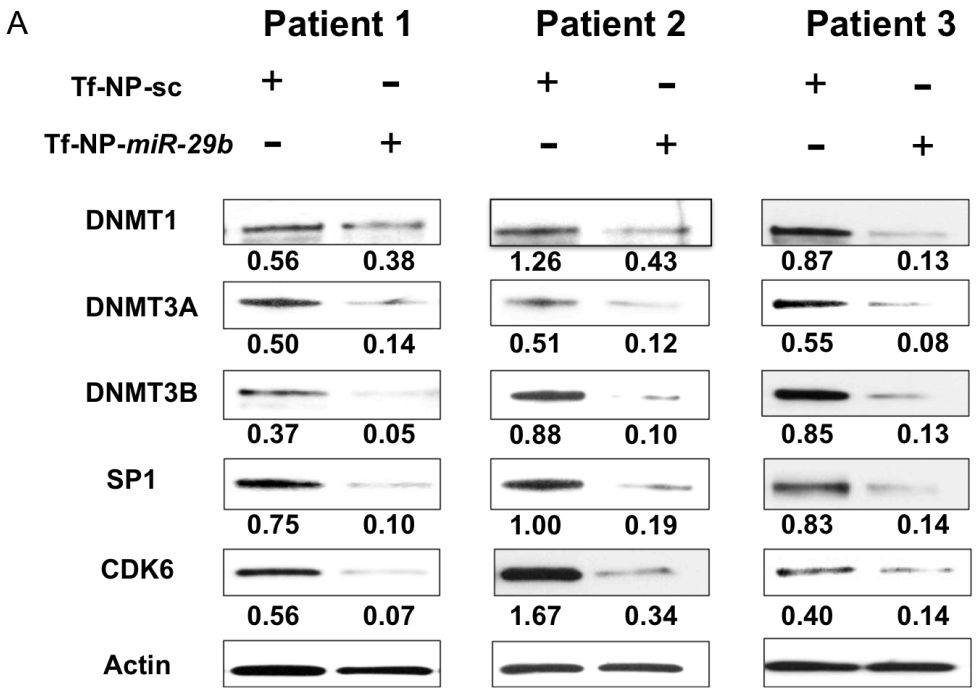

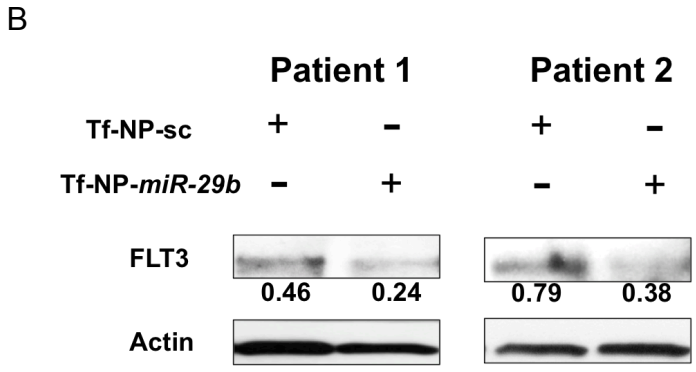

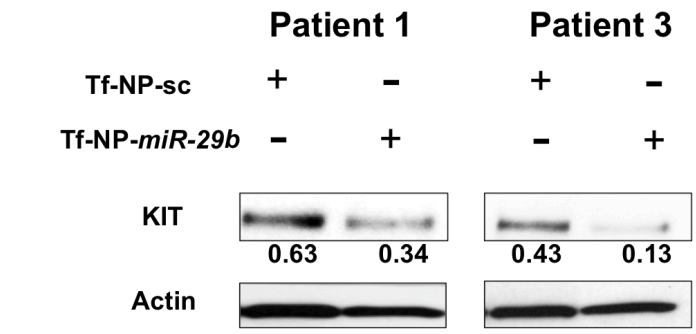

Continued

Figure 3. 9 : Continued

Tf-NP-*miR-29b* treatment down-regulated DNMT1, DNMT3A, DNMT3B, SP1, CDK6, FLT3 and KIT. DNMT1, DNMT3A, DNMT3B, SP1 and CDK6 expression (A) and FLT3 and KIT expression (B) in AML patient blasts after treatment with Tf-NP-*miR-29b* compared to Tf-NP-sc treatment. The number below each band represents the ratio of the band's intensity to actin used as a loading control.

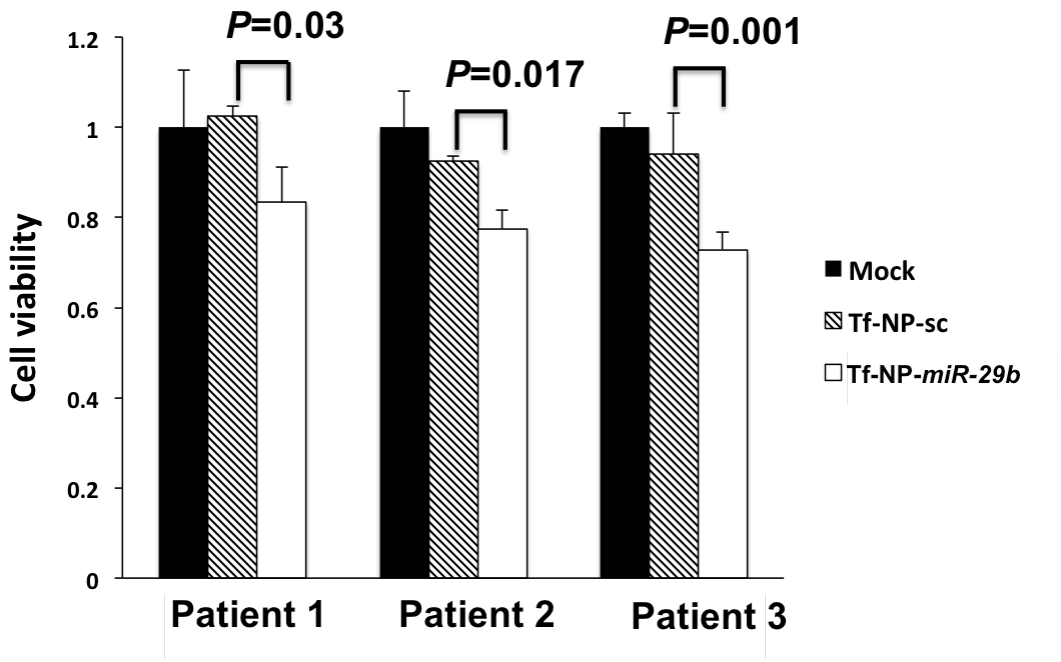

Figure 3. 10 Cell viability of three patient blast samples treated with Tf-NP-*miR-29b*, Tf-NP-sc or mock.

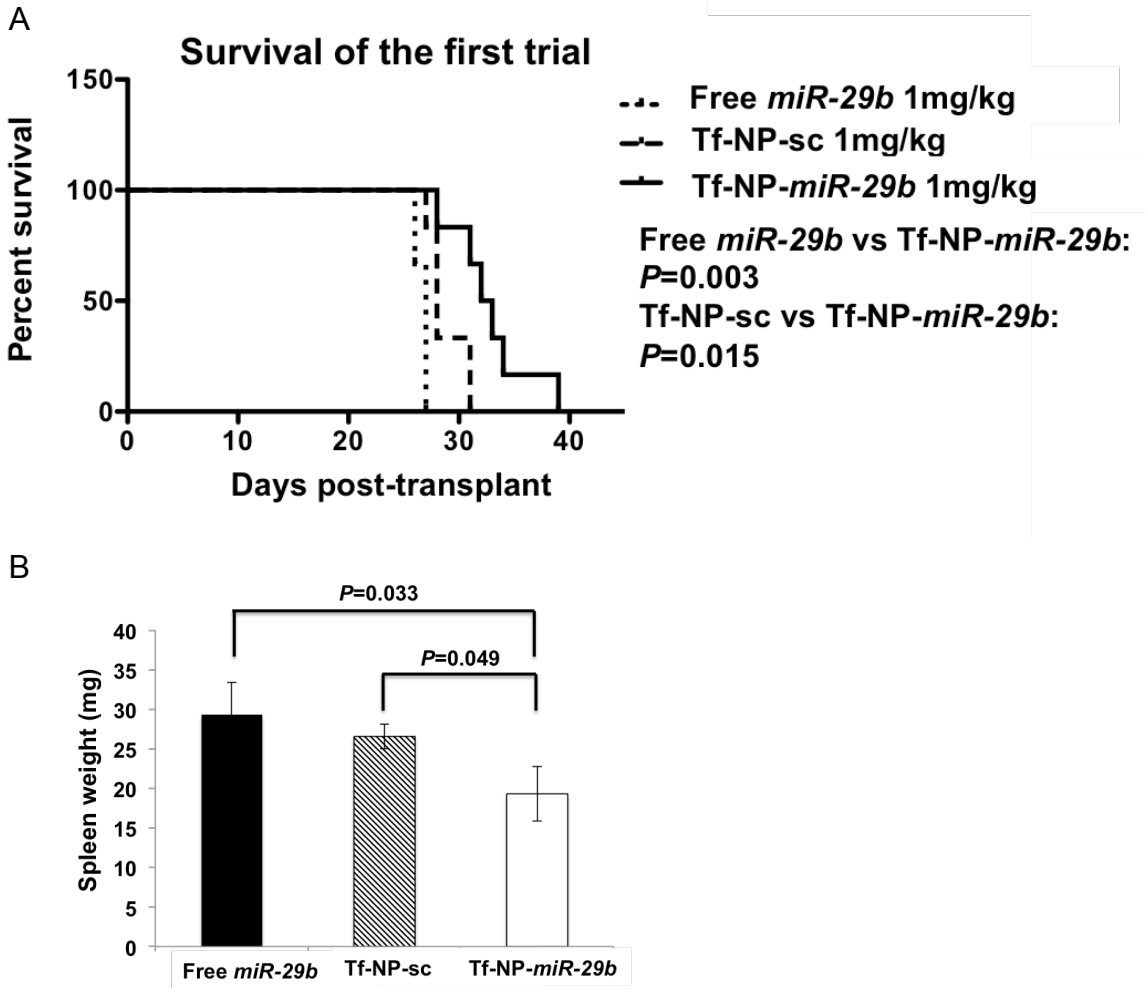

Figure 3. 11 *In vivo* evaluation of Tf-NP-*miR-29b* in preclinical model, first trial.

First trial: leukemic mice were treated with either free *miR-29b* mimic, Tf-NP-scramble or Tf-NP-*miR-29b*. (A) Survival curves of the mice according to distinct treatments are shown. (B) Corresponding spleen weights are shown.

Figure 3. 12 *In vivo* evaluation of Tf-NP-*miR-29b* in preclinical model, second trial.

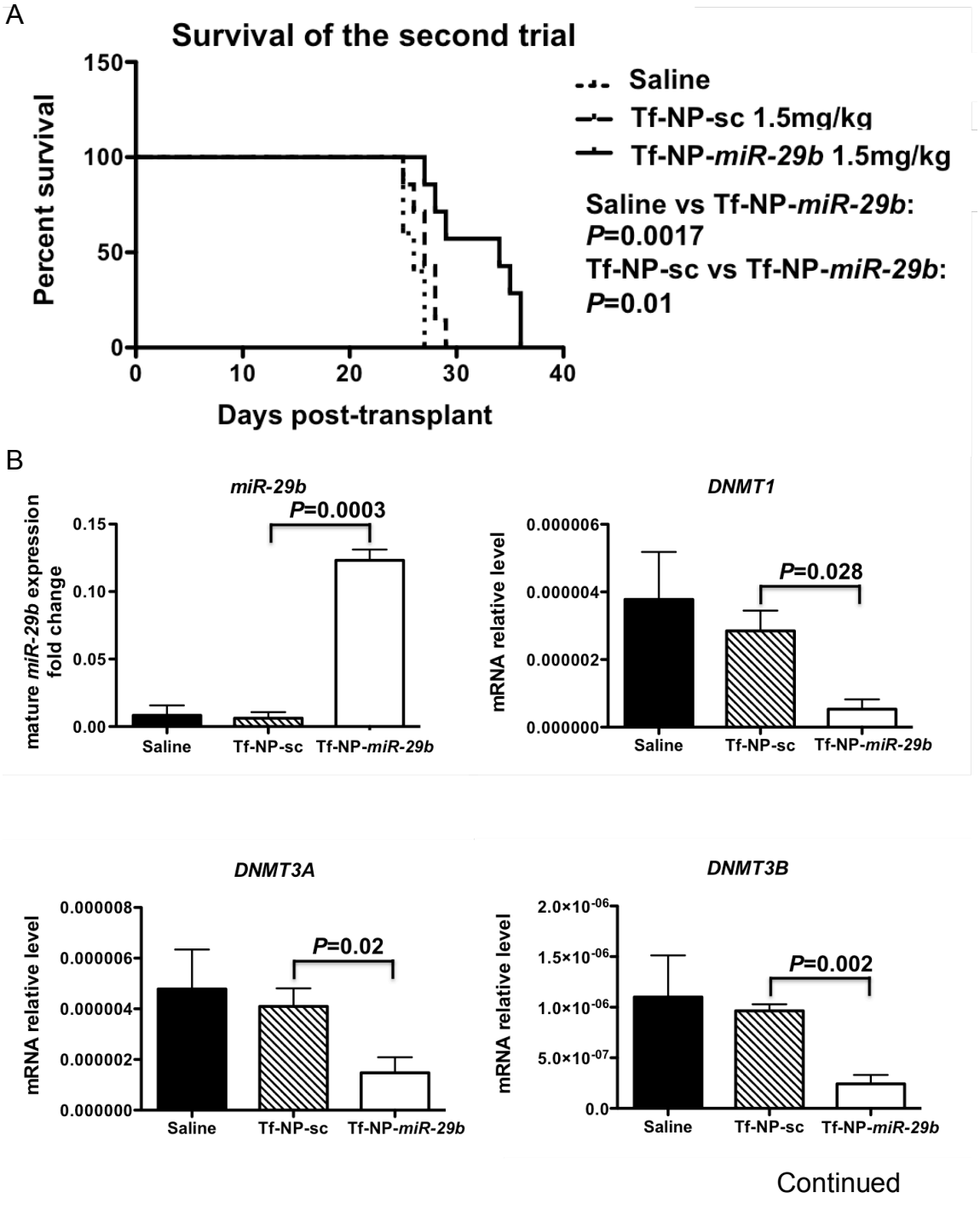

Continued

Figure 3. 12 : Continued

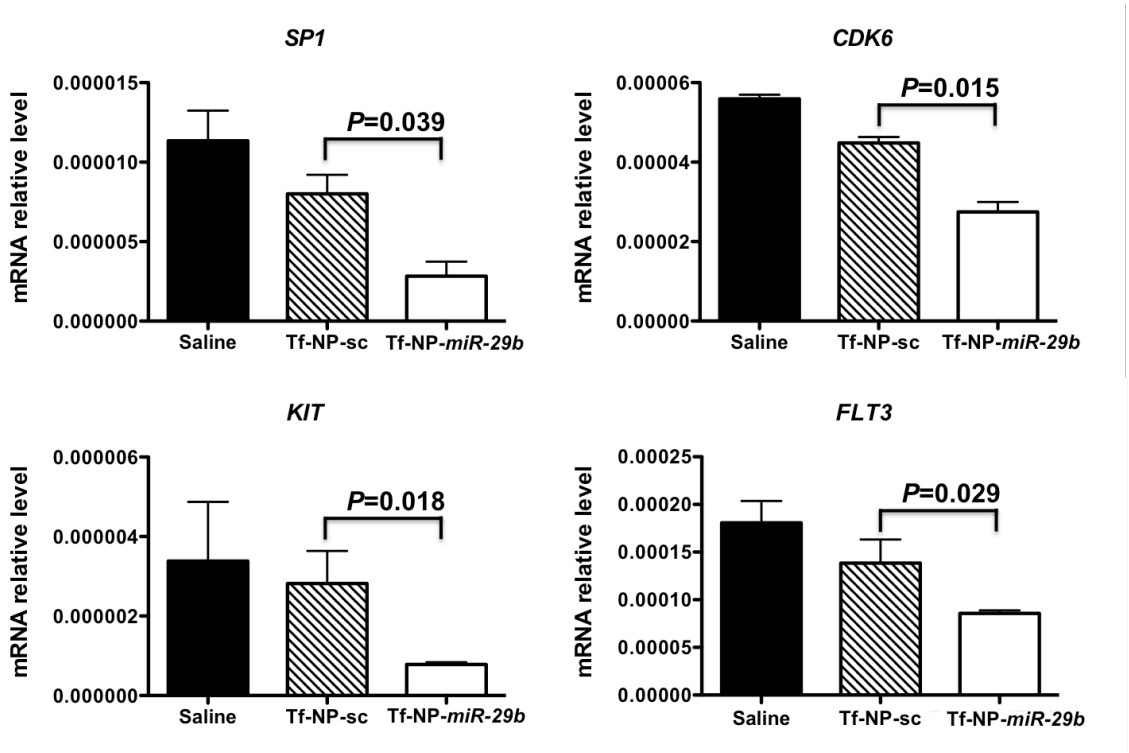

Figure 3. 12: Second trial: leukemic mice were treated with either saline, Tf-NP-sc or Tf-NP-*miR-29b*. (A) Survival curves of the mice according to distinct treatments are shown. (B) Intracellular levels of *miR-29b*, *DNMT1*, *DNMT3A*, *DNMT3B*, *SP1*, *CDK6*, *FLT3* and *KIT* at day 24.

Figure 3. 13 Anti-leukemic activity of Tf-NP-*miR-29b* followed by decitabine *in vitro* and *in vivo*.

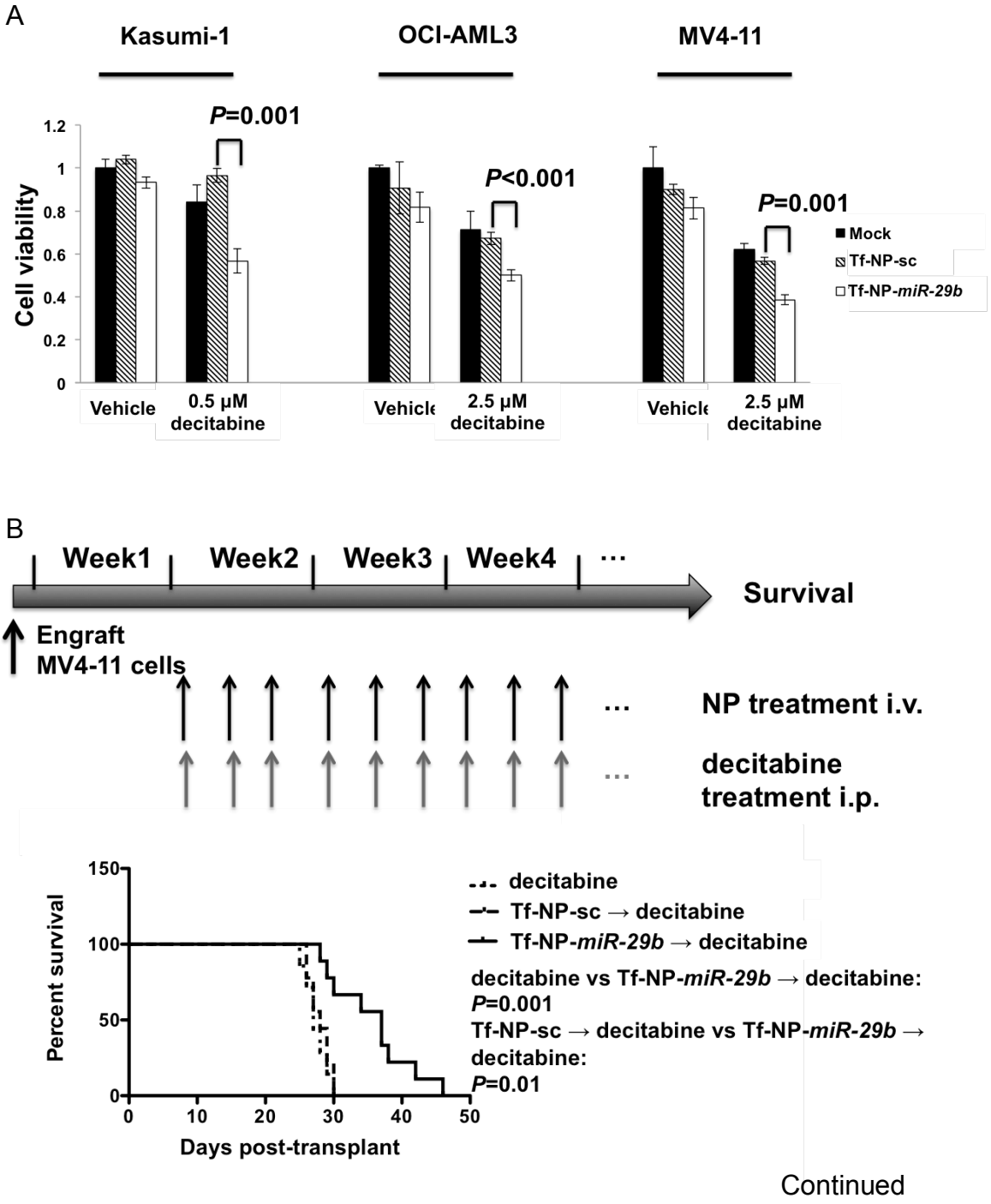

Continued

Figure 3. 13 : Continued

(A) Kasumi-1, OCI-AML3 and MV4-11 cells were pretreated with Tf-NP-*miR-29b*, Tf-NP-sc or mock for 48 hours before 48 hours decitabine treatment. (B) Leukemic mice were treated with decitabine, Tf-NP-sc followed by (→) decitabine or Tf-NP-*miR-29b*→decitabine ten days after engraftment. Survival curves of the mice according to distinct treatments are shown.

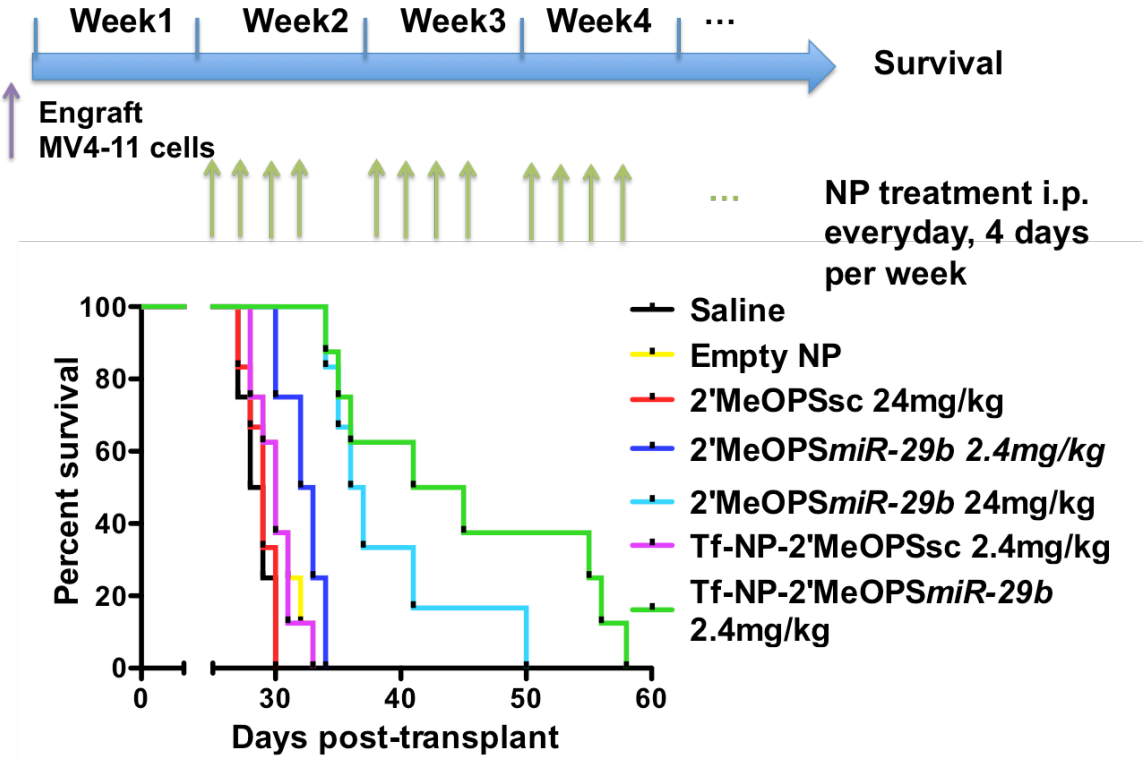

Figure 3. 14 Improvement of the potency of synthetic single-stranded 2′-O-Methylphophorothioate *miR-29b* (2′-MeOPSmiR-29b) by Tf-NP.

The engrafted AML mice were treated with 2.4mg/kg free 2′-MeOPSmiR-29b, 24mg/kg free 2′-MeOPSmiR-29b and 2.4mg/kg Tf-NP-2′-MeOPSmiR-29b. Saline, empty NP, 24mg/kg 2′-MeOPSsc and 2.4mg/kg 2′-MeOPSsc treatment were as controls. Survival curves of the mice according to distinct treatments are shown.

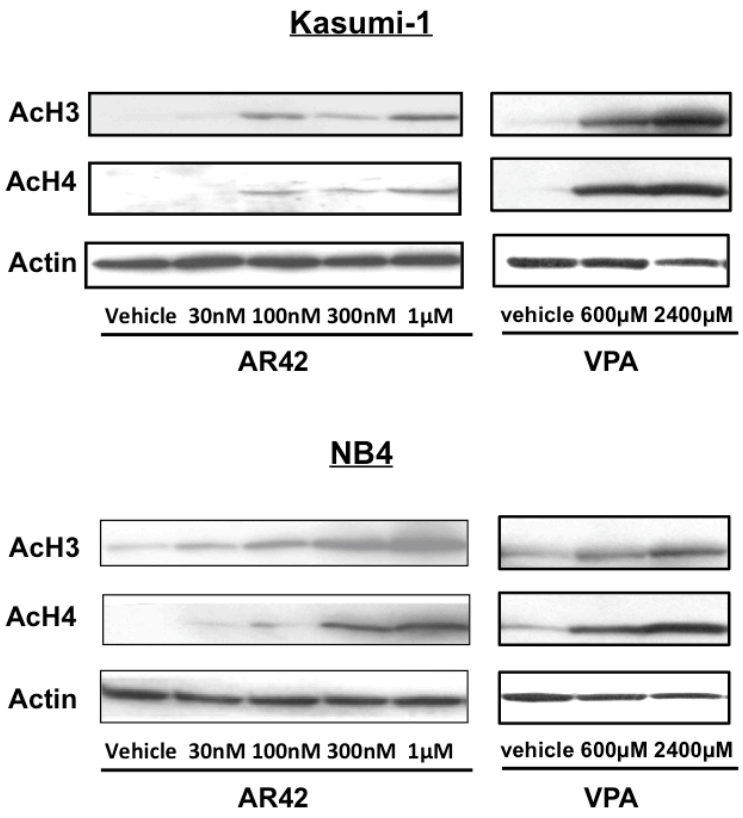

Figure 3. 15 AR-42 treatment inhibited HDAC activity in AML cell lines.

Increased histone acetylation in Kasumi-1 (upper) and NB4 (bottom) 48 hours after AR-42 or VPA treatment.

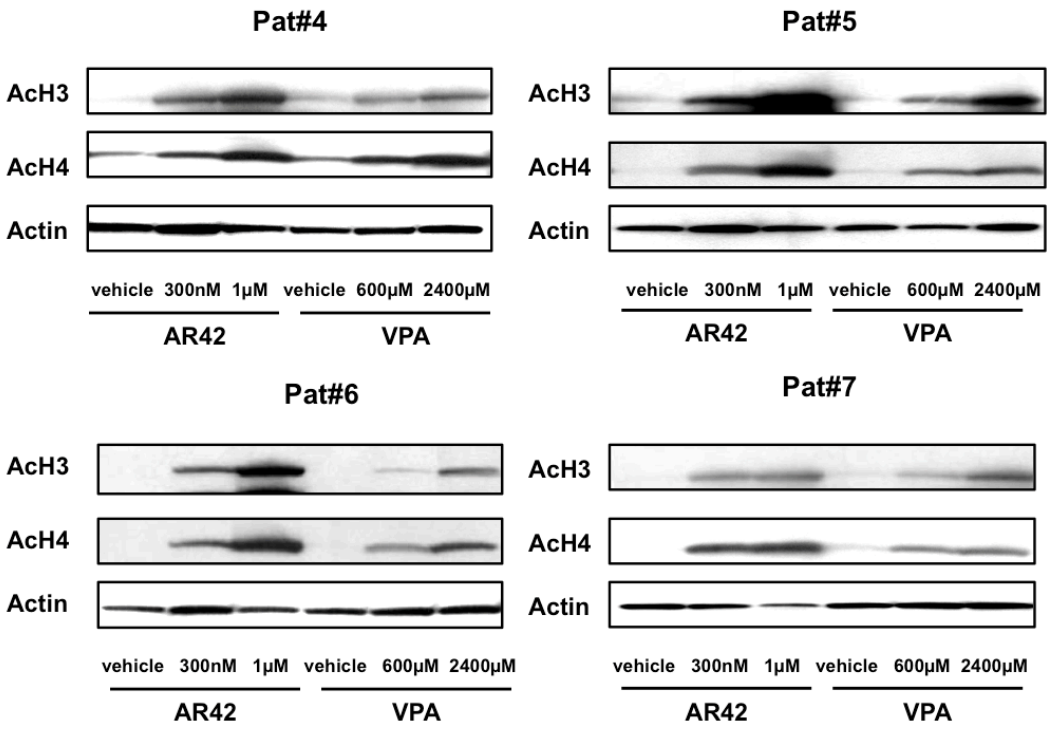

Figure 3. 16 AR-42 treatment inhibited HDAC activity in AML patient blasts. Increased histone acetylation in AML patient blasts (n=4) 48 hours after AR-42 or VPA treatment.

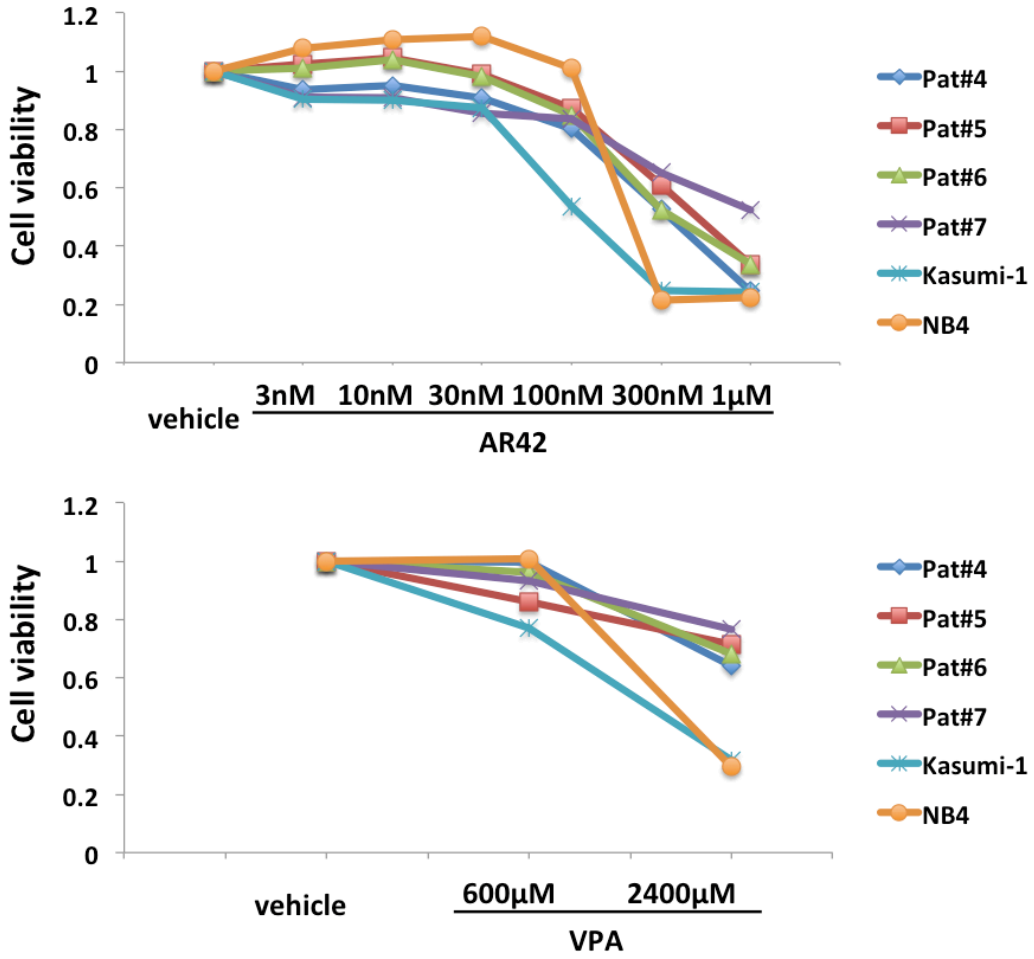

Figure 3. 17 AR-42 decreased proliferation of AML cells and patient blasts.

Proliferation of primary AML patient blasts (n=4) following treatment of AR-42 and VPA at different doses.

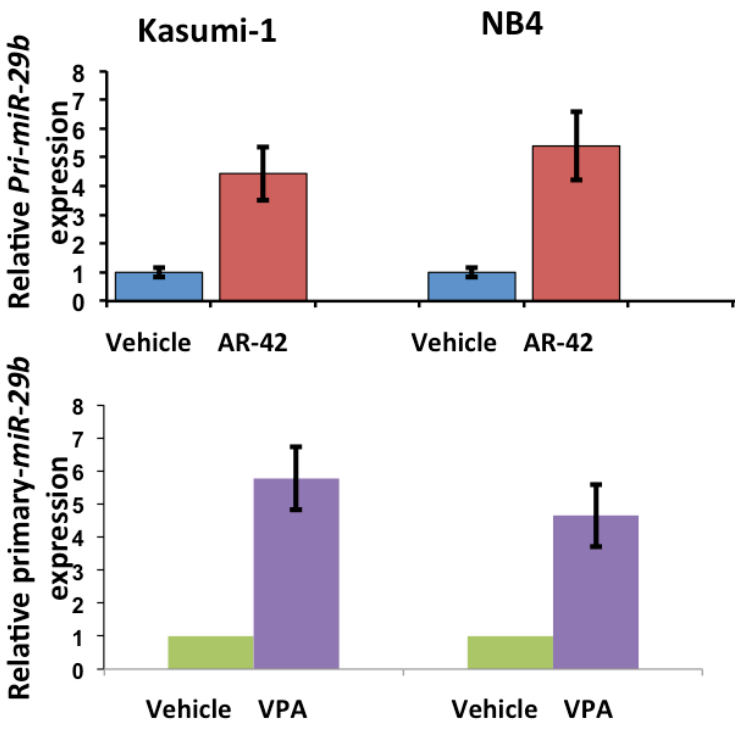

Figure 3. 18 *miR-29b* expression increases following AR-42 treatment in AML cell lines.

Kasumi-1 and NB4 were treated with either 1 μM AR-42 or 2400 μM VPA for 24 hours.

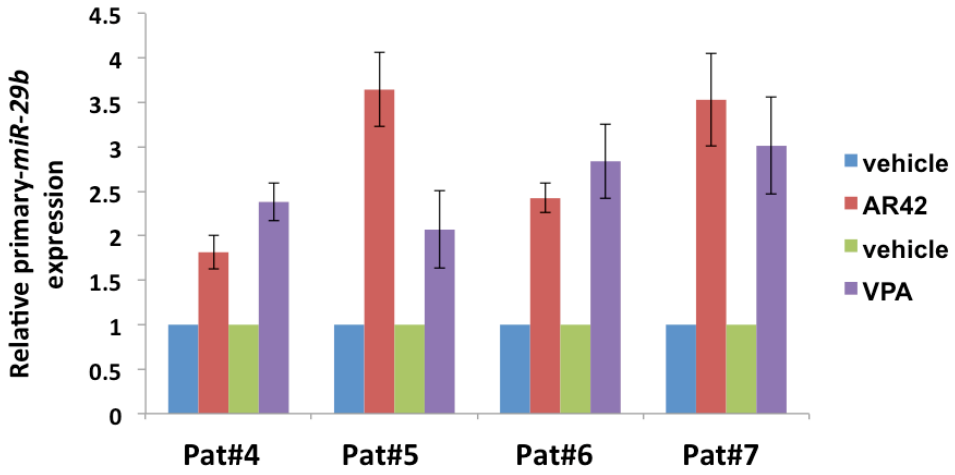

Figure 3. 19 *miR-29b* expression increases following AR-42 treatment in AML patient blasts (n=4).

Four patient blasts were treated with either 1 μM AR-42 or 2400 μM VPA for 24 hours.

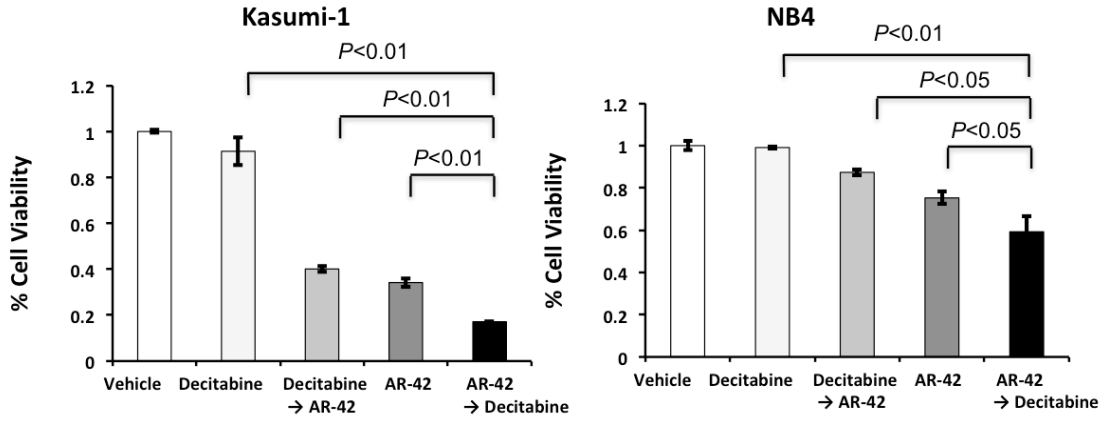

Figure 3. 20 AR-42 followed by decitabine has the strongest activity on cell viability.

Kasumi-1 and NB4 cells treated with vehicle, decitabine 0.5 μM for 72 hours, decitabine 0.5 μM for 72 hours with AR-42 0.3 μM added at 24 hours, AR-42 0.3 μM for 72 hours, or AR-42 0.3 μM for 72 hours with decitabine 0.5 μM added at 24 hours. Cells treated with AR-42 followed by decitabine showed lowest cell viability.

Chapter 4. Mechanism of MicroRNA-181a and Its Therapeutic Application in Acute Myeloid Leukemia

4.1 Introduction

The *miR-181* family comprises four mature miRs (*miR-181a*, *miR-181b*, *miR-181c*, *miR-181d*) and has been associated with the regulation of inflammatory mechanisms (*211, 212*). These miRs have been found dysregulated in several types of human cancers, including leukemias (*37, 79, 213-219*). In solid tumors the role of *miR-181* seems to be organ specific. High expression of *miR-181* has been associated with poor clinical outcome in patients with colorectal cancer (*213*) and lymph-node metastasis in oral squamous cell carcinoma (*214*). However in glioma high expression of *miR-181* seems to have tumor suppressor activity (*215*). In hematologic malignancies higher expression of *miR-181* is associated with better outcome (*37, 79, 219-221*). Indeed, we recently reported that the favorable impact of higher expression of *miR-181a* in both AML cytogenetically normal (CN) or abnormal (CA) patients (*37, 79, 221*). To date, however the molecular basis for the attenuation of disease aggressiveness by *miR-181a* in AML remains to be elucidated.

RAS proto-oncogenes encode small GTPase proteins, i.e. KRAS, NRAS and HRAS that are involved in homeostatic mechanisms of proliferation, differentiation and apoptosis of normal cells (*222*). While *KRAS* and *NRAS* are frequently mutated and activated in AML, *HRAS* mutations are rare and even the *HRAS* wild type expression is the lowest with respect to the other RAS isoforms (*222*). Aberrant activation of RAS signal transduction is often found in human neoplasia (*223-236*). In hematopoietic malignancies, including AML, activating oncogenic RAS mutations contribute to malignant phenotypes by phosphorylating and activating down-stream effectors such as the mitogen-activated protein kinase kinase (MAPKK, also known as MEK), mitogen-activated protein kinase (MAPK), and the PI3K-AKT downstream effectors, thereby promoting aberrant cell proliferation and survival (*222*). However, to date, an effective therapeutic RAS targeting approach in AML remains to be developed.

Recently, *KRAS* was shown to be a direct target of *miR-181a* in oral squamous cell carcinoma (*237*). Additionally, *NRAS* and the RAS-downstream effector *MAPK1*, are *in silico* predicted to be putative targets of *miR-181a*. Therefore, we hypothesized here that higher *miR-181a* levels may attenuate AML aggressiveness by targeting RAS and/or its downstream effectors in myeloid blasts, and, we reasoned, the delivery of synthetic *miR-181a* mimics may reverse low endogenous levels of *miR-181a* in AML blasts and leads to anti-leukemic activity.

4.2 Materials and Methods

4.2.1 Cell lines, patient samples and cell culture

KG1a, MV4-11, HEK 293T and HEK 293TN cells were obtained from ATCC; OCI-AML3 cells were obtained from DSMZ (Braunschweig, Germany). Primary, unselected AML blasts from apheresis samples collected from nine patients were obtained from The Ohio State University (OSU) Leukemia Tissue Bank. Patients signed an informed consent to store and use their tissue for discovery studies according to OSU institutional guidelines.

4.2.2 *miR-181a* lentivirus infection

The lentiviral-infections were performed as previously described (*81*). Briefly, for overexpression the stemloop of *miR-181a* with 200bp flanking sequence was cloned into the HIV based lentiviral dual promoter vector (pCDH-CMV-MCS-EF1-copGFP+Puro cDNA; System Biosciences, Montain View, CA, USA), utilizing the primers and PCR conditions described in Table 4.1. As a control, lentiviral scramble control miR was used (miRZiP000, System Biosciences). For each experiment 4 500µg lentiviral constructs were transfected into 293TN cells using 45 µg pPACKH1 (System Biosciences) and 55 µl PureFection (System Biosciences). After 48 hours and 72 hours, the supernatant containing the pseudoviral particles was collected and the virus was precipitated overnight at 4°C using 5 ml PEG-IT virus precipitation solution (System Biosciences). 200 µl Phosphate Buffered Saline (PBS) and 25 µM Hepes Buffer were used for

resuspension of the pelleted virus. 500 000 MV4-11 cells/ml were infected with 20 UI virus, using 5 µl Transdux Infection Reagent (System Biosciences). Ten Days later the infected cells were selected with Puromycin.

4.2.3 Luciferase assays

Luciferase assays were carried out as previously described (*81*). Briefly, the 3′-untranslated regions (UTRs) of the *KRAS, NRAS* and *MAPK1* gene were amplified by PCR from genomic DNA and inserted into the pGL4.24 control vector (Promega, Madison, WI, USA), using the EcoRI site immediately downstream from the stop codon of the luciferase coding region. We also generated mutated binding sites by using bi-directional mutation primers, exchanging 3 or 4 nucleotides of the respective predicted binding sequences. Primer sequences are listed in Table 4.1. HEK 293T cells were seeded in 12-well plates 24 hours before transfection. When the culture reached 80% confluency, the cells were transfected in triplicates with reporter and control constructs (Renilla, pGL4.74; Promega) using the Lipofectamine 2000 transfection reagent (Invitrogen, Carlsbad, CA, USA) according to the manufacturer's instructions. Cells were co-transfected with 10pmol of either *miR-181a* or miR-scramble control (Ambion, Austin, TX, USA). After 24 hours, protein lysates were assessed for firefly luciferase and Renilla luciferase activities according to the manufacturer's recommendations (Promega). For analysis, relative expression was normalized using co-transfected Renilla luciferase.

4.2.4 Nanoparticle preparation

The synthetic double-stranded *miR-181a*, miR-scramble (sc), and *KRAS*, *NRAS* and *MAPK1* siRNAs were purchased from Ambion. Nanoparticle preparation was performed as previously described (*238*). Briefly, polyethylenimine was used to capture miRs/siRNAs and the complex was loaded to pre-made anionic liposomal nanoparticles which consists of 1,2-dioleoyl-sn-glycero-3-phosphoethanolamine (DOPE), 1,2-dimyristoyl-sn-glycerol, methoxypolyethylene glycol (DMG-PEG) and linoleic acid. Transferrin was first conjugated with 1,2-distearoyl-sn-glycero-3-phosphoethanolamine-N-[maleimide(polyethylene glycol)-2000] (DSPE-PEG2000 maleimide) and then post-inserted to the miR loaded nanoparticle to form the final product.

4.2.5 Quantitative RT-PCR (qRT-PCR)

RNA extraction was performed as previously described (*238*). Briefly, total RNA was extracted using Trizol reagent (Invitrogen). Then cDNA was synthesized using Superscript III (Invitrogen) or the Taqman miR Reverse Transcription kit (Applied Biosystems, Foster City, CA, USA) for *miR-181a, miR-181b, miR-140* and *U44*. qRT-PCR was performed with Taqman gene expression assays (Applied Biosystems) following the manufacturer's protocols. *miR-181a, miR-181b* and *miR-140* expression were normalized to *U44*. *KRAS*, *NRAS* and *MAPK1* expression were normalized to *GAPDH*. The comparative cycle threshold (C_T) method as previously described was used for relative quantification of gene expression.

4.2.6 Western blot analysis

The protein expression was measured by Western blot as previously described (*238*). Anti-KRAS (ab55391) antibodies were purchased from Abcam (Cambridge, MA, USA). Anti-NRAS (C-20, sc-519) and Anti-MYC (N-262, sc-764) antibodies were purchased from Santa Cruz Biotechnology (Santa Cruz, CA, USA). Anti-MAPK1, –MEK1/2 (L38C12), –p-MEK1/2 (S217/221,41G9), AKT and p-AKT (S473, D9E) antibodies were purchased from Cell Signaling Technology (Beverly, MA, USA). Equivalent gel loading was confirmed by probing with antibodies against Actin (sc-1616; Santa Cruz). The intensity of the resulting bands was measured by ImageJ 1.45s (http://imagej.nih.gov/ij). The intensity ratio of each band respective to the corresponding actin intensity was used for relative quantification and is displayed in the respective figures.

4.2.7 Growth Curve

Lenti-virally transduced MV4-11 cells (1×10^5/mL) were plated in 12-well plates. KG1a, OCI-AML3 and MV4-11 cells (1×10^5/mL) were plated in 12-well plates and treated with nanoparticles (Tf-NP-scramble or Tf-NP-*miR-181a* at a final concentration of 10nM) or were mock treated (buffer only). Cells were harvested and counted at 24-hour intervals using a Bio-Rad TC20™ Automated Cell Counter (Bio-Rad, Berkeley, CA, USA). Each sample was run in triplicate.

4.2.8 Colony Assays

Methylcellulose colony formation assays were carried out as previously described (*208*) and counted after 15 days.

4.2.9 Apoptosis assays

MV4-11, OCI-AML3 cells and four AML patient blast samples cells were treated with Tf-NP-*miR-181a*, Tf-NP-sc and mock for 24 hours. The cells were then subsequently treated with daunorubicin (DNR; 0.01 μM for MV4-11, 0.04 μM for OCI-AML3, 0.04 μM for patient #1 and #3, 0.01 μM for patient #2 and #4 blasts; Sigma-Aldrich, St Louis, MO, USA) or vehicle control (phosphate-buffered saline; Sigma-Aldrich) for another 72 hours. Annexin V/ propidium iodide (PI) stain (BD Biosciences, San Jose, CA, USA) was performed.

4.2.10 *In vivo* studies

Animal studies were performed according to the Ohio State University institutional guidelines. A total 5 million lenti-viral transduced MV4-11 cells were injected subcutaneously into eight-week female NOD/SCID gamma mice (NSG; The Jackson Laboratory, Bar Harbor, ME, USA). At day 11, 3 mice from each lenti-*anti-181a* and lenti-sc group were sacrificed and tumors were weighed. At day 23, 3 mice from each lenti-sc and lenti-*181a* group were sacrificed and tumors were weighed.

For the functional study six-week-old NSG mice were injected with 0.15 million lenti-virally transduced MV4-11 cells intravenously through a tail vein (n=6 in each group: lenti-*anti-181a*, lenti-sc and lenti-*181a*).

For the therapeutic study six-week-old NSG mice were injected with 0.3 million MV4-11 cells intravenously through a tail vein. The treatment started 10 days after the engraftment. Mice were treated with saline (n=11), Tf-NP-scramble

(n=11) or Tf-NP-*miR-181a* (n=11; 1.5 mg/kg/d of miR molecules intravenously on Monday, Wednesday and Friday). Randomly 3 mice of each group were sacrificed after 8 doses of treatment for pathology and biomarker analysis. The treatment was continued for the remaining mice.

4.2.11 Statistical analysis

Data are presented as mean ±SD of at least 3 independent experiments and analyzed by the 2-tailed Student t test. The mean and SD were calculated and displayed in bar graphs as the height and the corresponding error bar, respectively. Mouse survival was calculated using the Kaplan–Meier method, and survival curves were compared by the log-rank test.

4.3 Results

4.3.1 Tumor suppressor role of miR-181a in AML

We previously reported that chemotherapy-treated AML patients with higher *miR-181a* expression achieved complete remission (CR) more frequently and had longer survivals compared to lower *miR-181a* expressing patients (*37, 79*). In line with these clinical observations we and others showed that *miR-181a* expression was associated with higher cytarabine sensitivity in AML cell-lines (*66, 239*).

These findings led us to postulate a putative tumor suppressor activity of *miR-181a* that we first tested by overexpressing or knocking-down *miR-181a* in an AML cell line MV4-11 by lentiviral infection (Figure 4.3A). Overexpression of *miR-181a* (lenti-*181a*) inhibited cell growth (Figure 4.3B; lenti-*181a* vs. lenti-sc:

P=0.009), whereas downregulation of *miR-181a* (lenti-*anti-181a*) enhanced cell proliferation, compared to cells transfected with a vector carrying a scramble sequence (lenti-sc) (Figure 4.3B; lenti-sc vs. lenti-*anti-181a*: *P*=0.028). We next engrafted 5×10^6 virally transduced MV4-11 cells into NOD/SCID mice subcutaneously (n=3 in each group). On day 11, the average tumor weights for animals engrafted with the lenti-*anti-181a* and lenti-sc transduced cells were 1.642±0.65 g and 0.076±0.022 g, respectively (Figure 4.3C). No tumor growth was evident in animals engrafted with lenti-*181a* transduced cells. On day 23, the average tumor weights for the lenti-sc and the lenti-*181a* transduced cell-engrafted groups were 0.65±0.49 g and 0.037±0.025 g, respectively (Figure 4.3C).

To further support the putative tumor suppressor activity of *miR-181a*, we engrafted NSG mice with virally transduced MV4-11 cells through a tail vein. The median survival for the animals engrafted with the lenti-*miR-181a*, lenti-sc and lenti-*anti-181a* transduced cells were 43 days, 33.5 days and 28.5 days, respectively (Figure 4.4A). Compared to the control group (lenti-sc), the lenti-*anti-181a* mice lived significantly shorter (*P*=0.002, log-rank test) and lenti-*miR-181a* mice significantly longer (*P*=0.02). Though the mice in three groups showed survival time differences, they all died from AML-like disease (Figure 4.4B).

Thus, we conclude that higher *miR-181a* expression leads to a less aggressive AML phenotype thereby validating the previously reported clinical prognostic results (*37, 79, 221*).

4.3.2 KRAS, NRAS and MAPK1 are the direct targets of *miR-181a*

The RAS-MAPK1 and RAS-AKT-pathways are often aberrantly activated in AML, and are known to contribute to myeloid leukemogenesis (*222-236*). *KRAS* has been shown to be a direct target of *miR-181a* in oral squamous cell carcinoma (*237*). Here we first tested whether *KRAS* and other genes involved in these pathways, including *NRAS* and its downstream effectors, were *miR-181a* targets in AML. Utilizing *in silico* tools (www.targetscan.org and http://diana.imis.athena-innovation.gr/) we first identified putative *miR-181a*-binding sites in the 3′-untranslated regions (3′-UTRs) of *KRAS*, *NRAS* and *MAPK1*. For *HRAS*, a gene rarely associated with AML, we could not identify putative *miR-181a* binding sites. We then tested whether *miR-181a* was able to reduce the expression of these genes in AML cells. *miR-181a* overexpression by a lenti-*181a* reduced KRAS, NRAS, and MAPK1 protein levels 5.2, 2.1, and 6.5-fold, respectively, compared to scramble expressing controls in MV4-11 cells (Figure 4.5A). Consistent with these results, knock-down of *miR-181a* by a lenti-*anti-181a* increased KRAS, NRAS and MAPK1 1.5, 1.5 and 1.8-fold compared to scramble controls (Figure 4.5A).

Next we showed that the modulation of KRAS, NRAS and MAPK1 expression by *miR-181a* was a result of the binding of the miR to the predicted binding sites in the respective 3′-UTRs. We first validated *KRAS* as a direct *miR-181a* target. We identified two *miR-181a*-binding sites in the *KRAS* 3′-UTR and observed a 28±4% (±Standard Deviation [SD]; *P*=0.003) and a 25±1% (±SD; *P*=0.007) downregulation of luciferase activity on site 1 and site 2 after co-transfecting

293T cells with *miR-181a* compared with scramble expressing controls (Figure 4.5B). Mutations in the seed sequences of the *KRAS* 3′-UTRs rescued the *miR-181a*-induced downregulation (Figure 4.5B). Next, to demonstrate that *NRAS* is also a direct *miR-181a* target, we cloned the predicted *miR-181a*-binding-site in the *NRAS* 3′-UTR into a luciferase reporter and we observed a 26±6% (P<0.0001) downregulation of luciferase activity (Figure 4.5C). An introduced mutation in the seed sequence rescued the *miR-181a*-induced downregulation (Figure 4.5C). We also identified two putative *miR-181a* binding sites in the *MAPK1* 3′-UTR. Due to the short distance between the two binding sites (149 base pairs), we cloned the two binding sites into the same luciferase reporter construct. We observed a 33±2% (±SD; P=0.0002) downregulation of luciferase activity with *miR-181a* treatment compared to cells with scramble control treatment (Figure 4.5D). When mutated the two sites separately, we still observed a 13±3% (±SD; P=0.004) and a 15±3% (±SD; P=0.006) *miR-181a*-induced downregulation of the luciferase activity respectively in site 1 and site 2 (Figure 4.5D). In contrast, mutations on both sites of *MAPK1* could completely rescue the *miR-181a*-induced downregulation (Figure 4.5D). Collectively these results support that KRAS, NRAS and MAPK1 are direct *miR-181a* targets.

4.3.3 Delivery of synthetic *miR-181a* mimic by transferrin conjugated nanoparticles enhances *miR-181a* levels and inhibited RAS-dependent signaling pathways in AML

Since higher *miR-181a* levels associate with improved outcomes in AML and *miR-181a* targets the RAS-MAPK1 and RAS-AKT-kinase-pathways, we reasoned that increasing *miR-181a* may have therapeutic value in AML. We have previously demonstrated the successful delivery of microRNAs to AML blasts by utilizing transferrin (Tf)-targeted anionic lipid-based lipopolyplex nanoparticles (NP) (*238*). Here we used a similar approach to deliver synthetic *miR-181a* mimics to AML cells. Following treatment with Tf-NPs encapsulating *miR-181a* double-stranded mimic molecules (Tf-NP-*miR-181a*; 10 nM) or scramble control molecules (Tf-NP-sc; 10 nM), levels of mature *miR-181a* levels were measured by qRT-PCR in KG1a, OCI-AML3 and MV4-11 cells (all of which have activated RAS by mutations or aberrantly activated upstream members of the pathway; Figure 4.1 and 4.2). After 24 hours exposure, mature *miR-181a* levels increased 211±31, 880±10 and 142±10-fold in KG1a, OCI-AML3 and MV4-11, respectively, while levels of *miR-181b* and unrelated *miR-140* remained unchanged (Figure 4.6).

Having shown that the Tf-NP-delivery-system was able to successfully deliver *miR-181a* to AML blasts, we next tested the impact of Tf-NP-*miR-181a* on RAS activity. First, we found that the delivered synthetic *miR-181a* was functional, as it downregulated KRAS, NRAS and MAPK1 proteins (KG1a: 4.3, 4.4 and 5.5-fold; OCI-AML3: 3.2, 3.9 and 2.2-fold; MV4-11: 1.5, 4.4 and 4.6-fold, respectively)

compared to Tf-NP-scramble treatment (Figure 4.7). Compared to Tf-NP-scramble, Tf-NP-*miR-181a* decreased p-MEK protein by 6.8, 2.2 and 4.5-fold and p-AKT protein by 2.0, 2.5 and 5.7-fold in KG1a, OCI-AML3 and MV4-11 cells, respectively (Figure 4.7). Finally, we assessed the expression of the oncogenic transcription factor MYC, whose protein stability is known to be enhanced by the RAS-MAPK1 phosphorylation pathway (*240*). There was a 4.8, 4.3 and 7.8-fold reduction of MYC protein in KG1a, OCI-AML3 and MV4-11 treated with Tf-NP-*miR-181a* compared to those treated with Tf-NP-scramble control (Figure 4.7).

To validate these results, we treated primary AML blasts from three AML patients (Patient No 1-3; details of the patients in Table 4.2; all of the analyzed patients had activated RAS; Figure 4.1 and 4.2) with Tf-NP-*miR-181a*. Similar to the results from the AML cell lines we observed an increase of *miR-181a* (Figure 4.8). After 24 hours mature *miR-181a* levels increased 45±4, 35±0.1 and 125±16-fold, respectively, in the three patient blasts samples compared to Tf-NP-scramble treated blasts, while levels of *miR-181b* and unrelated *miR-140* remained unchanged (Figure 4.8). Increased levels of *miR-181a* resulted in decreased protein levels of KRAS, NRAS and MAPK1 in all three treated patient samples by 3.4, 5.5 and 5-fold in patient 1; 6.3, 1.6 and 15-fold in patient 2; and 2.3, 2.4 and 3-fold in patient 3, respectively (Figure 4.9). Downregulation of RAS and MAPK1 resulted in RAS-MAPK1 inhibition, decreased MEK and AKT phosphorylation and decreased MYC levels. We observed a 2, 2.9 and 2.2-fold decrease of p-MEK, 1.8, 8 and 1.7-fold decrease of p-AKT, as well as 4.9, 9 and

3.4-fold decrease of MYC normalized in the three patient blasts treated with Tf-NP-*miR-181a* compared to Tf-NP-scramble treatment (Figure 4.9).

In summary, these results support that Tf-conjugated nanoparticles can effectively deliver *miR-181a* and downregulate KRAS, NRAS and MAPK1, thereby inhibiting the RAS-MAPK1 and RAS-AKT-kinase cascade signaling pathways.

4.3.4 Tf-NP-miR-181a reduced cell growth, impaired colony formation ability and induced apoptosis of AML cells

Next, we demonstrated the anti-leukemic activity of the Tf-NP-*miR-181a* treatment, which led to reduced proliferation of KG1a cells by 40% (P=0.015), OCI-AML3 cells by 25% (P=0.023) and MV4-11 cells by 32% (P<0.0001) after 72 hours compared to Tf-NP-scramble treatment (Figure 4.10A). To validate the RAS-MAPK1 and RAS-AKT-kinase-pathways as relevant anti-leukemic *miR-181a* targets, we treated KG1a and MV4-11 cells with Tf-NP loaded with siRNAs for *KRAS*, *NRAS* and *MAPK1* (Figure 4.11A). Following this treatment we observed a similar anti-leukemic effect. The combined siRNAs treatment reduced proliferation of KG1a cells by 32% and MV4-11 cells by 30% compared with scramble siRNA treatment (Figure 4.11B). We also observed more than 50% reduction of colony formation following Tf-NP-*miR-181a* treatment in the three cell lines after 2 weeks (Figure 4.10B). The average number of colonies formed with mock treatment (buffer only), Tf-NP-scramble control and Tf-NP-*miR-181a* treatment were 145±7 (±SD), 145±11 and 44±3 (P=0.0002 compared to Tf-NP-

scramble) for KG1a, 176±11, 172±8 and 80±6 (*P*<0.0001 compared to Tf-NP-scramble) for OCI-AML3 and 217±42, 180±17 and 82±15 (*P*=0.0001 compared to Tf-NP-scramble) for MV4-11, respectively.

Treatment with Tf-NP-*miR-181a* induced apoptosis in both MV4-11 (28.69±5.88% vs. 15.92±0.7% annexin V+, *P*=0.02) and OCI-AML3 cells (20.15±2.58% vs. 8.54±1.42% annexin V+, *P*<0.0001) compared to Tf-NP-scramble treatment at 96 hours (Figure 4.12A and C). In addition, after 24 hours of priming cells with *miR-181a*, DNR was added to treat the cells for another 72 hours. We observed that *miR-181a* treatment enhanced the apoptotic effect of DNR in both cell lines, MV4-11 (*miR-181a*->0.01μM DNR: 45.27±5.99% vs. scramble->0.01μM DNR: 22.88±4.61% annexin V+, *P*=0.001) and OCI-AML3 (*miR-181a*->0.04μM DNR: 70.92±5.01% vs. scramble->0.04μM DNR: 53.25±7.06% annexin V+, *P*=0.02; Figure 4.12B and C). We then validated our observation in primary patient blasts. Tf-NP-*miR-181a* alone induced apoptosis in all four treated patient blast samples compared to the respective Tf-NP-scramble control (patient 1: 17.04±4.22% vs. 6.66±1.73% annexin V+, *P*=0.03; patient 2: 58.53±0.81% vs. 35.73±2.41% annexin V+, *P*=0.01; patient 3: 20.86±1.55% vs. 10.32±1.1% annexin V+, *P*=0.025; patient 4: 39.28±4.19% vs. 26.70±2.95% annexin V+, *P*=0.006; Figure 4.13A and C). When exposed to DNR for 72 hours, the *miR-181a*-overexpressing cells exhibited increased apoptosis compared with control cells (patient 1 exposed to 0.04 μM DNR: 27.28±0.87% vs. 14.75±1.36% annexin V+, *P*=0.01; patient 2 exposed to 0.01 μM DNR: 75.16±0.71 vs. 55.91±2.42% annexin V+, *P*=0.006; patient 3 exposed to 0.04 μM DNR: 57.61±3.77% vs. 43.99±4.7%

annexin V+, *P*=0.03; patient 4 exposed to 0.01 μM DNR: 51.61±0.68% vs. 28.06±3.42% annexin V+, *P*=0.005) (Figure 4.13B and C).

4.3.5 Systemic delivery of Tf-NP-miR-181a had therapeutic effect in an AML mouse model

Next, we examined the anti-leukemic activity of Tf-NP-*miR-181a in vivo*. Saline (control), Tf-NP-scramble or Tf-NP-*miR-181a* were administrated (1.5 mg/kg/d miR on Monday, Wednesday and Friday per week) through a tail vain 10 days after the engraftment of MV4-11 cells in NSG mice Randomly three mice from each group (i.e. of the saline, Tf-NP-scramble or Tf-NP-*miR-181a* treated group) were sacrificed after eight treatment doses. The spleen weights were measured and resulted in 187.3±25.93 mg (±SD), 174.3±13.65 mg and 77±50 mg (vs. Tf-NP-sc; *P*=0.03) in the saline, Tf-NP-scramble and Tf-NP-*miR-181a* group, respectively (Figure 4.14). Cytospins of bone marrow cells and histopathology of sternum, spleen and liver sections from MV4-11 cell engrafted mice treated with either saline or Tf-NP-scramble showed extensive infiltration of blast cells. In contrast, cytospins of bone marrow cells and histopathology of sternum, spleen and liver from Tf-NP-*miR-181a* treated leukemic mice were similar to that of the age-matched control groups (Figure 4.15). Thus Tf-NP-*miR-181a* treatment led to a reduction of AML tumor burden.

White blood cells (WBC) showed a 27-fold increase in intracellular mature *miR-181a* levels, as well as a 3-fold decrease in *KRAS*, 2-fold decrease in *NRAS* and 2.2-fold decrease in *MAPK1* at the RNA level in Tf-NP-*miR-181a* treated mice

compared with the Tf-NP-scramble treated group after eight treatment doses (Figure 4.16). In addition, we observed a 2.6-fold increase of *miR-181a* level in bone marrow cells and a 35-fold increase of *miR-181a* in spleen cells in Tf-NP-*miR-181a* treated mice compared to the Tf-NP-scramble treated group. RAS and MAPK1 were downregulated with Tf-NP-*miR-181a* treatment in bone marrow and spleen at the protein level (Figure 4.17 and 4.18).

The median survival time of the remaining mice was 26, 28.5 and 35 days for the saline, Tf-NP-scramble and Tf-NP-*miR-181a* treated group, respectively. Thus Tf-NP-*miR-181a* treatment reduced the disease burden and prolonged the survival of leukemic mice compared to Tf-NP-scramble (*P*=0.0002) or saline (*P*=0.0001) treatment (Figure 4.19).

4.4 Discussion

MicroRNAs have been implicated in leukemogenesis, and the expression levels of several miRs have been shown to impact on the prognosis of AML patients (*37, 64, 67, 78-82, 203, 241-243*). Lower expression of *miR-181a* is associated with worse outcomes in AML patients (*37, 79, 221*). Here we provided evidence that AML cells with reduced levels of *miR-181a* had a more aggressive AML phenotype and validated this clinical observation functionally at the bench.

In other types of cancers *miR-181a* has been associated with both tumor suppressor and oncogene functions (*213-221*), implying context specific effects. While in colorectal cancer (*213*) and patients with lymph-node metastasis in oral squamous cell carcinoma (*214*) a high *miR-181* level seems to associate with

worse clinical outcome, in glioma the miR has tumor suppressor function (*215*). In these brain tumors *miR-181a* was shown to target the anti-apoptotic genes *BCL2* and *MCL1* and downregulated *miR-181a* reduced glucose-deprivation induced apoptosis and caused mitochondrial dysfunction in astrocytes (*215, 244, 245*). The *miR-181*-family has been reported to be an effector in inflammatory response by TNF-α, IL-6, IL-1β, IL-8 and IL-10 (*211, 212, 246-248*). With regard to AML, we previously provided preliminary evidence that *miR-181* may targets elements of the "inflammasome" that ultimately lead to NF-kB activation and leukemia growth, while Li et al. showed that *miR-181* promoted apoptosis, reduced viability and delayed leukemogenesis in MLL-rearranged AML by downregulating the homeobox gene *PBX3* (*221*). However, the mechanisms through which *miR-181a* attenuate disease aggressiveness in AML still remains to be fully understood.

Here we first demonstrated *miR-181a* targets the RAS-MAPK1- and RAS-AKT-pathway that are frequently activated in AML and support leukemia growth (*249-253*). Despite extensive efforts to inhibit these pathways by small molecules, to date this approach has not been very successful and the RAS proteins and the RAS-MAPK1 and RAS-AKT-kinase pathways have often been termed "undruggable" (*254*). Our results however show that the protein level of KRAS and NRAS and MAPK1 can be reduced by utilizing RNA compounds mimicking *miR-181a*. The efficient delivery of *miR-181a* mimics decreased the downstream AKT and MEK phosphorylation and MYC level. The protein stability of MYC is known to be enhanced by the MAPK phosphorylation (*240*). And we did not

identify any *miR-181a* binding-site on MYC sequence. Thus downregulation of MYC by increasing *miR-181a* was probably due to reduced level of phosphorylation of MAPK. In sum, these effects led to an anti-leukemic activity and may support *miR-181a* replacement as an effective RAS targeting strategy not only in AML but also in other RAS-dependent tumors.

The therapeutic advantage of using miR mimics is evident as one miR can simultaneously targeting the cross-talk among multiple, different signal transduction pathways (STPs) (*231*). Indeed, a therapeutic use of the synthetic mimics has been postulated for several types of cancers and is currently being tested in clinical trials (e.g. for *miR-34* in NCT01829971). However, the delivery of miRs remains challenging as these oligonucleotides are subject to rapid hepatic uptake and metabolism and easily degraded by endonucleases in biological matrices. Nevertheless, we recently reported a novel anionic lipopolyplex nanocarrier system that was designed for the purpose of allowing for efficient miR delivery to AML cells (*238*). Here we show that this system could also be adapted to the delivery of *miR-181a* mimics and exert an efficient inhibitory effect on the RAS-MAPK1 and RAS-AKT-kinase pathways thereby resulting in a significant antileukemia activity. As expected, however, the *miR-181a*-NP did not cure the mice from the disease but showed that may specifically enhance malignant cell killing in combination with other effective drugs including chemotherapeutics (I.e., daunorubicin).

Other strategies to increase *miR-181a* have been tested by our group. In a previous study we demonstrated that lenalidomide increases endogenous *miR-*

181a (*66*), by enhancing the expression of C/EBPα isoforms, which bind to the *miR-181a* promoter and induce the transcription of *miR-181a*. However, lenalidomide has several unwanted side-effects at the doses necessary to achieve plasma concentrations at which *miR-181a* was increased. Thus, the targeting NPs that we reported here may present the advantage to be more specifically direct to AML blasts thereby sparing normal tissues and perhaps reducing unwanted toxicity. Our preclinical studies showed encouraging results with no toxicity of in NP-treated mice at doses inducing the anti-leukemic activity (*238*).

In summary, we unveil here a previously unreported activity of *miR-181a* that directly downregulates NRAS, KRAS and MAPK1 and RAS-dependent downstream signals supporting leukemia growth. We proved that a nanoparticle-based delivery system could be used to efficiently increase otherwise low baseline levels of *miR-181a* and achieve anti-leukemic activity in AML models with no evident toxicity. We believe that *miR-181a*-NP may warrant further preclinical evaluation for future clinical application.

4.5 Tables and Figures

Table 4. 1 PCR primers

Primer	**Sequence**
miR-181a-1 Forward	gcgtgctagcCCGATCCTTTTCTCTCATAC
miR-181a-1 Reverse	gcgtggatccGATGGAATATCTGTTGATTG
KRAS S1 Forward	gtgcgaattcactaatttcagttgagaccttc
KRAS S1 Reverse	gtgcgaattctaatagtttccattgccttg
KRAS S1 mutation Forward	catccctgatgTTCgtaaagttac
KRAS S1 mutation Reverse	gtaactttacGAAcatcagggatg
KRAS S2 Forward	gtgcgaattccacagagctaactgggttac
KRAS S2 Reverse	gtgcgaattcgatatgaccaacattcctaggtc
KRAS S2 mutation Forward	catgtttacctggaaCCCattttaac
KRAS S2 mutation Reverse	gttaaaatGGGttccaggtaaacatg
NRAS Forward	gtgcgaattctgagtctatcctagtcttca
NRAS Reverse	gtgcgaattctttcatctttctcctgggaa
NRAS mutation Forward	atccttatgcatgaaatgCCCgtctgag
NRAS mutation Reverse	ctcagacGGGcatttcatgcataaggat
MAPK1 Forward	gtgcgaattcgtactgttggtgccttcttggtat
MAPK1 Reverse	gtgcgaattccaggtgccataaacattcaaataatccatc
MAPK1 S1 mutation Forward	ggaagattttattaagaatctgTCAAtttattc
MAPK1 S1 mutation Reverse	gaataaaTTGAcagattcttaataaaatcttcc
MAPK1 S2 mutation Reverse	gtgcgaattccaggtgccataaaTTGAcaaataatccatc

Table 4. 2 Characteristics of AML Patients

	Karyotype	*FLT3*-ITD	*NPM1*	*CEBPA*
Pat #1	46, XX	present	mutated	wild-type
Pat #2	46, XX	present	wild-type	wild-type
Pat #3	46, XX	present	wild-type	wild-type
Pat #4	46, XX	present	wild-type	mutated
Pat #5	46,XX	absent	mutated	wild-type
Pat #6	46, XY, inv(16)(p13q22)/46, XY	absent	wild-type	wild-type
Pat #7	46, XY, del(11)(p13p15)/46, XY	absent	wild-type	wild-type
Pat #8	NA	present	mutated	wild-type
Pat #9	complex karyotype	absent	wild-type	wild-type

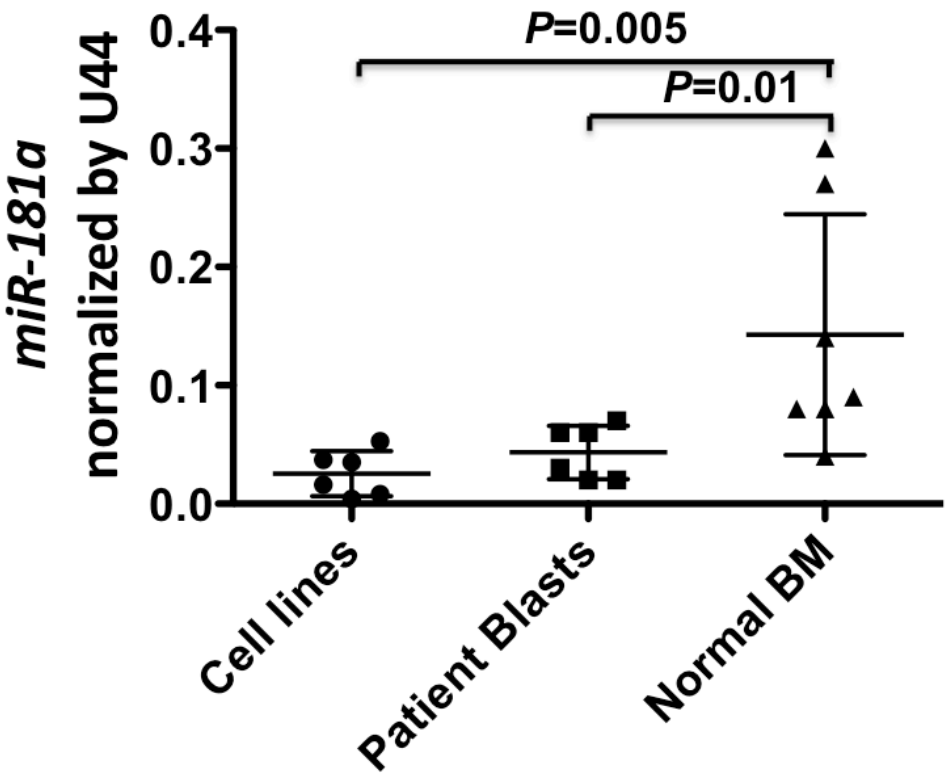

Figure 4. 1 *miR-181a* level in AML cell lines and patient blasts and in normal bone marrow cells.

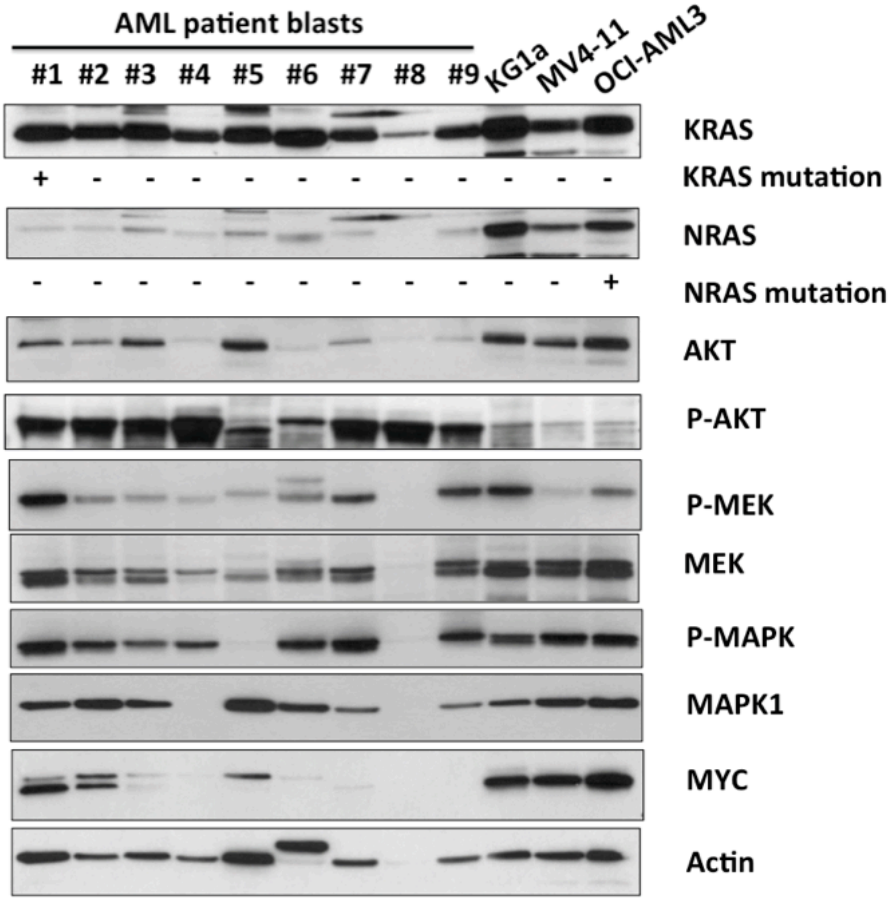

Figure 4. 2 RAS mutations and activation of RAS signaling pathway in AML cells.

KRAS and NRAS mutation status and KRAS, NRAS, p-MEK, MEK, p-AKT, AKT, p-MAPK, MAPK1, and MYC protein expression in blasts cells from nine AML patients and KG1a, OCI-AML3 and MV4-11 cells.

Figure 4. 3 Higher levels of *miR-181a* associated with a less aggressive phenotype in AML cells.

A

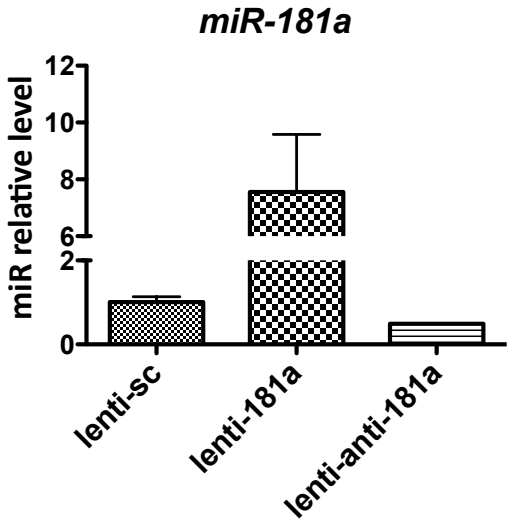

B

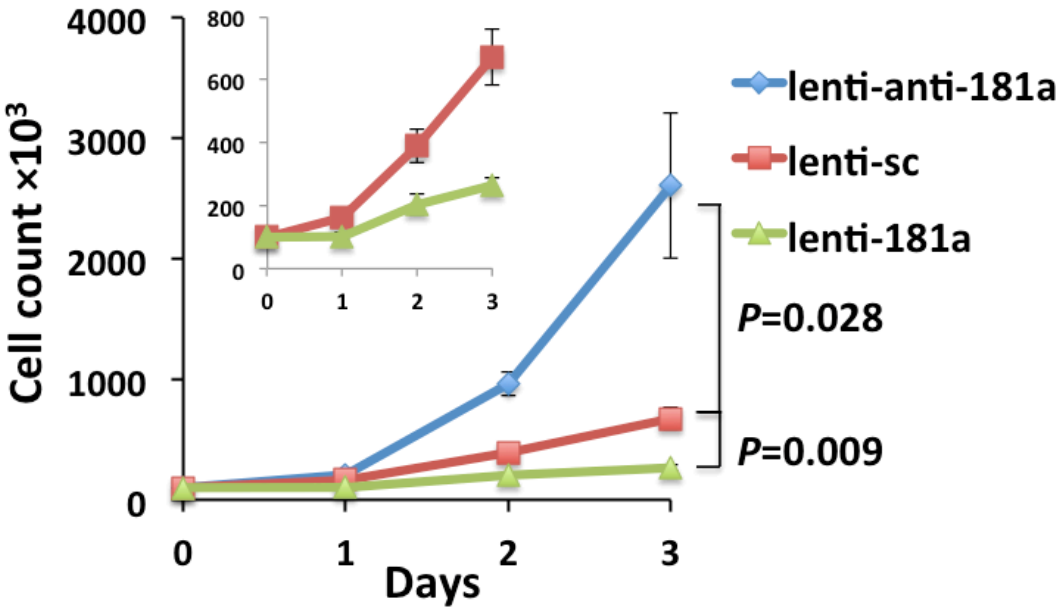

Continued

Figure 4. 3 : Continued

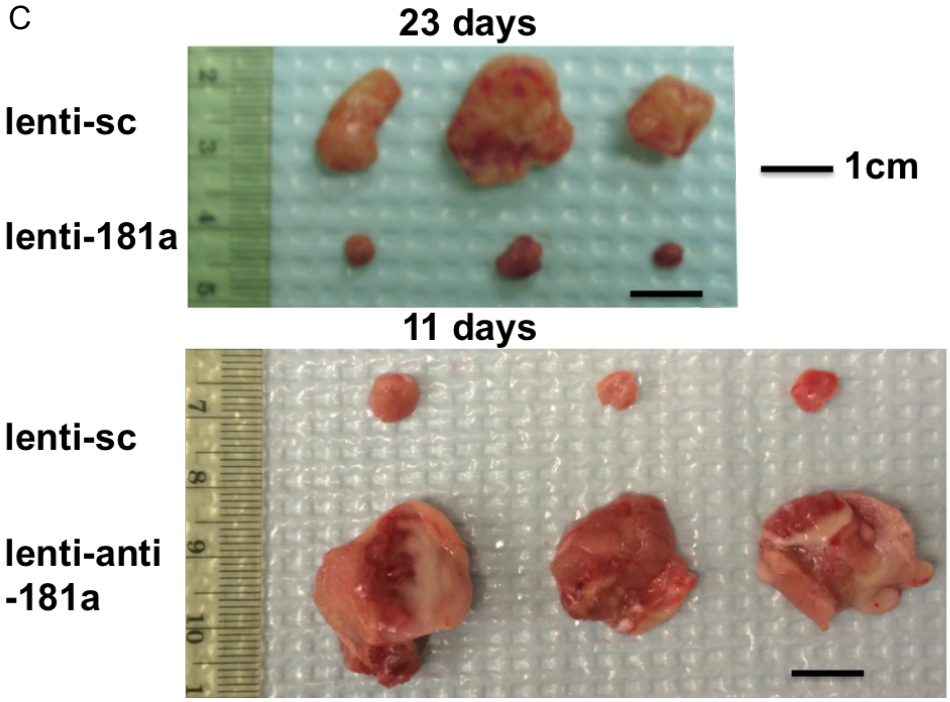

Figure 4. 3: A. *miR-181a* expression of MV4-11 cells transduced with lenti-viral constructs either overexpressing *miR-181a* (lenti-181a), expressing a scramble sequence (lenti-sc; = control) or a knock-down construct of *miR-181a* (lenti-anti-181a). B. growth curve of three groups of lenti-viral infected MV4-11 cells. C. 5 million lenti-viral transduced cells were engrafted subcutaneously in NOD/SCID mice. At day 11, tumors from lenti-anti-181a and lenti-sc group (n=3 in each group) were isolated and weighed (no tumor in lenti-181a group). At day 23, tumors from lenti-181a and lenti-sc group (n=3 in each group) were isolated and weighed.

A

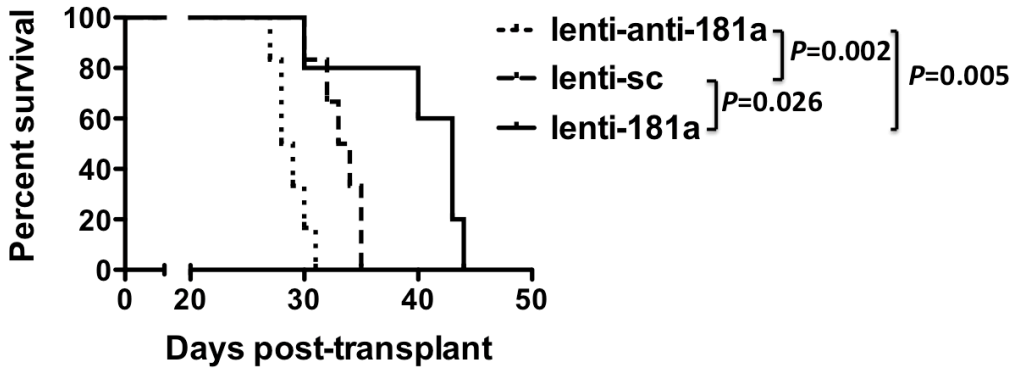

B

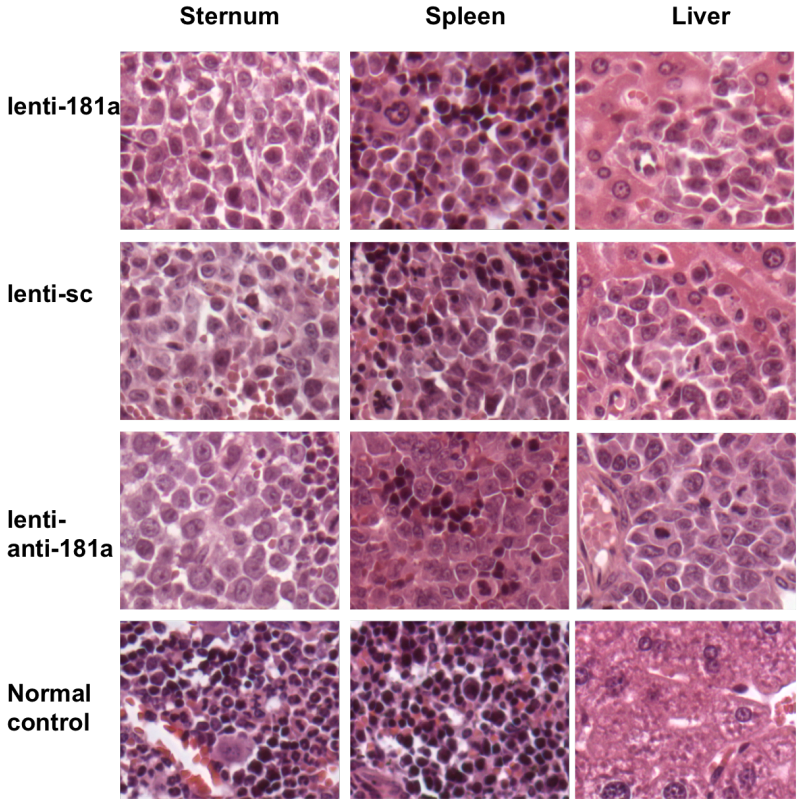

Figure 4. 4 Higher levels of *miR-181a* associated with longer survival in a murine AML model.

A. 1.5 million lenti-viral transduced MV4-11 cells were engrafted into NSG mice. Survival curves of the mice in the three groups. B. H&E staining of sections from sternum, spleen and liver sections of virally transduced-MV4-11 engrafted mice at the end point.

Figure 4. 5 KRAS, NRAS and MAPK1 are direct targets of *miR-181a.*

A

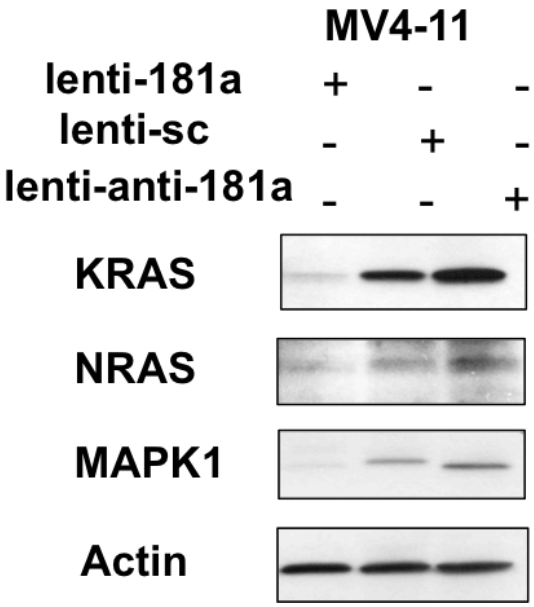

B

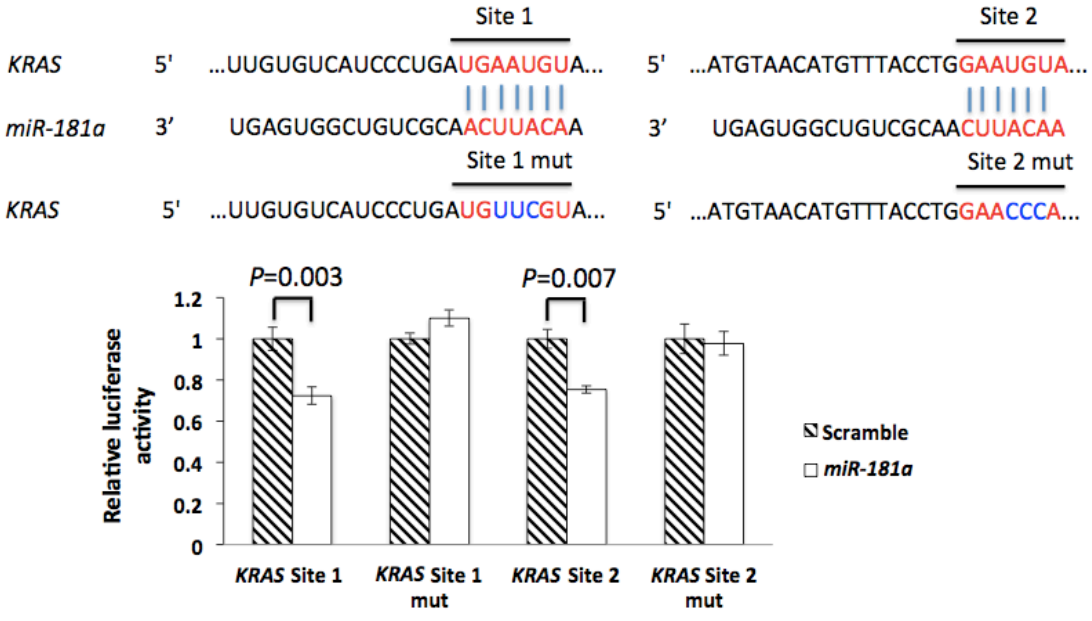

Continued

Figure 4. 5 : Continued

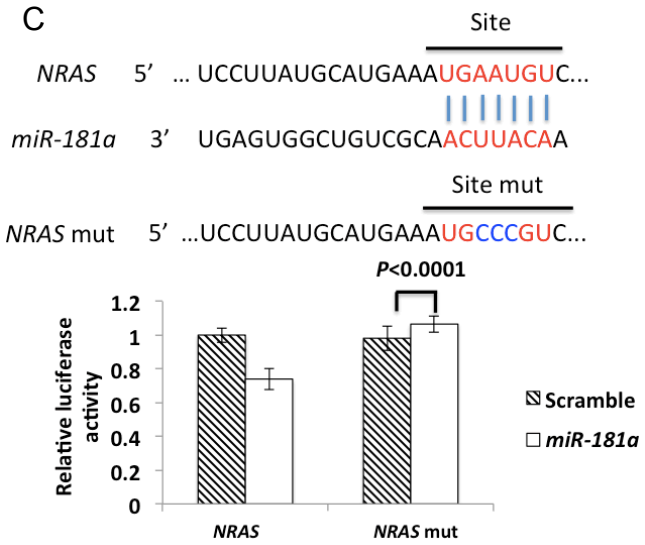

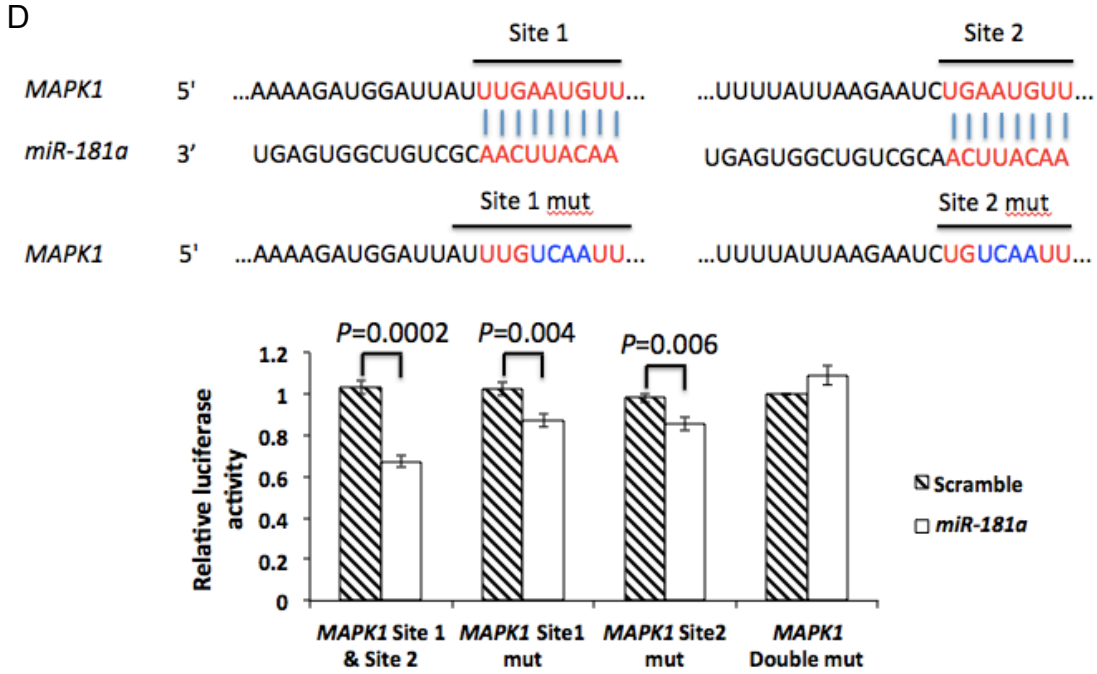

Continued

Figure 4. 5 : Continued

(A) NRAS, KRAS and MAPK1 protein expression in infected MV4-11 with lenti-181a, lenti-sc or lenti-anti-181a. Dual luciferase assays of HEK293T cells co-transfected with firefly luciferase constructs containing the *KRAS* (B), *NRAS* (C) and *MAPK1* (D) wild-type or mutated 3′-UTRs and *miR-181a* mimics or scramble mimics (as controls). The firefly luciferase activity was normalized to Renilla luciferase activity. The data are shown as relative luciferase activity of *miR-181a* mimic transfected cells with the respect to the scramble control of nine data points from three independent transfections. Error bars represent the standard deviation (SD).

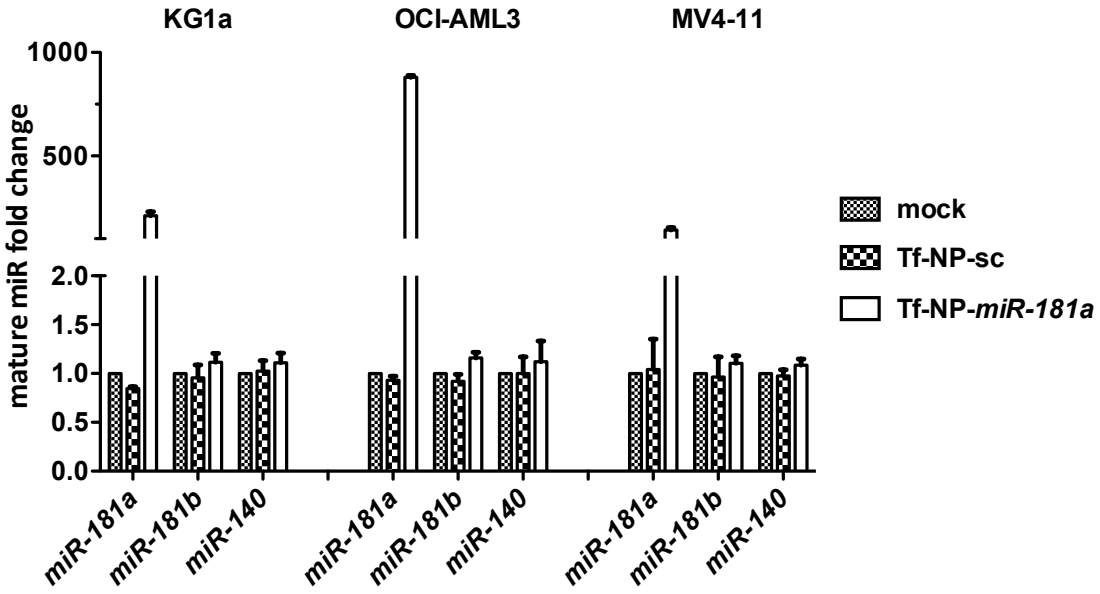

Figure 4. 6 Treatment with Tf-NP-miR-181a increased mature miR-181a level. Mature *miR-181a*, *miR-181b* and *miR-140* expression levels in KG1a, OCI-AML3 and MV4-11 cells treated with mock, Tf-NP-sc and Tf-NP-*miR-181a.*

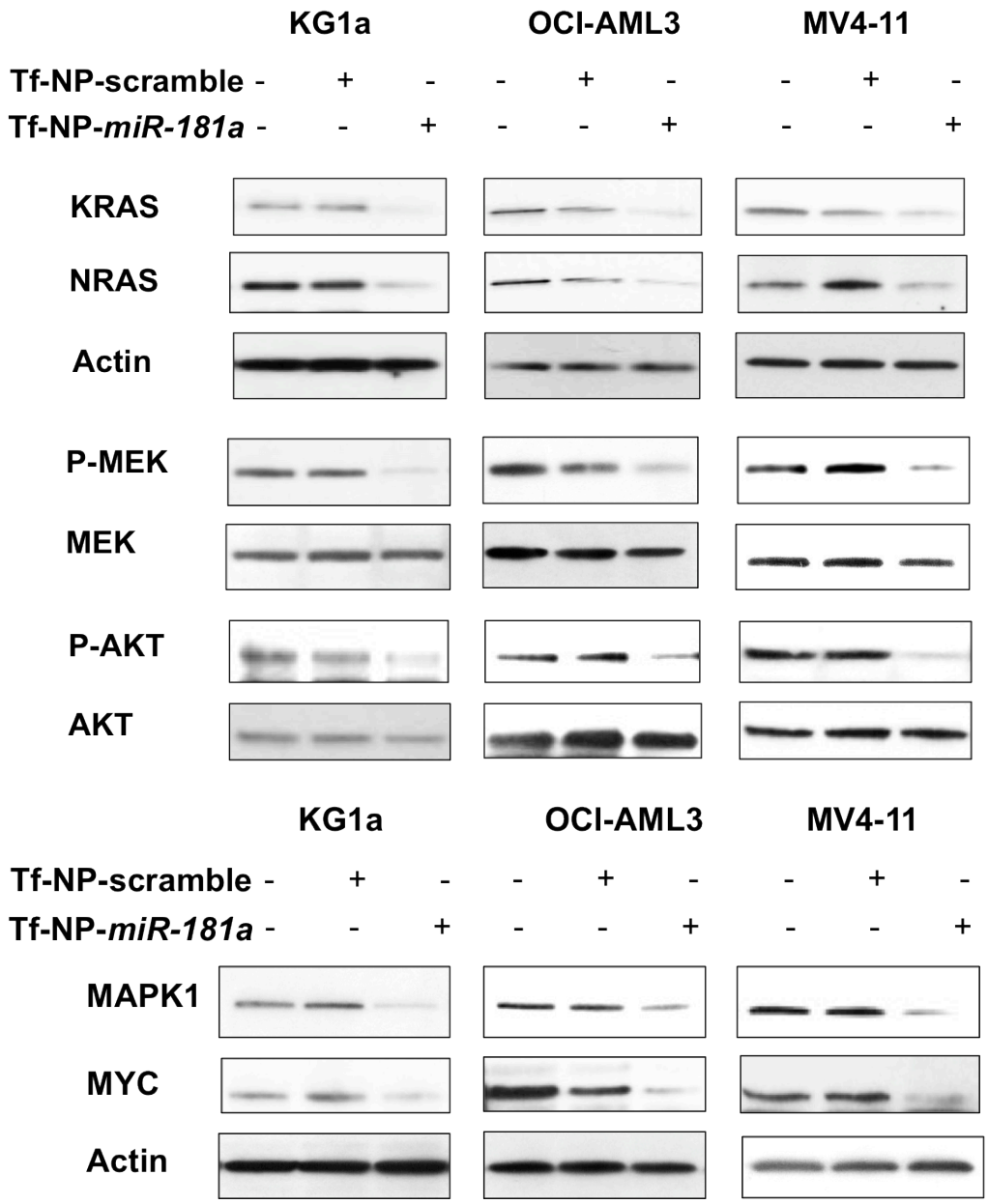

Figure 4. 7 Treatment with Tf-NP-miR-181a downregulated KRAS and NRAS and MAPK1 and inhibited the RAS-MAPK1 signaling pathway in AML cell lines.

NRAS, KRAS, p-MEK, MEK, p-AKT, AKT, MAPK1, and MYC expression in KG1a, OCI-AML3 and MV4-11 cells treated with mock, Tf-NP-sc and Tf-NP-*miR-181a*.

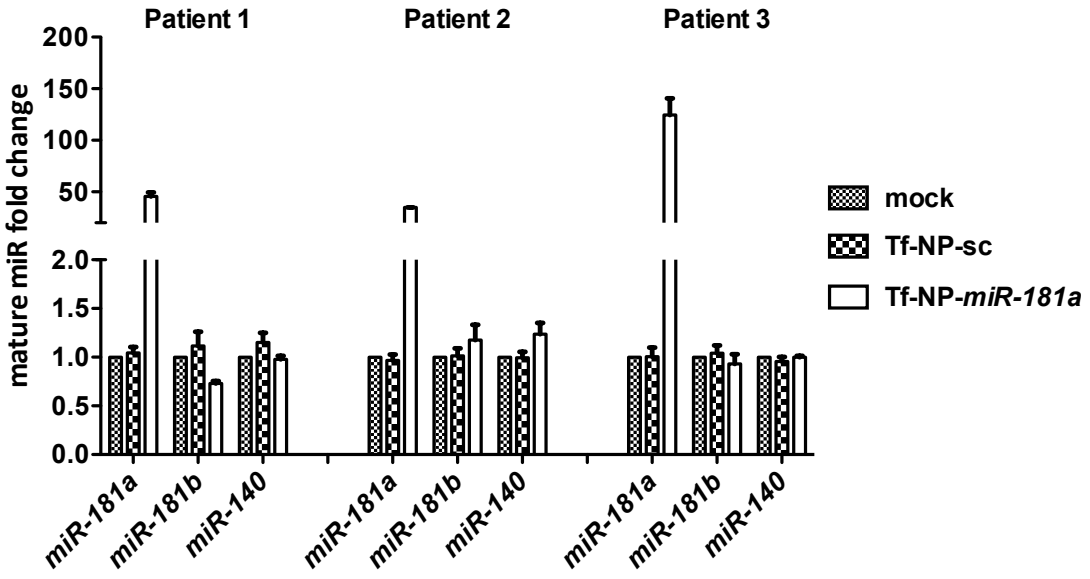

Figure 4. 8 Treatment with Tf-NP-*miR-181a* increased mature *miR-181a* level. Mature *miR-181a*, *miR-181b* and *miR-140* expression levels in primary patient blasts (n=3) treated with mock, Tf-NP-sc and Tf-NP-*miR-181a*.

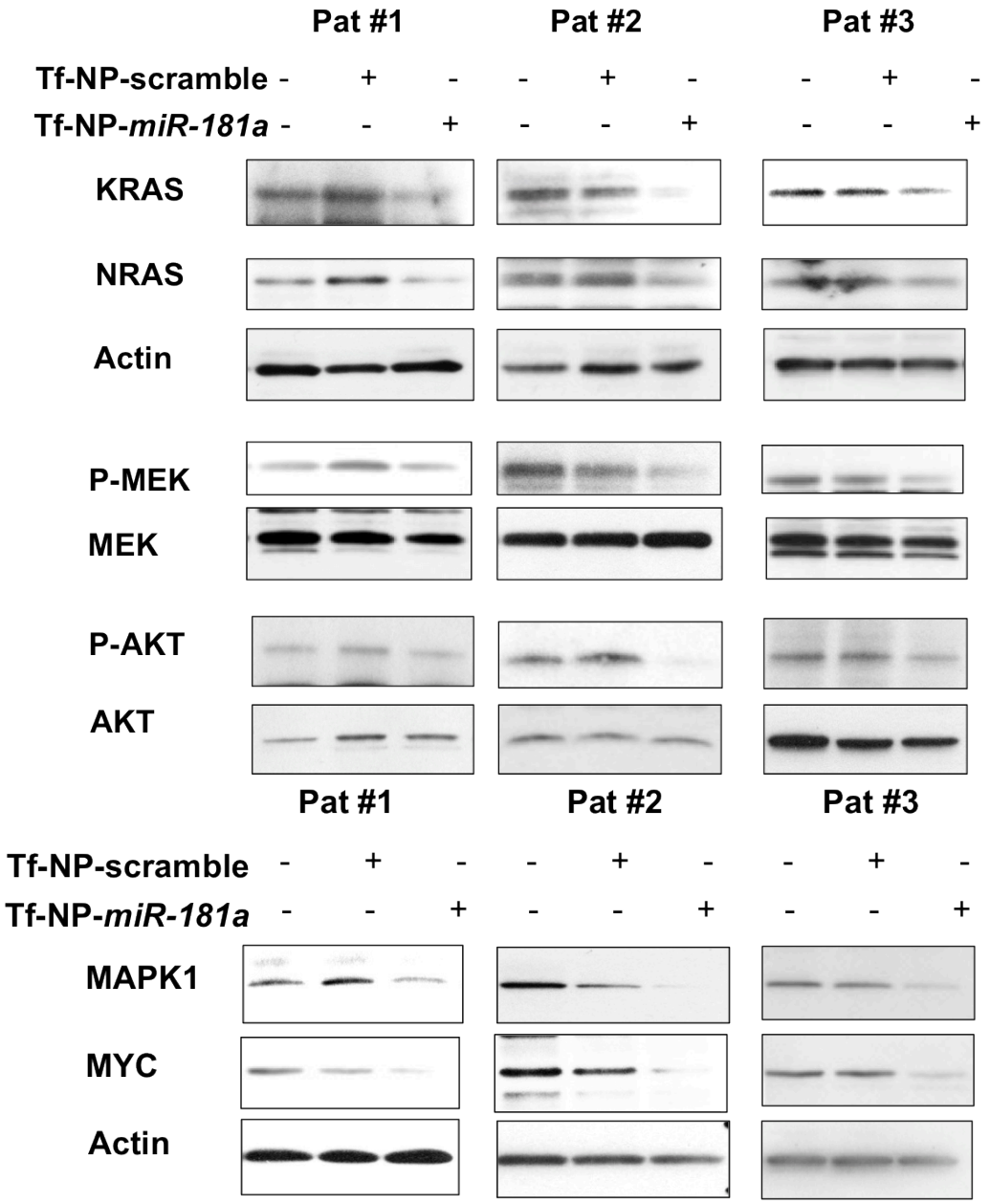

Figure 4. 9 Treatment with Tf-NP-*miR-181a* downregulated KRAS and NRAS and MAPK1 and inhibited the RAS-MAPK1 signaling pathway in AML patient blasts. .

NRAS, KRAS, p-MEK, MEK, p-AKT, AKT, MAPK1, and MYC expression in primary patient blasts (n=3) treated with mock, Tf-NP-sc and Tf-NP-*miR-181a*.

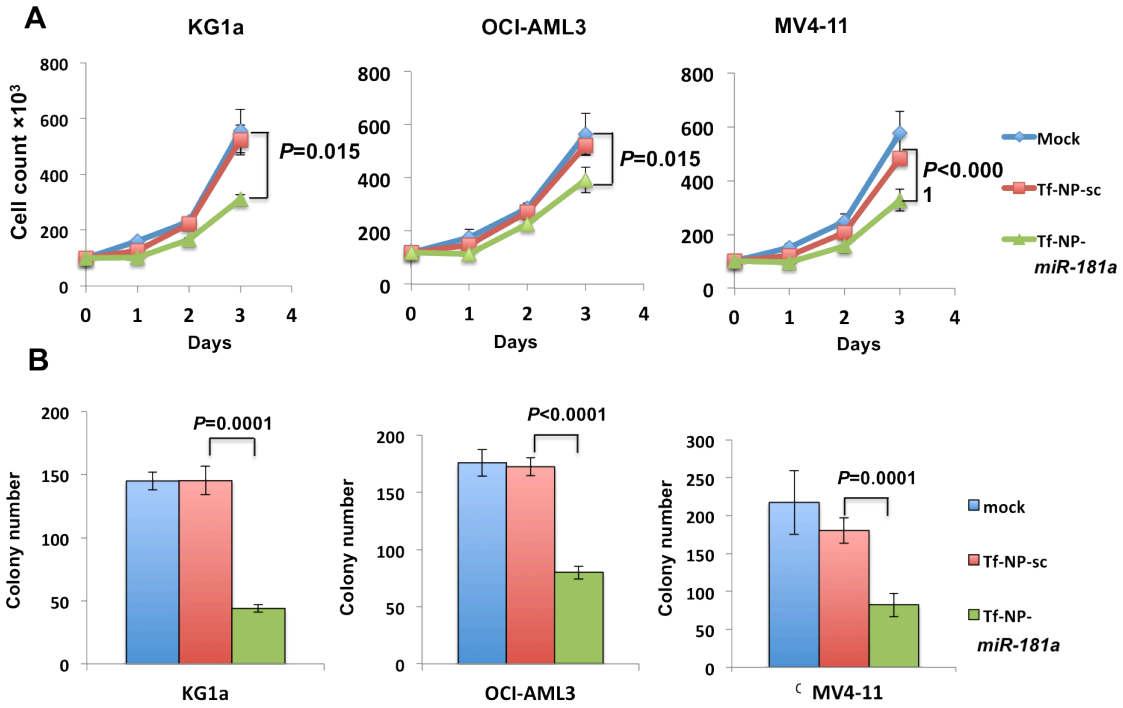

Figure 4. 10 Treatment with Tf-NP-*miR-181a* reduce the proliferation and colony formation in AML cells.

Cell growth curve (A) and colony numbers (B) of KG1a, OCI-AML3 and MV4-11 cells treated with Tf-NP-*miR-181a*, Tf-NP-sc or mock. Error bars represent SD.

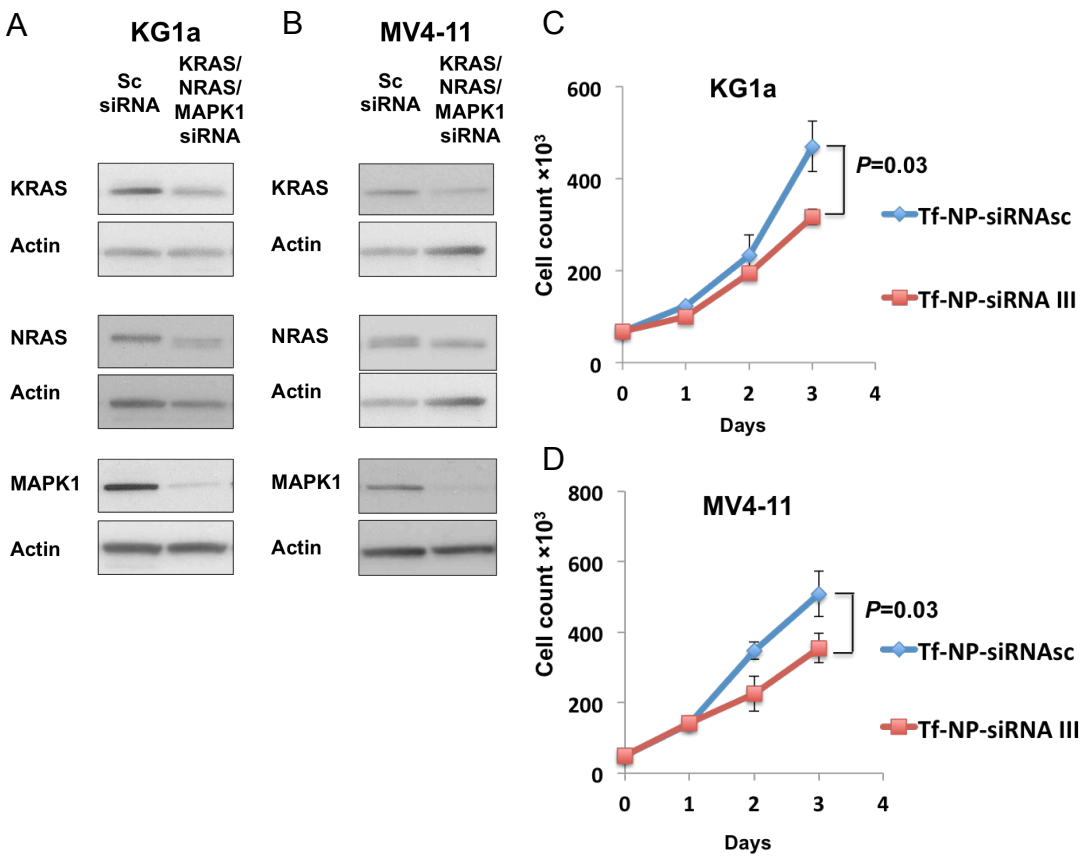

Figure 4. 11 Inhibition of AML cells growth by downregulation of KRAS, NRAS and MAPK1.

Downregulation of KRAS, NRAS and MAPK1 proteins following their respective siRNA treatments in KG1a (A) and MV4-11 (B). Three siRNAs against KRAS, NRAS and MAPK1 (siRNAIII) were equally mixed and encapsulated into Tf-nanoparticles. Two AML cell lines, KG1a and MV4-11 were treated with Tf-NP-siRNAIII at a concentration of 20nM for each KRAS, NRAS and MAPK1 siRNA. 60nM of scramble siRNA contained Tf-NP as a control. Growth curve of KG1a (C) and MV4-11 (D) cell lines after KRAS/NRAS/MAPK1 siRNAs treatments compared with scramble siRNA treatment.

Figure 4. 12 Treatment with Tf-NP-*miR-181a* induced apoptosis and enhanced the effect of daunorubicin (DNR) in AML cell lines.

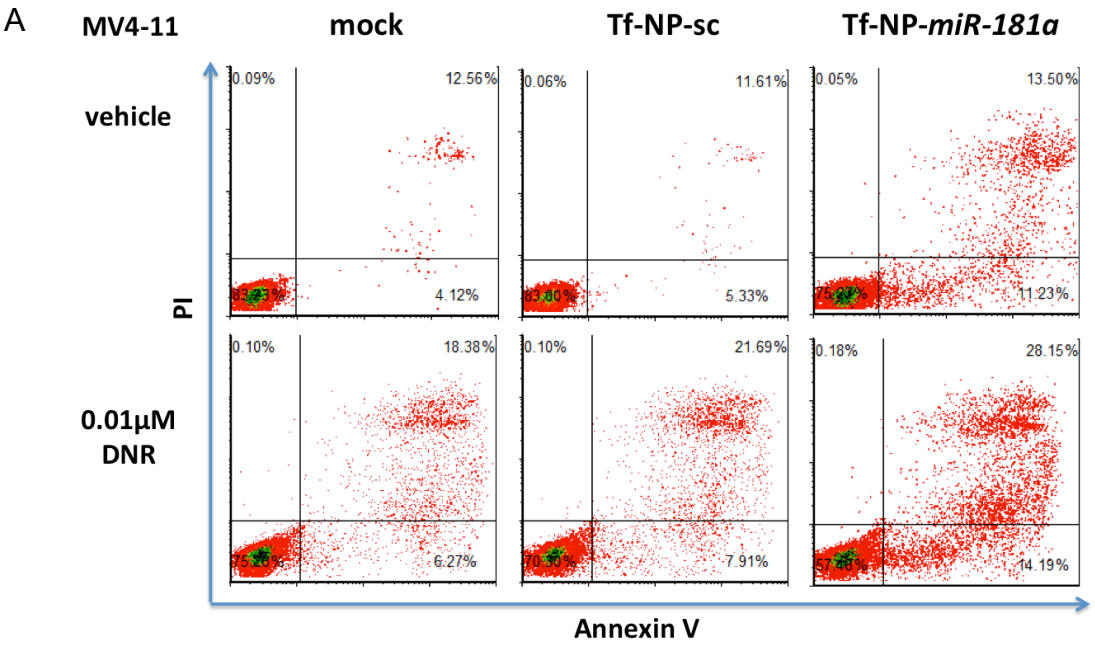

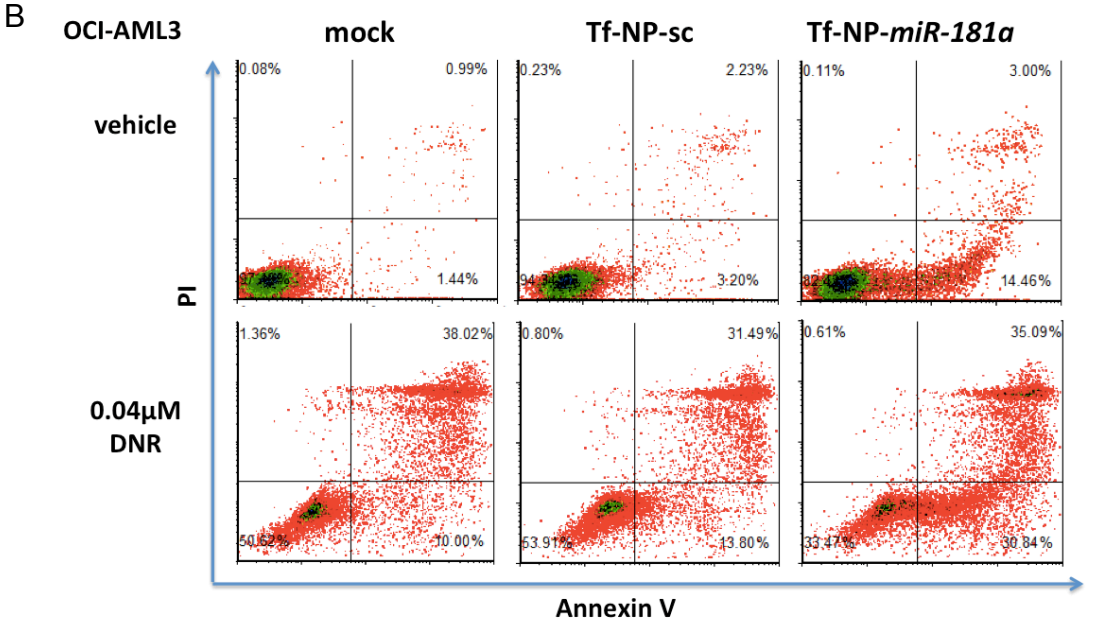

Continued

Figure 4. 12 : Continued

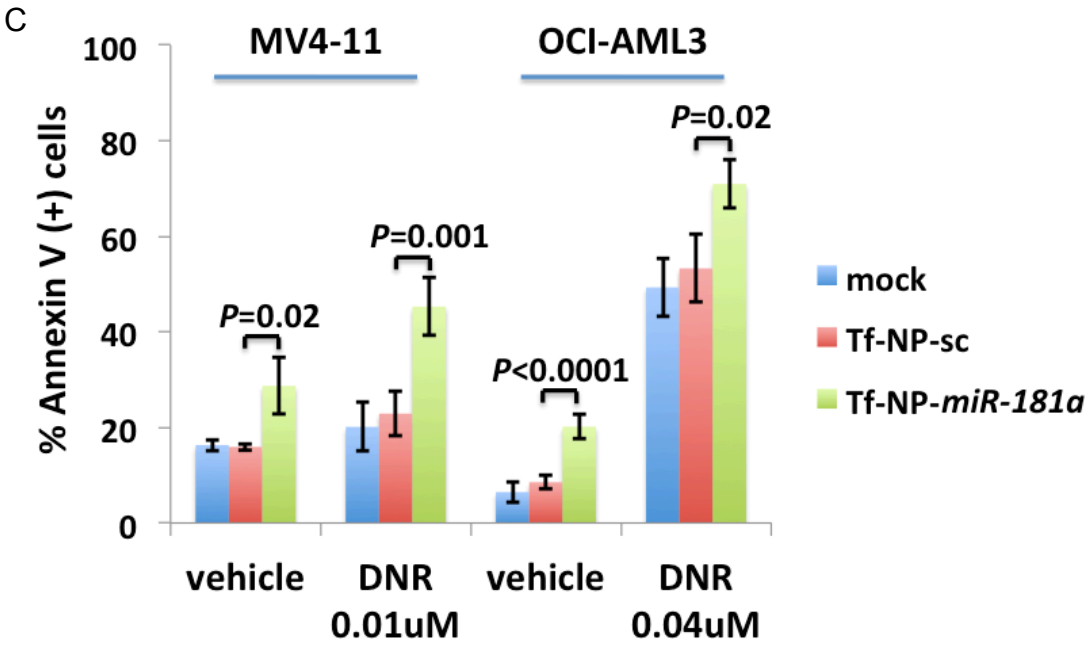

Figure 4. 12: Annexin V assays in MV4-11 (A, C) and OCI-AML3 cells (B, C) treated with Tf-NP-*miR-181a*, Tf-NP-sc or mock in the presence or absence of daunorubicin (DNR, 0.01μM for MV4-11, 0.04μM for OCI-AML3). DNR was added 24 hours after priming cells with nanoparticle-miR treatment for another 72 hours.

Figure 4. 13 Treatment with Tf-NP-*miR-181a* induced apoptosis and enhanced the effect of daunorubicin (DNR) in AML patient blasts.

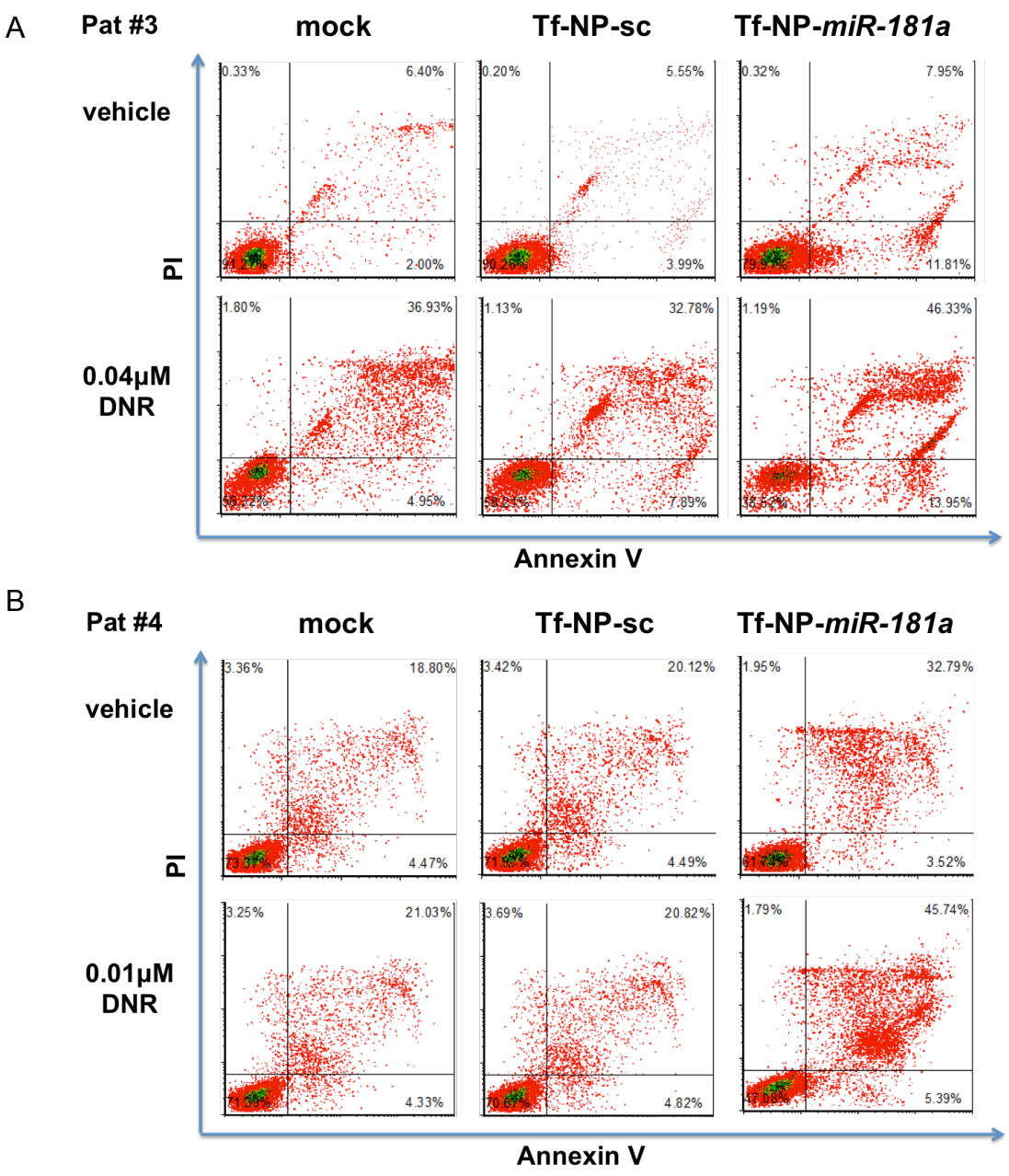

Continued

Figure 4. 13 : continued

C

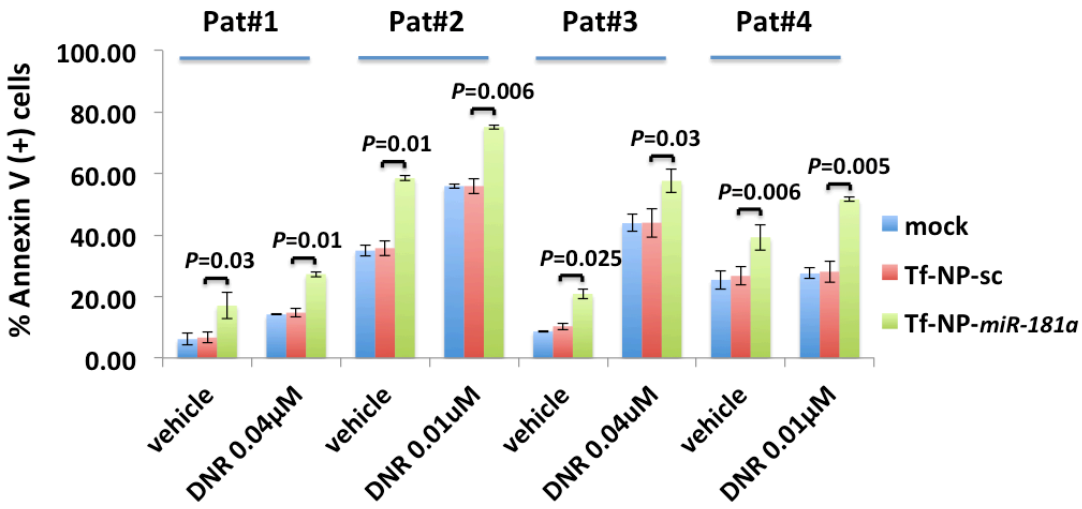

Figure 4. 13: Annexin V assays in patient blast cells (Pat#1 C; Pat#2 C; Pat#3 A and C; Pat#4 B and C) treated with Tf-NP-*miR-181a*, Tf-NP-sc or mock in the presence or absence of daunorubicin (0.01μM for Pat #1 and #3, 0.04μM for Pat #2 and #4 blasts). DNR was added 24 hours after priming cells with nanoparticle-miR treatment for another 72 hours.

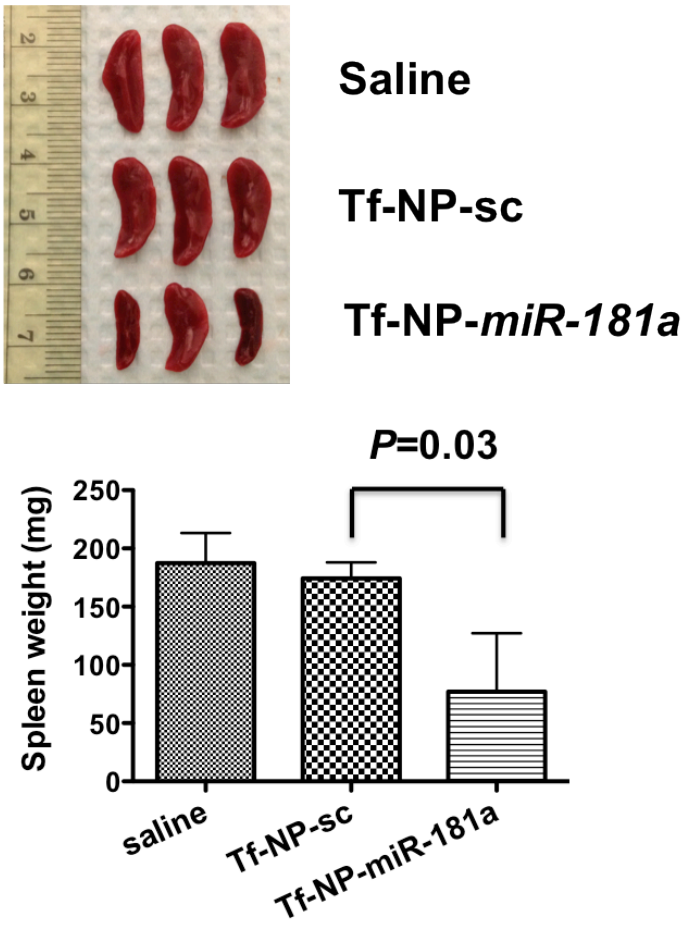

Figure 4. 14 Tf-NP-*miR-181a* treatment slowed the expansion of engrafted AML cells.

Spleens and spleen weights from mice sacrificed after 8 doses of treatment from each group, saline, Tf-NP-sc and Tf-NP-*miR-181a* (n=3).

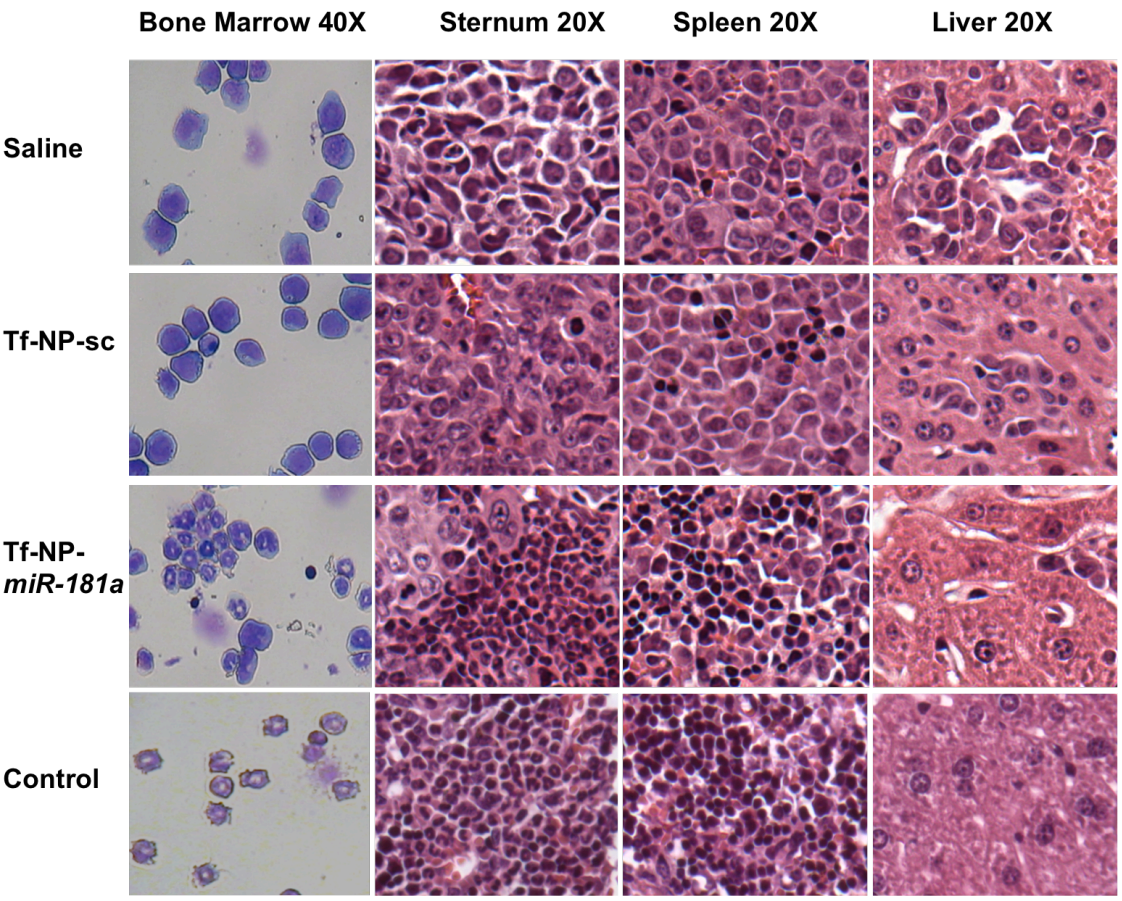

Figure 4. 15 Tf-NP-*miR-181a* treatment reduced AML cells accumulated in bone marrow, spleen and liver.

May-Grumwald/Giemsa staining of bone marrow cells and H&E staining of sections from sternum, spleen and liver of MV4-11 engrafted mice treated with saline, Tf-NP-sc and Tf-NP-*miR-181a*. NSG mice without MV4-11 engraftment were also used as controls.

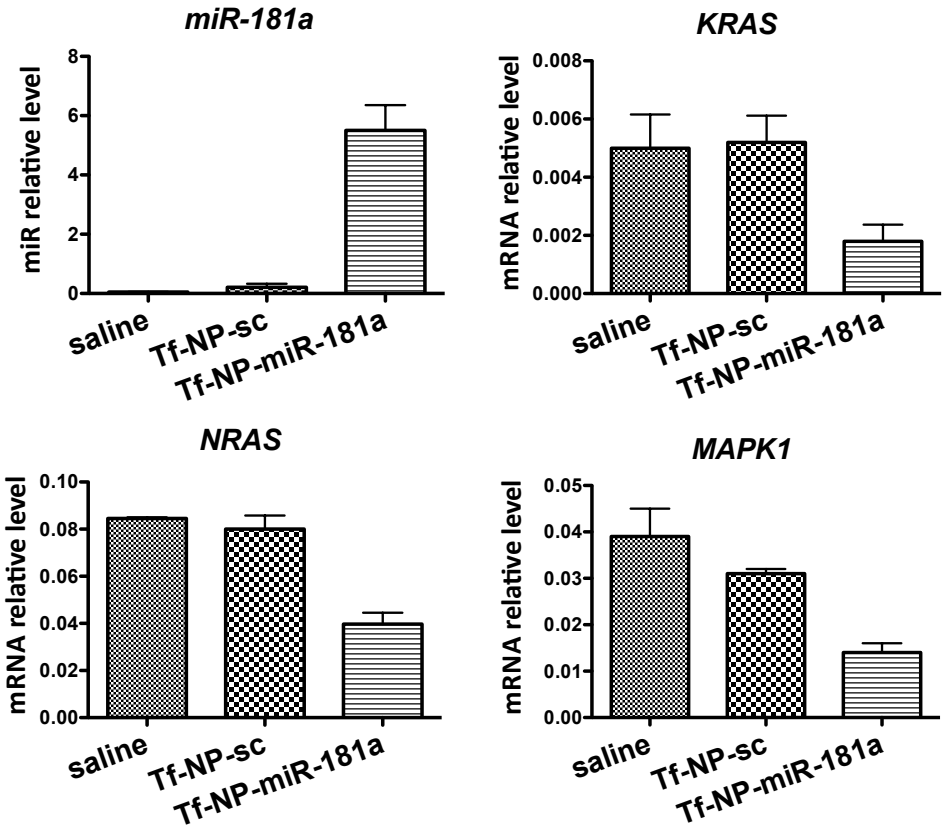

Figure 4. 16 Tf-NP-*miR-181a* treatment increased mature *miR-181a* level and decreased its targets expression in white blood cells (WBC).

Mature *miR-181a* level and *KRAS*, *NRAS* and *MAPK1* RNA level in WBC isolated from the mice after 8 doses of treatment from each group.

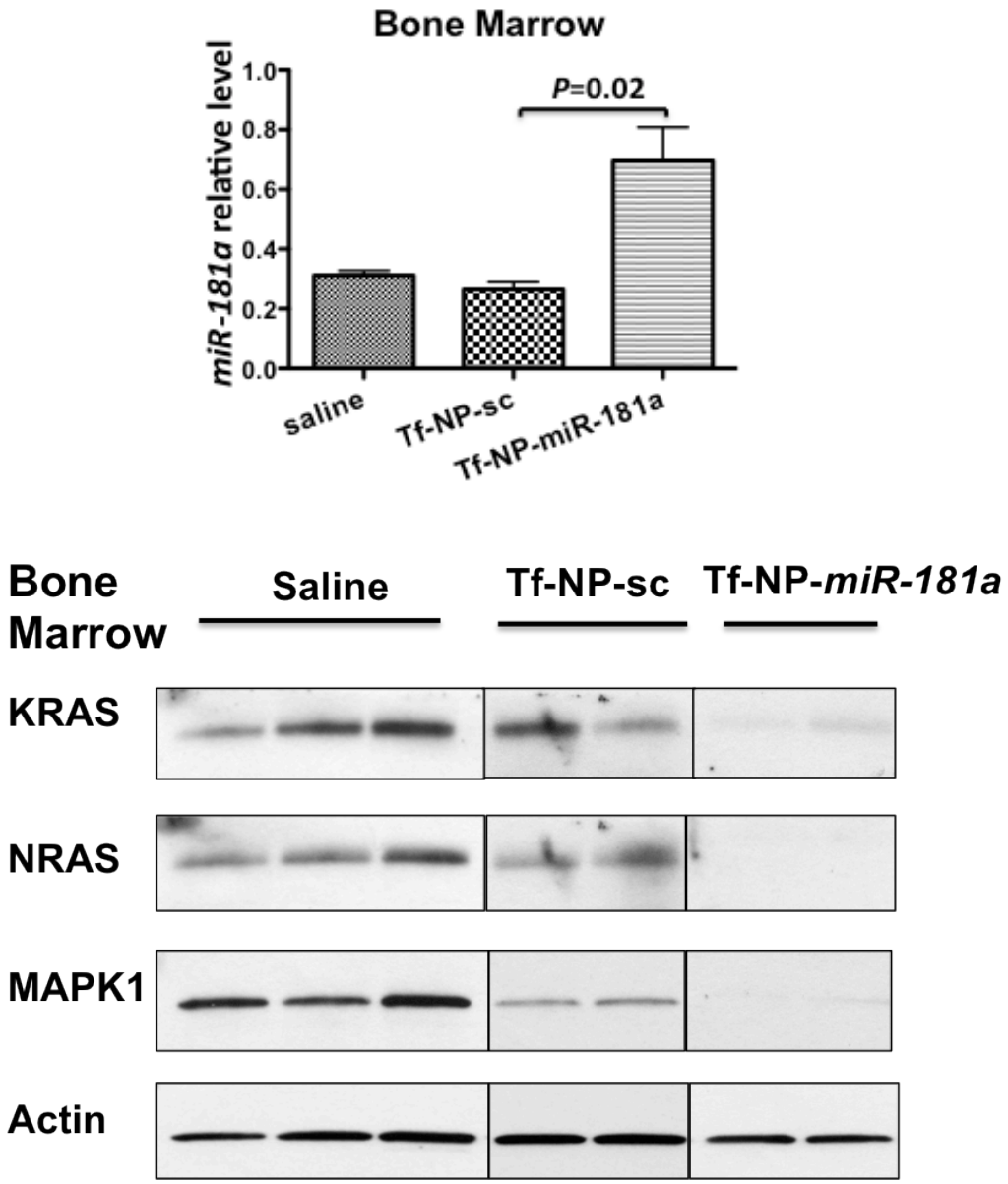

Figure 4. 17 Tf-NP-*miR-181a* treatment increased mature *miR-181a* level and decreased its targets expression in bone marrow.

Mature *miR-181a* level (upper) and KRAS, NRAS and MAPK1 protein expression (bottom) in spleen isolated from the mice after 8 doses of treatment from each group. Error bars represent SD.

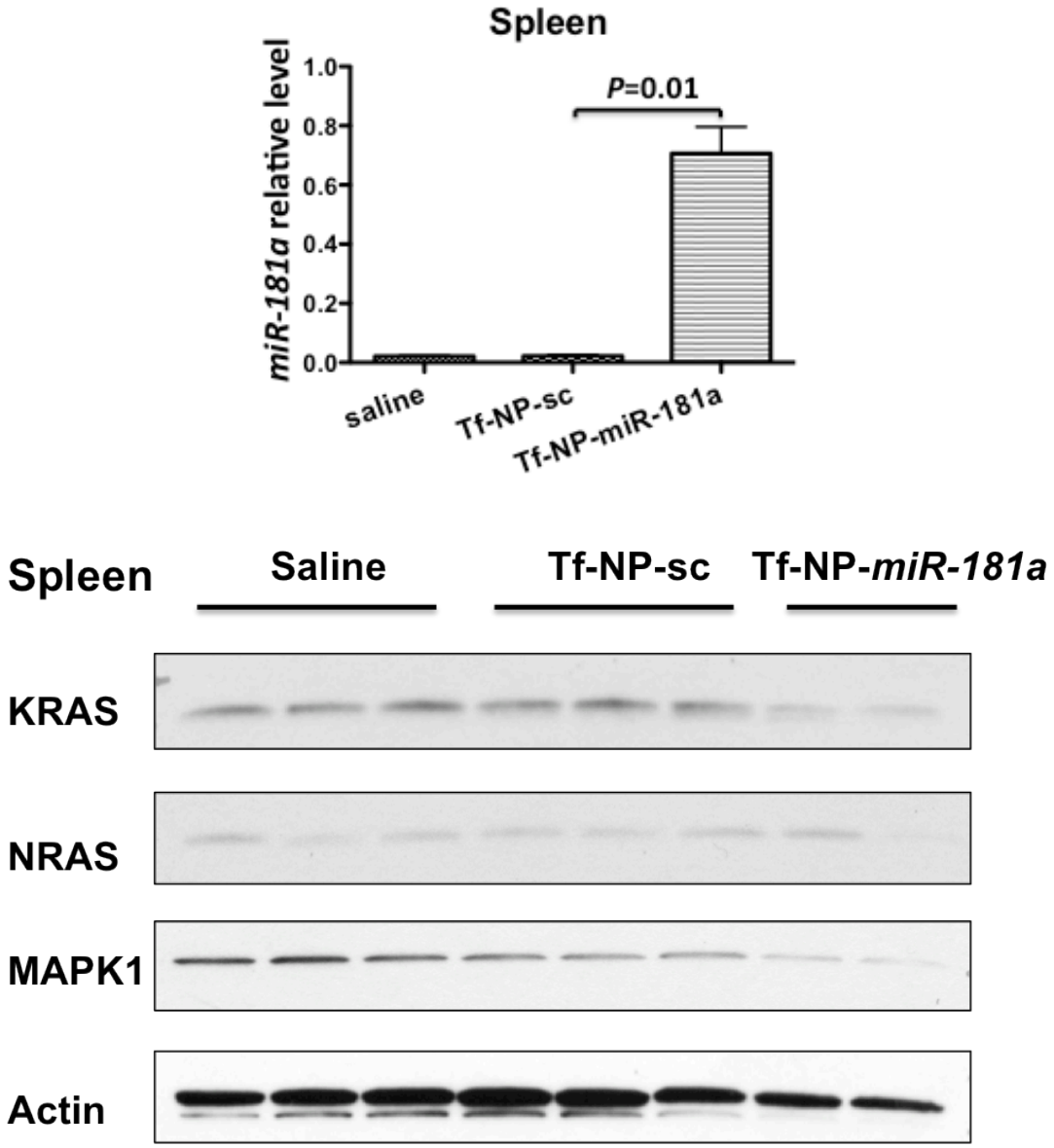

Figure 4. 18 Tf-NP-*miR-181a* treatment increased mature *miR-181a* level and decreased its targets expression in spleen.

Mature *miR-181a* level (upper) and KRAS, NRAS and MAPK1 protein expression (bottom) in spleen isolated from the mice after 8 doses of treatment from each group. Error bars represent SD.

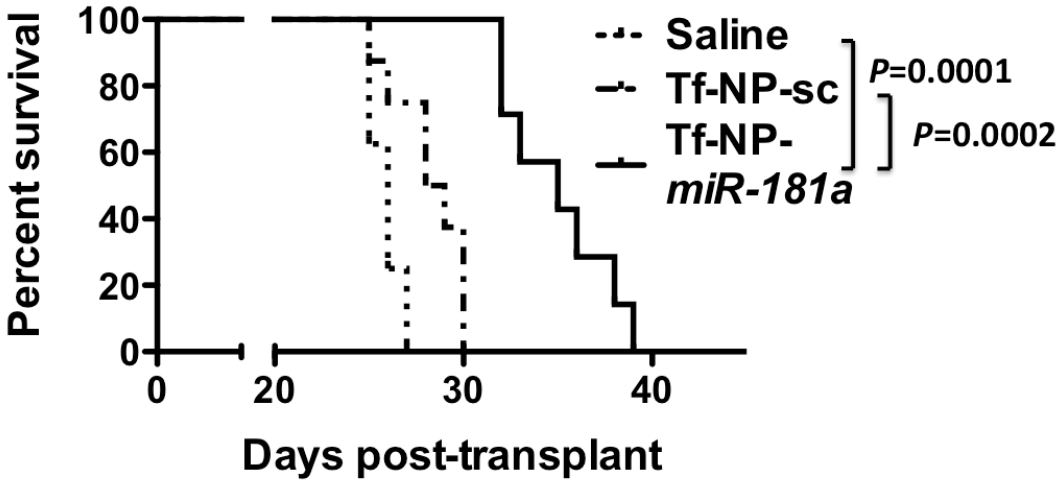

Figure 4. 19 Tf-NP-*miR-181a* treatment prolonged the survival of AML mice.

Survival curve of the mice according to the indicated treatment.

Chapter 5. Summery and Future Direction

By using high-throughput genome-scale technologies, we have learnt more about the complexity and biological heterogeneity of AML. The importance of miRNA increase not only our basic knowledge about the pathology of leukemias but also their therapeutic potentials. Some pitfalls that could be encountered in clinical translation include dosage, efficacy, functionality, delivery, nonspecific toxicity and immune activation (*84, 85*).

To overcome some of above-mentioned difficulties regarding clinical application of miRNAs, development of targeted nanoparticle-based delivery system for miRNA replacement therapy is the goal of this thesis. We developed an anionic lipid based lipopolyplex nanoparticle system for miRNA delivery. The lipid carrier consisted of DOPE, linoleic acid and DMG-PEG at a ratio of 50/48/2. PEI was used to provide positive charge to capture the miRNA molecules and loaded into lipid carrier. Because of the high level of transferrin receptor on the surface of AML cells, we conjugated the nanoparticles with transferrin (Tf-NP) for targeting and efficient delivery. The size of Tf-NP-miRNA was around 150 nm and ζ-potential was 5.8 ± 1.9 mV. The achieved size and charge of the nanoparticles has been previously shown to be optimal for a long-lasting *in vivo* circulation (*87, 148*). Entrapment efficacy of this lipopolyplex was almost 100%. The qualitative

intracellular FAM-miR uptake by AML cells following Tf-NP treatment was confirmed by confocal microscopy that showed an accumulation of FAM-miR mostly in the cytoplasm. Then *in vivo* toxicity profile was generated and there was no significant liver and kidney function impairment, no body weight loss and no normal bone marrow function impairment.

The microRNA *miR-29b* has been shown to have tumor suppressor activity by targeting genes involved in myeloid leukemogenesis, i.e., *DNMT*s, *CDK6, SP1, KIT* and *FLT3* (*202*). And a higher *miR-29b* pretreatment expression is associated with improved response to decitabine and better outcome in AML (*82, 194, 198, 203*). Thus, increasing *miR-29b* in AML blasts may be beneficial. In Chapter 3, we showed that Tf-NP-*miR-29b* treatment resulted in >200-fold increase of mature *miR-29b* compared to free *miR-29b* and was about twice as efficient as treatment with non-Tf-conjugated NP-*miR-29b.* Tf-NP-*miR-29b* treatment significantly downregulated DNMTs, CDK6, SP1, KIT and FLT3, decreased AML cell growth by 30-50%, and impaired colony formation by approximately 50%. Mice engrafted with AML cells and then treated with Tf-NP-*miR-29b* had significantly longer survival compared to Tf-NP-scramble (P=0.015) or free *miR-29b* (P=0.003). Furthermore, priming AML cells with Tf-NP-*miR-29b* before decitabine resulted in strong cell viability decrease *in vitro* and showed improved anti-leukemic activity compared with decitabine alone (P=0.001) *in vivo*. Tf-NP effectively delivered functional *miR-29b,* resulting in target downregulation and anti-leukemic activity. This warrants further investigation as a novel therapeutic approach in AML.

Several studies showed that lower *miR-181a* expression is associated with worse clinical outcomes (*37, 79*). However, unlike *miR-29b*, the exact mechanisms by which *miR-181a* mediates this effect remain elusive. In Chapter 4, we focused on revealing the mechanism of tumor suppressor function of *miR-181a* and also using Tf-NP to explore the therapeutic potential of *miR-181a*. Aberrant activation of the RAS-pathway by mutation or overexpression is frequent in AML and contributes to leukemogenesis. Here we report that *miR-181a* directly binds to the 3'-UTRs and downregulates KRAS, NRAS and MAPK1, leading to anti-leukemia activity. Therefore, we reasoned that an efficient delivery of *miR-181a* double-stranded mimics to target AML cells using transferrin-targeting lipopolyplex nanoparticles (NP) would result in significant anti-leukemic activity. NP treatment indeed increased mature *miR-181a*, downregulated KRAS, NRAS and MAPK1, resulted in decreased phosphorylation of the downstream RAS effectors AKT and MEK, and ultimately downregulated the MAKP1-downstream target and oncogenic transcription factor MYC in AML cell lines and primary blasts. NP mediated *miR-181a* upregulation also lead to reduced proliferation, impaired colony formation and increased sensitivity to daunorubicin. Finally, treatment with *miR-181a*-NP in mice engrafted with MV4-11 AML cells resulted in longer survival compared to mice treated with scramble-NP control. Altogether these data support that targeting the RAS-MAPK-pathway by *miR-181a* mimics is a novel and promising therapeutic approach for AML.

To our knowledge, our targeted nanoparticle system represents the first nanoparticle miRNA delivery system for AML cells. Using Tf as a targeting

molecule does not only enhance the delivery to AML bulk population but also facilitate the cellular uptake of miRNA in leukemia stem cells. As shown in this study, the level of a down-regulated tumor suppressor, *miR-29b*, can be restored by synthetic *miR-29b* double stranded mimic delivered by Tf-NP and then leads to anti-leukemia activity. Our work also highlights that priming AML cells with *miR-29b* could improve decitabine treatment, which could be a novel treatment for older AML patients in clinic. *MiR-181a*, though has been shown to be associated with clinical outcome, still not clear in its mechanism. We demonstrated that *miR-181a* as a novel target for aiming at the therapeutically elusive RAS-MAPK1 and RAS-AKT-kinase pathways in AML. We also show the therapeutic potential of *miR-181a*-delivering AML blasts targeting-nanoparticles. As microRNA mimics start to make their way into the clinic and are currently being tested in clinical trials (i.e., MRX34, a miR-34 mimic compound), we believe this research is well-timed and further expands the horizon of the potential applications of microRNA-based therapeutic approaches in leukemia.

The next step would be a comprehensive study of toxicity, pharmacokinetic (PK) and pharmacodynamics (PD) with different doses, schedule and administration route (i.e. i.v. and i.p.) to identify an optimal dose and schedule of Tf-NP-*miR-29b* or *miR-181a* treatment. More often, the tumor suppressive activity of miRNAs can sensitize tumor cells to chemo-drugs. Priming tumor cells with miRNAs, patients may only need lower dose of drugs, which minimize their side effects and unwanted toxicity. Thus, incorporating miRNA replacement therapy into standard chemotherapy may achieve better outcome. Moreover, the idea of

applying of cocktail therapies with multiple miRNA mimics and antagomiRs targeting different pathways and subgroups of cell populations (including bulk population and LSC) simultaneously, delivery through nanoparticles, should be further explored.

Bibliography

1. Estey E, Dohner H. Acute myeloid leukaemia. *Lancet* 2006 Nov 25; **368**(9550)**:** 1894-1907.

2. Vardiman JW, Thiele J, Arber DA, Brunning RD, Borowitz MJ, Porwit A*, et al.* The 2008 revision of the World Health Organization (WHO) classification of myeloid neoplasms and acute leukemia: rationale and important changes. *Blood* 2009 Jul 30; **114**(5)**:** 937-951.

3. Estey EH. Acute myeloid leukemia: 2012 update on diagnosis, risk stratification, and management. *Am J Hematol* 2012 Jan; **87**(1)**:** 89-99.

4. Vardiman JW, Harris NL, Brunning RD. The World Health Organization (WHO) classification of the myeloid neoplasms. *Blood* 2002 Oct 1; **100**(7)**:** 2292-2302.

5. Grimwade D, Walker H, Oliver F, Wheatley K, Harrison C, Harrison G*, et al.* The importance of diagnostic cytogenetics on outcome in AML: analysis of 1,612 patients entered into the MRC AML 10 trial. The Medical Research Council Adult and Children's Leukaemia Working Parties. *Blood* 1998 Oct 1; **92**(7)**:** 2322-2333.

6. Becker H, Maharry K, Mrozek K, Volinia S, Eisfeld AK, Radmacher MD*, et al.* Prognostic gene mutations and distinct gene- and microRNA-expression signatures in acute myeloid leukemia with a sole trisomy 8. *Leukemia* 2014 Mar 21.

7. Schwind S, Edwards CG, Nicolet D, Mrozek K, Maharry K, Wu YZ*, et al.* inv(16)/t(16;16) acute myeloid leukemia with non-type A CBFB-MYH11 fusions associate with distinct clinical and genetic features and lack KIT mutations. *Blood* 2013 Jan 10; **121**(2)**:** 385-391.

8. Garzon R, Garofalo M, Martelli MP, Briesewitz R, Wang L, Fernandez-Cymering C*, et al.* Distinctive microRNA signature of acute myeloid

leukemia bearing cytoplasmic mutated nucleophosmin. *Proc Natl Acad Sci U S A* 2008 Mar 11; **105**(10)**:** 3945-3950.

9. Whitman SP, Archer KJ, Feng L, Baldus C, Becknell B, Carlson BD*, et al.* Absence of the wild-type allele predicts poor prognosis in adult de novo acute myeloid leukemia with normal cytogenetics and the internal tandem duplication of FLT3: a cancer and leukemia group B study. *Cancer Res* 2001 Oct 1; **61**(19)**:** 7233-7239.

10. Whitman SP, Maharry K, Radmacher MD, Becker H, Mrozek K, Margeson D*, et al.* FLT3 internal tandem duplication associates with adverse outcome and gene- and microRNA-expression signatures in patients 60 years of age or older with primary cytogenetically normal acute myeloid leukemia: a Cancer and Leukemia Group B study. *Blood* 2010 Nov 4; **116**(18)**:** 3622-3626.

11. Falini B, Mecucci C, Tiacci E, Alcalay M, Rosati R, Pasqualucci L*, et al.* Cytoplasmic nucleophosmin in acute myelogenous leukemia with a normal karyotype. *N Engl J Med* 2005 Jan 20; **352**(3)**:** 254-266.

12. Dohner K, Schlenk RF, Habdank M, Scholl C, Rucker FG, Corbacioglu A*, et al.* Mutant nucleophosmin (NPM1) predicts favorable prognosis in younger adults with acute myeloid leukemia and normal cytogenetics: interaction with other gene mutations. *Blood* 2005 Dec 1; **106**(12)**:** 3740-3746.

13. Schnittger S, Schoch C, Kern W, Mecucci C, Tschulik C, Martelli MF*, et al.* Nucleophosmin gene mutations are predictors of favorable prognosis in acute myelogenous leukemia with a normal karyotype. *Blood* 2005 Dec 1; **106**(12)**:** 3733-3739.

14. Becker H, Marcucci G, Maharry K, Radmacher MD, Mrozek K, Margeson D*, et al.* Favorable prognostic impact of NPM1 mutations in older patients with cytogenetically normal de novo acute myeloid leukemia and associated gene- and microRNA-expression signatures: a Cancer and Leukemia Group B study. *J Clin Oncol* 2010 Feb 1; **28**(4)**:** 596-604.

15. Frohling S, Schlenk RF, Stolze I, Bihlmayr J, Benner A, Kreitmeier S*, et al.* CEBPA mutations in younger adults with acute myeloid leukemia and normal cytogenetics: prognostic relevance and analysis of cooperating mutations. *J Clin Oncol* 2004 Feb 15; **22**(4)**:** 624-633.

16. Preudhomme C, Sagot C, Boissel N, Cayuela JM, Tigaud I, de Botton S*, et al.* Favorable prognostic significance of CEBPA mutations in patients

with de novo acute myeloid leukemia: a study from the Acute Leukemia French Association (ALFA). *Blood* 2002 Oct 15; **100**(8)**:** 2717-2723.

17. Marcucci G, Maharry K, Radmacher MD, Mrozek K, Vukosavljevic T, Paschka P*, et al.* Prognostic significance of, and gene and microRNA expression signatures associated with, CEBPA mutations in cytogenetically normal acute myeloid leukemia with high-risk molecular features: a Cancer and Leukemia Group B Study. *J Clin Oncol* 2008 Nov 1; **26**(31)**:** 5078-5087.

18. Dufour A, Schneider F, Metzeler KH, Hoster E, Schneider S, Zellmeier E*, et al.* Acute myeloid leukemia with biallelic CEBPA gene mutations and normal karyotype represents a distinct genetic entity associated with a favorable clinical outcome. *J Clin Oncol* 2010 Feb 1; **28**(4)**:** 570-577.

19. Dufour A, Schneider F, Hoster E, Benthaus T, Ksienzyk B, Schneider S*, et al.* Monoallelic CEBPA mutations in normal karyotype acute myeloid leukemia: independent favorable prognostic factor within NPM1 mutated patients. *Ann Hematol* 2012 Jul; **91**(7)**:** 1051-1063.

20. Tang JL, Hou HA, Chen CY, Liu CY, Chou WC, Tseng MH*, et al.* AML1/RUNX1 mutations in 470 adult patients with de novo acute myeloid leukemia: prognostic implication and interaction with other gene alterations. *Blood* 2009 Dec 17; **114**(26)**:** 5352-5361.

21. Mendler JH, Maharry K, Radmacher MD, Mrozek K, Becker H, Metzeler KH*, et al.* RUNX1 mutations are associated with poor outcome in younger and older patients with cytogenetically normal acute myeloid leukemia and with distinct gene and MicroRNA expression signatures. *J Clin Oncol* 2012 Sep 1; **30**(25)**:** 3109-3118.

22. Caligiuri MA, Strout MP, Lawrence D, Arthur DC, Baer MR, Yu F*, et al.* Rearrangement of ALL1 (MLL) in acute myeloid leukemia with normal cytogenetics. *Cancer Res* 1998 Jan 1; **58**(1)**:** 55-59.

23. Dohner K, Tobis K, Ulrich R, Frohling S, Benner A, Schlenk RF*, et al.* Prognostic significance of partial tandem duplications of the MLL gene in adult patients 16 to 60 years old with acute myeloid leukemia and normal cytogenetics: a study of the Acute Myeloid Leukemia Study Group Ulm. *J Clin Oncol* 2002 Aug 1; **20**(15)**:** 3254-3261.

24. Marcucci G, Maharry K, Wu YZ, Radmacher MD, Mrozek K, Margeson D*, et al.* IDH1 and IDH2 gene mutations identify novel molecular subsets within de novo cytogenetically normal acute myeloid leukemia: a Cancer

and Leukemia Group B study. *J Clin Oncol* 2010 May 10; **28**(14)**:** 2348-2355.

25. Paschka P, Schlenk RF, Gaidzik VI, Habdank M, Kronke J, Bullinger L*, et al.* IDH1 and IDH2 mutations are frequent genetic alterations in acute myeloid leukemia and confer adverse prognosis in cytogenetically normal acute myeloid leukemia with NPM1 mutation without FLT3 internal tandem duplication. *J Clin Oncol* 2010 Aug 1; **28**(22)**:** 3636-3643.

26. Boissel N, Nibourel O, Renneville A, Gardin C, Reman O, Contentin N*, et al.* Prognostic impact of isocitrate dehydrogenase enzyme isoforms 1 and 2 mutations in acute myeloid leukemia: a study by the Acute Leukemia French Association group. *J Clin Oncol* 2010 Aug 10; **28**(23)**:** 3717-3723.

27. Wagner K, Damm F, Gohring G, Gorlich K, Heuser M, Schafer I*, et al.* Impact of IDH1 R132 mutations and an IDH1 single nucleotide polymorphism in cytogenetically normal acute myeloid leukemia: SNP rs11554137 is an adverse prognostic factor. *J Clin Oncol* 2010 May 10; **28**(14)**:** 2356-2364.

28. Langer C, Radmacher MD, Ruppert AS, Whitman SP, Paschka P, Mrozek K*, et al.* High BAALC expression associates with other molecular prognostic markers, poor outcome, and a distinct gene-expression signature in cytogenetically normal patients younger than 60 years with acute myeloid leukemia: a Cancer and Leukemia Group B (CALGB) study. *Blood* 2008 Jun 1; **111**(11)**:** 5371-5379.

29. Metzeler KH, Dufour A, Benthaus T, Hummel M, Sauerland MC, Heinecke A*, et al.* ERG expression is an independent prognostic factor and allows refined risk stratification in cytogenetically normal acute myeloid leukemia: a comprehensive analysis of ERG, MN1, and BAALC transcript levels using oligonucleotide microarrays. *J Clin Oncol* 2009 Oct 20; **27**(30)**:** 5031-5038.

30. Marcucci G, Maharry K, Whitman SP, Vukosavljevic T, Paschka P, Langer C*, et al.* High expression levels of the ETS-related gene, ERG, predict adverse outcome and improve molecular risk-based classification of cytogenetically normal acute myeloid leukemia: a Cancer and Leukemia Group B Study. *J Clin Oncol* 2007 Aug 1; **25**(22)**:** 3337-3343.

31. Port M, Bottcher M, Thol F, Ganser A, Schlenk R, Wasem J*, et al.* Prognostic significance of FLT3 internal tandem duplication, nucleophosmin 1, and CEBPA gene mutations for acute myeloid leukemia patients with normal karyotype and younger than 60 years: a systematic review and meta-analysis. *Ann Hematol* 2014 May 7.

32. Kiyoi H, Naoe T, Nakano Y, Yokota S, Minami S, Miyawaki S*, et al.* Prognostic implication of FLT3 and N-RAS gene mutations in acute myeloid leukemia. *Blood* 1999 May 1; **93**(9)**:** 3074-3080.

33. Sallmyr A, Fan J, Datta K, Kim KT, Grosu D, Shapiro P*, et al.* Internal tandem duplication of FLT3 (FLT3/ITD) induces increased ROS production, DNA damage, and misrepair: implications for poor prognosis in AML. *Blood* 2008 Mar 15; **111**(6)**:** 3173-3182.

34. Shih LY, Huang CF, Wu JH, Lin TL, Dunn P, Wang PN*, et al.* Internal tandem duplication of FLT3 in relapsed acute myeloid leukemia: a comparative analysis of bone marrow samples from 108 adult patients at diagnosis and relapse. *Blood* 2002 Oct 1; **100**(7)**:** 2387-2392.

35. Falini B, Bolli N, Liso A, Martelli MP, Mannucci R, Pileri S*, et al.* Altered nucleophosmin transport in acute myeloid leukaemia with mutated NPM1: molecular basis and clinical implications. *Leukemia* 2009 Oct; **23**(10)**:** 1731-1743.

36. Falini B, Nicoletti I, Martelli MF, Mecucci C. Acute myeloid leukemia carrying cytoplasmic/mutated nucleophosmin (NPMc+ AML): biologic and clinical features. *Blood* 2007 Feb 1; **109**(3)**:** 874-885.

37. Marcucci G, Radmacher MD, Maharry K, Mrozek K, Ruppert AS, Paschka P*, et al.* MicroRNA expression in cytogenetically normal acute myeloid leukemia. *N Engl J Med* 2008 May 1; **358**(18)**:** 1919-1928.

38. Marcucci G, Haferlach T, Dohner H. Molecular genetics of adult acute myeloid leukemia: prognostic and therapeutic implications. *J Clin Oncol* 2011 Feb 10; **29**(5)**:** 475-486.

39. Ross SE, Radomska HS, Wu B, Zhang P, Winnay JN, Bajnok L*, et al.* Phosphorylation of C/EBPalpha inhibits granulopoiesis. *Mol Cell Biol* 2004 Jan; **24**(2)**:** 675-686.

40. Pabst T, Mueller BU. Transcriptional dysregulation during myeloid transformation in AML. *Oncogene* 2007 Oct 15; **26**(47)**:** 6829-6837.

41. Dohner H, Estey EH, Amadori S, Appelbaum FR, Buchner T, Burnett AK*, et al.* Diagnosis and management of acute myeloid leukemia in adults: recommendations from an international expert panel, on behalf of the European LeukemiaNet. *Blood* 2010 Jan 21; **115**(3)**:** 453-474.

42. Pastore F, Dufour A, Benthaus T, Metzeler KH, Maharry KS, Schneider S*, et al.* Combined molecular and clinical prognostic index for relapse and survival in cytogenetically normal acute myeloid leukemia. *J Clin Oncol* 2014 May 20; **32**(15)**:** 1586-1594.

43. Hannon GJ. RNA interference. *Nature* 2002 Jul 11; **418**(6894)**:** 244-251.

44. He L, Thomson JM, Hemann MT, Hernando-Monge E, Mu D, Goodson S*, et al.* A microRNA polycistron as a potential human oncogene. *Nature* 2005 Jun 9; **435**(7043)**:** 828-833.

45. Murchison EP, Hannon GJ. miRNAs on the move: miRNA biogenesis and the RNAi machinery. *Curr Opin Cell Biol* 2004 Jun; **16**(3)**:** 223-229.

46. Denli AM, Tops BB, Plasterk RH, Ketting RF, Hannon GJ. Processing of primary microRNAs by the Microprocessor complex. *Nature* 2004 Nov 11; **432**(7014)**:** 231-235.

47. Yi R, Qin Y, Macara IG, Cullen BR. Exportin-5 mediates the nuclear export of pre-microRNAs and short hairpin RNAs. *Genes Dev* 2003 Dec 15; **17**(24)**:** 3011-3016.

48. Lund E, Guttinger S, Calado A, Dahlberg JE, Kutay U. Nuclear export of microRNA precursors. *Science* 2004 Jan 2; **303**(5654)**:** 95-98.

49. Bohnsack MT, Czaplinski K, Gorlich D. Exportin 5 is a RanGTP-dependent dsRNA-binding protein that mediates nuclear export of pre-miRNAs. *RNA* 2004 Feb; **10**(2)**:** 185-191.

50. Bernstein E, Caudy AA, Hammond SM, Hannon GJ. Role for a bidentate ribonuclease in the initiation step of RNA interference. *Nature* 2001 Jan 18; **409**(6818)**:** 363-366.

51. Ketting RF, Fischer SE, Bernstein E, Sijen T, Hannon GJ, Plasterk RH. Dicer functions in RNA interference and in synthesis of small RNA involved in developmental timing in C. elegans. *Genes Dev* 2001 Oct 15; **15**(20)**:** 2654-2659.

52. Chendrimada TP, Gregory RI, Kumaraswamy E, Norman J, Cooch N, Nishikura K*, et al.* TRBP recruits the Dicer complex to Ago2 for microRNA processing and gene silencing. *Nature* 2005 Aug 4; **436**(7051)**:** 740-744.

53. Schwarz DS, Hutvagner G, Du T, Xu Z, Aronin N, Zamore PD. Asymmetry in the assembly of the RNAi enzyme complex. *Cell* 2003 Oct 17; **115**(2)**:** 199-208.

54. Calin GA, Croce CM. MicroRNA signatures in human cancers. *Nat Rev Cancer* 2006 Nov; **6**(11)**:** 857-866.

55. Garzon R, Calin GA, Croce CM. MicroRNAs in Cancer. *Annu Rev Med* 2009; **60:** 167-179.

56. Lu J, Getz G, Miska EA, Alvarez-Saavedra E, Lamb J, Peck D*, et al.* MicroRNA expression profiles classify human cancers. *Nature* 2005 Jun 9; **435**(7043)**:** 834-838.

57. Li Z, Lu J, Sun M, Mi S, Zhang H, Luo RT*, et al.* Distinct microRNA expression profiles in acute myeloid leukemia with common translocations. *Proc Natl Acad Sci U S A* 2008 Oct 7; **105**(40)**:** 15535-15540.

58. Jongen-Lavrencic M, Sun SM, Dijkstra MK, Valk PJ, Lowenberg B. MicroRNA expression profiling in relation to the genetic heterogeneity of acute myeloid leukemia. *Blood* 2008 May 15; **111**(10)**:** 5078-5085.

59. Cammarata G, Augugliaro L, Salemi D, Agueli C, La Rosa M, Dagnino L*, et al.* Differential expression of specific microRNA and their targets in acute myeloid leukemia. *Am J Hematol* 2010 May; **85**(5)**:** 331-339.

60. Dixon-McIver A, East P, Mein CA, Cazier JB, Molloy G, Chaplin T*, et al.* Distinctive patterns of microRNA expression associated with karyotype in acute myeloid leukaemia. *PLoS One* 2008; **3**(5)**:** e2141.

61. Garzon R, Volinia S, Liu CG, Fernandez-Cymering C, Palumbo T, Pichiorri F*, et al.* MicroRNA signatures associated with cytogenetics and prognosis in acute myeloid leukemia. *Blood* 2008 Mar 15; **111**(6)**:** 3183-3189.

62. Wang Y, Li Z, He C, Wang D, Yuan X, Chen J*, et al.* MicroRNAs expression signatures are associated with lineage and survival in acute leukemias. *Blood Cells Mol Dis* 2010 Mar 15; **44**(3)**:** 191-197.

63. Diaz-Beya M, Navarro A, Ferrer G, Diaz T, Gel B, Camos M*, et al.* Acute myeloid leukemia with translocation (8;16)(p11;p13) and MYST3-CREBBP rearrangement harbors a distinctive microRNA signature targeting RET proto-oncogene. *Leukemia* 2013 Mar; **27**(3)**:** 595-603.

64. Rucker FG, Russ AC, Cocciardi S, Kett H, Schlenk RF, Botzenhardt U*, et al.* Altered miRNA and gene expression in acute myeloid leukemia with complex karyotype identify networks of prognostic relevance. *Leukemia* 2013 Feb; **27**(2)**:** 353-361.

65. Faraoni I, Laterza S, Ardiri D, Ciardi C, Fazi F, Lo-Coco F. MiR-424 and miR-155 deregulated expression in cytogenetically normal acute myeloid leukaemia: correlation with NPM1 and FLT3 mutation status. *J Hematol Oncol* 2012; **5:** 26.

66. Hickey CJ, Schwind S, Radomska HS, Dorrance AM, Santhanam R, Mishra A*, et al.* Lenalidomide-mediated enhanced translation of C/EBPalpha-p30 protein up-regulates expression of the antileukemic microRNA-181a in acute myeloid leukemia. *Blood* 2013 Jan 3; **121**(1)**:** 159-169.

67. Diaz-Beya M, Brunet S, Nomdedeu J, Tejero R, Diaz T, Pratcorona M*, et al.* MicroRNA expression at diagnosis adds relevant prognostic information to molecular categorization in patients with intermediate-risk cytogenetic acute myeloid leukemia. *Leukemia* 2014 Apr; **28**(4)**:** 804-812.

68. Marcucci G, Metzeler KH, Schwind S, Becker H, Maharry K, Mrozek K*, et al.* Age-related prognostic impact of different types of DNMT3A mutations in adults with primary cytogenetically normal acute myeloid leukemia. *J Clin Oncol* 2012 Mar 1; **30**(7)**:** 742-750.

69. Metzeler KH, Maharry K, Radmacher MD, Mrozek K, Margeson D, Becker H*, et al.* TET2 mutations improve the new European LeukemiaNet risk classification of acute myeloid leukemia: a Cancer and Leukemia Group B study. *J Clin Oncol* 2011 Apr 1; **29**(10)**:** 1373-1381.

70. Schwind S, Marcucci G, Maharry K, Radmacher MD, Mrozek K, Holland KB*, et al.* BAALC and ERG expression levels are associated with outcome and distinct gene and microRNA expression profiles in older patients with de novo cytogenetically normal acute myeloid leukemia: a Cancer and Leukemia Group B study. *Blood* 2010 Dec 16; **116**(25)**:** 5660-5669.

71. Langer C, Marcucci G, Holland KB, Radmacher MD, Maharry K, Paschka P*, et al.* Prognostic importance of MN1 transcript levels, and biologic insights from MN1-associated gene and microRNA expression signatures in cytogenetically normal acute myeloid leukemia: a cancer and leukemia group B study. *J Clin Oncol* 2009 Jul 1; **27**(19)**:** 3198-3204.

72. Schwind S, Marcucci G, Kohlschmidt J, Radmacher MD, Mrozek K, Maharry K*, et al.* Low expression of MN1 associates with better treatment response in older patients with de novo cytogenetically normal acute myeloid leukemia. *Blood* 2011 Oct 13; **118**(15)**:** 4188-4198.

73. Bonnet D, Dick JE. Human acute myeloid leukemia is organized as a hierarchy that originates from a primitive hematopoietic cell. *Nat Med* 1997 Jul; **3**(7)**:** 730-737.

74. Lapidot T, Fajerman Y, Kollet O. Immune-deficient SCID and NOD/SCID mice models as functional assays for studying normal and malignant human hematopoiesis. *J Mol Med (Berl)* 1997 Sep; **75**(9)**:** 664-673.

75. Eppert K, Takenaka K, Lechman ER, Waldron L, Nilsson B, van Galen P*, et al.* Stem cell gene expression programs influence clinical outcome in human leukemia. *Nat Med* 2011 Sep; **17**(9)**:** 1086-1093.

76. Metzeler KH, Maharry K, Kohlschmidt J, Volinia S, Mrozek K, Becker H*, et al.* A stem cell-like gene expression signature associates with inferior outcomes and a distinct microRNA expression profile in adults with primary cytogenetically normal acute myeloid leukemia. *Leukemia* 2013 Oct; **27**(10)**:** 2023-2031.

77. Li Z, Huang H, Chen P, He M, Li Y, Arnovitz S*, et al.* miR-196b directly targets both HOXA9/MEIS1 oncogenes and FAS tumour suppressor in MLL-rearranged leukaemia. *Nat Commun* 2012; **3:** 688.

78. Sun SM, Rockova V, Bullinger L, Dijkstra MK, Dohner H, Lowenberg B*, et al.* The prognostic relevance of miR-212 expression with survival in cytogenetically and molecularly heterogeneous AML. *Leukemia* 2013 Jan; **27**(1)**:** 100-106.

79. Schwind S, Maharry K, Radmacher MD, Mrozek K, Holland KB, Margeson D*, et al.* Prognostic significance of expression of a single microRNA, miR-181a, in cytogenetically normal acute myeloid leukemia: a Cancer and Leukemia Group B study. *J Clin Oncol* 2010 Dec 20; **28**(36)**:** 5257-5264.

80. Marcucci G, Maharry KS, Metzeler KH, Volinia S, Wu YZ, Mrozek K*, et al.* Clinical role of microRNAs in cytogenetically normal acute myeloid leukemia: miR-155 upregulation independently identifies high-risk patients. *J Clin Oncol* 2013 Jun 10; **31**(17)**:** 2086-2093.

81. Eisfeld AK, Marcucci G, Maharry K, Schwind S, Radmacher MD, Nicolet D*, et al.* miR-3151 interplays with its host gene BAALC and independently affects outcome of patients with cytogenetically normal acute myeloid leukemia. *Blood* 2012 Jul 12; **120**(2)**:** 249-258.

82. Blum W, Garzon R, Klisovic RB, Schwind S, Walker A, Geyer S*, et al.* Clinical response and miR-29b predictive significance in older AML

patients treated with a 10-day schedule of decitabine. *Proc Natl Acad Sci U S A* 2010 Apr 20; **107**(16)**:** 7473-7478.

83. Havelange V, Ranganathan P, Geyer S, Nicolet D, Huang X, Yu X*, et al.* Implications of the miR-10 family in chemotherapy response of NPM1-mutated AML. *Blood* 2014 Apr 10; **123**(15)**:** 2412-2415.

84. Schoof CR, Botelho EL, Izzotti A, Vasques Ldos R. MicroRNAs in cancer treatment and prognosis. *Am J Cancer Res* 2012; **2**(4)**:** 414-433.

85. Chen J, Odenike O, Rowley JD. Leukaemogenesis: more than mutant genes. *Nat Rev Cancer* 2010 Jan; **10**(1)**:** 23-36.

86. Kim BY, Rutka JT, Chan WC. Nanomedicine. *N Engl J Med* 2010 Dec 16; **363**(25)**:** 2434-2443.

87. Alexis F, Pridgen E, Molnar LK, Farokhzad OC. Factors affecting the clearance and biodistribution of polymeric nanoparticles. *Mol Pharm* 2008 Jul-Aug; **5**(4)**:** 505-515.

88. Prencipe G, Tabakman SM, Welsher K, Liu Z, Goodwin AP, Zhang L*, et al.* PEG branched polymer for functionalization of nanomaterials with ultralong blood circulation. *J Am Chem Soc* 2009 Apr 8; **131**(13)**:** 4783-4787.

89. Hobbs SK, Monsky WL, Yuan F, Roberts WG, Griffith L, Torchilin VP*, et al.* Regulation of transport pathways in tumor vessels: role of tumor type and microenvironment. *Proc Natl Acad Sci U S A* 1998 Apr 14; **95**(8)**:** 4607-4612.

90. Farokhzad OC, Langer R. Impact of nanotechnology on drug delivery. *ACS Nano* 2009 Jan 27; **3**(1)**:** 16-20.

91. Davis ME, Chen ZG, Shin DM. Nanoparticle therapeutics: an emerging treatment modality for cancer. *Nat Rev Drug Discov* 2008 Sep; **7**(9)**:** 771-782.

92. Deng Y, Wang CC, Choy KW, Du Q, Chen J, Wang Q*, et al.* Therapeutic potentials of gene silencing by RNA interference: principles, challenges, and new strategies. *Gene* 2014 Apr 1; **538**(2)**:** 217-227.

93. Davidson BL, McCray PB, Jr. Current prospects for RNA interference-based therapies. *Nat Rev Genet* 2011 May; **12**(5)**:** 329-340.

94. Kole R, Krainer AR, Altman S. RNA therapeutics: beyond RNA interference and antisense oligonucleotides. *Nat Rev Drug Discov* 2012 Feb; **11**(2)**:** 125-140.

95. Crooke ST. *Antisense Drug Technology: Principles: Strategies, and Applications*. CRC Press2001, pp 47-74.

96. Lu QL, Rabinowitz A, Chen YC, Yokota T, Yin H, Alter J*, et al.* Systemic delivery of antisense oligoribonucleotide restores dystrophin expression in body-wide skeletal muscles. *Proc Natl Acad Sci U S A* 2005 Jan 4; **102**(1)**:** 198-203.

97. Sazani P, Gemignani F, Kang SH, Maier MA, Manoharan M, Persmark M*, et al.* Systemically delivered antisense oligomers upregulate gene expression in mouse tissues. *Nat Biotechnol* 2002 Dec; **20**(12)**:** 1228-1233.

98. Roberts J, Palma E, Sazani P, Orum H, Cho M, Kole R. Efficient and persistent splice switching by systemically delivered LNA oligonucleotides in mice. *Mol Ther* 2006 Oct; **14**(4)**:** 471-475.

99. Kim DH, Rossi JJ. Strategies for silencing human disease using RNA interference. *Nat Rev Genet* 2007 Mar; **8**(3)**:** 173-184.

100. Whitehead KA, Langer R, Anderson DG. Knocking down barriers: advances in siRNA delivery. *Nat Rev Drug Discov* 2009 Feb; **8**(2)**:** 129-138.

101. Couto LB, High KA. Viral vector-mediated RNA interference. *Curr Opin Pharmacol* 2010 Oct; **10**(5)**:** 534-542.

102. Boudreau RL, McBride JL, Martins I, Shen S, Xing Y, Carter BJ*, et al.* Nonallele-specific silencing of mutant and wild-type huntingtin demonstrates therapeutic efficacy in Huntington's disease mice. *Mol Ther* 2009 Jun; **17**(6)**:** 1053-1063.

103. Harper SQ, Staber PD, He X, Eliason SL, Martins IH, Mao Q*, et al.* RNA interference improves motor and neuropathological abnormalities in a Huntington's disease mouse model. *Proc Natl Acad Sci U S A* 2005 Apr 19; **102**(16)**:** 5820-5825.

104. Rodriguez-Lebron E, Denovan-Wright EM, Nash K, Lewin AS, Mandel RJ. Intrastriatal rAAV-mediated delivery of anti-huntingtin shRNAs induces partial reversal of disease progression in R6/1 Huntington's disease transgenic mice. *Mol Ther* 2005 Oct; **12**(4)**:** 618-633.

105. Kota J, Chivukula RR, O'Donnell KA, Wentzel EA, Montgomery CL, Hwang HW*, et al.* Therapeutic microRNA delivery suppresses tumorigenesis in a murine liver cancer model. *Cell* 2009 Jun 12; **137**(6)**:** 1005-1017.

106. Grimm D, Streetz KL, Jopling CL, Storm TA, Pandey K, Davis CR*, et al.* Fatality in mice due to oversaturation of cellular microRNA/short hairpin RNA pathways. *Nature* 2006 May 25; **441**(7092)**:** 537-541.

107. Grimm D, Wang L, Lee JS, Schurmann N, Gu S, Borner K*, et al.* Argonaute proteins are key determinants of RNAi efficacy, toxicity, and persistence in the adult mouse liver. *J Clin Invest* 2010 Sep; **120**(9)**:** 3106-3119.

108. Castanotto D, Sakurai K, Lingeman R, Li H, Shively L, Aagaard L*, et al.* Combinatorial delivery of small interfering RNAs reduces RNAi efficacy by selective incorporation into RISC. *Nucleic Acids Res* 2007; **35**(15)**:** 5154-5164.

109. Soutschek J, Akinc A, Bramlage B, Charisse K, Constien R, Donoghue M*, et al.* Therapeutic silencing of an endogenous gene by systemic administration of modified siRNAs. *Nature* 2004 Nov 11; **432**(7014)**:** 173-178.

110. Wolfrum C, Shi S, Jayaprakash KN, Jayaraman M, Wang G, Pandey RK*, et al.* Mechanisms and optimization of in vivo delivery of lipophilic siRNAs. *Nat Biotechnol* 2007 Oct; **25**(10)**:** 1149-1157.

111. Guo P, Coban O, Snead NM, Trebley J, Hoeprich S, Guo S*, et al.* Engineering RNA for targeted siRNA delivery and medical application. *Adv Drug Deliv Rev* 2010 Apr 30; **62**(6)**:** 650-666.

112. Salva E, Turan SO, Kabasakal L, Alan S, Ozkan N, Eren F*, et al.* Investigation of the therapeutic efficacy of codelivery of psiRNA-vascular endothelial growth factor and pIL-4 into chitosan nanoparticles in the breast tumor model. *J Pharm Sci* 2014 Mar; **103**(3)**:** 785-795.

113. Matokanovic M, Barisic K, Filipovic-Grcic J, Maysinger D. Hsp70 silencing with siRNA in nanocarriers enhances cancer cell death induced by the inhibitor of Hsp90. *Eur J Pharm Sci* 2013 Sep 27; **50**(1)**:** 149-158.

114. Xia H, Jun J, Wen-Ping L, Yi-Feng P, Xiao-Ling C. Chitosan nanoparticle carrying small interfering RNA to platelet-derived growth factor B mRNA

inhibits proliferation of smooth muscle cells in rabbit injured arteries. *Vascular* 2013 Mar 21.

115. Malmo J, Sandvig A, Varum KM, Strand SP. Nanoparticle mediated P-glycoprotein silencing for improved drug delivery across the blood-brain barrier: a siRNA-chitosan approach. *PLoS One* 2013; **8**(1)**:** e54182.

116. Yang J, Li S, Guo F, Zhang W, Wang Y, Pan Y. Induction of apoptosis by chitosan/HPV16 E7 siRNA complexes in cervical cancer cells. *Mol Med Rep* 2013 Mar; **7**(3)**:** 998-1002.

117. Chaturvedi K, Ganguly K, Kulkarni AR, Kulkarni VH, Nadagouda MN, Rudzinski WE*, et al.* Cyclodextrin-based siRNA delivery nanocarriers: a state-of-the-art review. *Expert Opin Drug Deliv* 2011 Nov; **8**(11)**:** 1455-1468.

118. Hu-Lieskovan S, Heidel JD, Bartlett DW, Davis ME, Triche TJ. Sequence-specific knockdown of EWS-FLI1 by targeted, nonviral delivery of small interfering RNA inhibits tumor growth in a murine model of metastatic Ewing's sarcoma. *Cancer Res* 2005 Oct 1; **65**(19)**:** 8984-8992.

119. Liu J, Gu C, Cabigas EB, Pendergrass KD, Brown ME, Luo Y*, et al.* Functionalized dendrimer-based delivery of angiotensin type 1 receptor siRNA for preserving cardiac function following infarction. *Biomaterials* 2013 May; **34**(14)**:** 3729-3736.

120. Liu X, Li G, Su Z, Jiang Z, Chen L, Wang J*, et al.* Poly(amido amine) is an ideal carrier of miR-7 for enhancing gene silencing effects on the EGFR pathway in U251 glioma cells. *Oncol Rep* 2013 Apr; **29**(4)**:** 1387-1394.

121. Arima H, Yoshimatsu A, Ikeda H, Ohyama A, Motoyama K, Higashi T*, et al.* Folate-PEG-appended dendrimer conjugate with alpha-cyclodextrin as a novel cancer cell-selective siRNA delivery carrier. *Mol Pharm* 2012 Sep 4; **9**(9)**:** 2591-2604.

122. Liu XX, Rocchi P, Qu FQ, Zheng SQ, Liang ZC, Gleave M*, et al.* PAMAM dendrimers mediate siRNA delivery to target Hsp27 and produce potent antiproliferative effects on prostate cancer cells. *ChemMedChem* 2009 Aug; **4**(8)**:** 1302-1310.

123. Grijalvo S, Avino A, Eritja R. Oligonucleotide delivery: a patent review (2010 - 2013). *Expert Opin Ther Pat* 2014 May 5.

124. Behlke MA. Progress towards in vivo use of siRNAs. *Mol Ther* 2006 Apr; **13**(4)**:** 644-670.

125. Kim SS, Garg H, Joshi A, Manjunath N. Strategies for targeted nonviral delivery of siRNAs in vivo. *Trends Mol Med* 2009 Nov; **15**(11)**:** 491-500.

126. de Fougerolles A, Vornlocher HP, Maraganore J, Lieberman J. Interfering with disease: a progress report on siRNA-based therapeutics. *Nat Rev Drug Discov* 2007 Jun; **6**(6)**:** 443-453.

127. Gomes-da-Silva LC, Fonseca NA, Moura V, Pedroso de Lima MC, Simoes S, Moreira JN. Lipid-based nanoparticles for siRNA delivery in cancer therapy: paradigms and challenges. *Acc Chem Res* 2012 Jul 17; **45**(7)**:** 1163-1171.

128. Tabernero J, Shapiro GI, LoRusso PM, Cervantes A, Schwartz GK, Weiss GJ*, et al.* First-in-humans trial of an RNA interference therapeutic targeting VEGF and KSP in cancer patients with liver involvement. *Cancer Discov* 2013 Apr; **3**(4)**:** 406-417.

129. van der Meel R, Vehmeijer LJ, Kok RJ, Storm G, van Gaal EV. Ligand-targeted particulate nanomedicines undergoing clinical evaluation: current status. *Adv Drug Deliv Rev* 2013 Oct; **65**(10)**:** 1284-1298.

130. Huebers HA, Finch CA. The physiology of transferrin and transferrin receptors. *Physiol Rev* 1987 Apr; **67**(2)**:** 520-582.

131. Aisen P, Leibman A, Zweier J. Stoichiometric and site characteristics of the binding of iron to human transferrin. *J Biol Chem* 1978 Mar 25; **253**(6)**:** 1930-1937.

132. Richardson DR, Ponka P. The molecular mechanisms of the metabolism and transport of iron in normal and neoplastic cells. *Biochim Biophys Acta* 1997 Mar 14; **1331**(1)**:** 1-40.

133. Daniels TR, Delgado T, Rodriguez JA, Helguera G, Penichet ML. The transferrin receptor part I: Biology and targeting with cytotoxic antibodies for the treatment of cancer. *Clin Immunol* 2006 Nov; **121**(2)**:** 144-158.

134. Tortorella S, Karagiannis TC. Transferrin receptor-mediated endocytosis: a useful target for cancer therapy. *J Membr Biol* 2014 Apr; **247**(4)**:** 291-307.

135. Davis ME. The first targeted delivery of siRNA in humans via a self-assembling, cyclodextrin polymer-based nanoparticle: from concept to clinic. *Mol Pharm* 2009 May-Jun; **6**(3)**:** 659-668.

136. Heidel JD, Liu JY, Yen Y, Zhou B, Heale BS, Rossi JJ*, et al.* Potent siRNA inhibitors of ribonucleotide reductase subunit RRM2 reduce cell proliferation in vitro and in vivo. *Clin Cancer Res* 2007 Apr 1; **13**(7)**:** 2207-2215.

137. Cerqueira NM, Pereira S, Fernandes PA, Ramos MJ. Overview of ribonucleotide reductase inhibitors: an appealing target in anti-tumour therapy. *Curr Med Chem* 2005; **12**(11)**:** 1283-1294.

138. Xu L, Tang WH, Huang CC, Alexander W, Xiang LM, Pirollo KF*, et al.* Systemic p53 gene therapy of cancer with immunolipoplexes targeted by anti-transferrin receptor scFv. *Mol Med* 2001 Oct; **7**(10)**:** 723-734.

139. Pirollo KF, Rait A, Zhou Q, Zhang XQ, Zhou J, Kim CS*, et al.* Tumor-targeting nanocomplex delivery of novel tumor suppressor RB94 chemosensitizes bladder carcinoma cells in vitro and in vivo. *Clin Cancer Res* 2008 Apr 1; **14**(7)**:** 2190-2198.

140. Park JW, Hong K, Kirpotin DB, Colbern G, Shalaby R, Baselga J*, et al.* Anti-HER2 immunoliposomes: enhanced efficacy attributable to targeted delivery. *Clin Cancer Res* 2002 Apr; **8**(4)**:** 1172-1181.

141. Mamot C, Drummond DC, Greiser U, Hong K, Kirpotin DB, Marks JD*, et al.* Epidermal growth factor receptor (EGFR)-targeted immunoliposomes mediate specific and efficient drug delivery to EGFR- and EGFRvIII-overexpressing tumor cells. *Cancer Res* 2003 Jun 15; **63**(12)**:** 3154-3161.

142. Mamot C, Drummond DC, Noble CO, Kallab V, Guo Z, Hong K*, et al.* Epidermal growth factor receptor-targeted immunoliposomes significantly enhance the efficacy of multiple anticancer drugs in vivo. *Cancer Res* 2005 Dec 15; **65**(24)**:** 11631-11638.

143. Zhang G, Guo B, Wu H, Tang T, Zhang BT, Zheng L*, et al.* A delivery system targeting bone formation surfaces to facilitate RNAi-based anabolic therapy. *Nat Med* 2012 Feb; **18**(2)**:** 307-314.

144. Ni X, Zhang Y, Ribas J, Chowdhury WH, Castanares M, Zhang Z*, et al.* Prostate-targeted radiosensitization via aptamer-shRNA chimeras in human tumor xenografts. *J Clin Invest* 2011 Jun; **121**(6)**:** 2383-2390.

145. Hrkach J, Von Hoff D, Mukkaram Ali M, Andrianova E, Auer J, Campbell T*, et al.* Preclinical development and clinical translation of a PSMA-targeted docetaxel nanoparticle with a differentiated pharmacological profile. *Sci Transl Med* 2012 Apr 4; **4**(128)**:** 128ra139.

146. Zhang X, Koh CG, Yu B, Liu S, Piao L, Marcucci G*, et al.* Transferrin receptor targeted lipopolyplexes for delivery of antisense oligonucleotide g3139 in a murine k562 xenograft model. *Pharm Res* 2009 Jun; **26**(6)**:** 1516-1524.

147. Zorko NA, Bernot KM, Whitman SP, Siebenaler RF, Ahmed EH, Marcucci GG*, et al.* Mll partial tandem duplication and Flt3 internal tandem duplication in a double knock-in mouse recapitulates features of counterpart human acute myeloid leukemias. *Blood* 2012 Aug 2; **120**(5)**:** 1130-1136.

148. Litzinger DC, Buiting AM, van Rooijen N, Huang L. Effect of liposome size on the circulation time and intraorgan distribution of amphipathic poly(ethylene glycol)-containing liposomes. *Biochim Biophys Acta* 1994 Feb 23; **1190**(1)**:** 99-107.

149. Lapidot T, Sirard C, Vormoor J, Murdoch B, Hoang T, Caceres-Cortes J*, et al.* A cell initiating human acute myeloid leukaemia after transplantation into SCID mice. *Nature* 1994 Feb 17; **367**(6464)**:** 645-648.

150. Lechman ER, Gentner B, van Galen P, Giustacchini A, Saini M, Boccalatte FE*, et al.* Attenuation of miR-126 activity expands HSC in vivo without exhaustion. *Cell Stem Cell* 2012 Dec 7; **11**(6)**:** 799-811.

151. de Leeuw DC, Denkers F, Olthof MC, Rutten AP, Pouwels W, Jan Schuurhuis G*, et al.* Attenuation of microRNA-126 expression that drives CD34+38- stem/progenitor cells in acute myeloid leukemia leads to tumor eradication. *Cancer Res* 2014 Apr 1; **74**(7)**:** 2094-2105.

152. Pihlmann M, Askou AL, Aagaard L, Bruun GH, Svalgaard JD, Holm-Nielsen MH*, et al.* Adeno-associated virus-delivered polycistronic microRNA-clusters for knockdown of vascular endothelial growth factor in vivo. *J Gene Med* 2012 May; **14**(5)**:** 328-338.

153. Kasar S, Salerno E, Yuan Y, Underbayev C, Vollenweider D, Laurindo MF*, et al.* Systemic in vivo lentiviral delivery of miR-15a/16 reduces malignancy in the NZB de novo mouse model of chronic lymphocytic leukemia. *Genes Immun* 2012 Feb; **13**(2)**:** 109-119.

154. Amendola M, Passerini L, Pucci F, Gentner B, Bacchetta R, Naldini L. Regulated and multiple miRNA and siRNA delivery into primary cells by a lentiviral platform. *Mol Ther* 2009 Jun; **17**(6)**:** 1039-1052.

155. Trang P, Medina PP, Wiggins JF, Ruffino L, Kelnar K, Omotola M*, et al.* Regression of murine lung tumors by the let-7 microRNA. *Oncogene* 2010 Mar 18; **29**(11)**:** 1580-1587.

156. Rai K, Takigawa N, Ito S, Kashihara H, Ichihara E, Yasuda T*, et al.* Liposomal delivery of MicroRNA-7-expressing plasmid overcomes epidermal growth factor receptor tyrosine kinase inhibitor-resistance in lung cancer cells. *Mol Cancer Ther* 2011 Sep; **10**(9)**:** 1720-1727.

157. Chiou GY, Cherng JY, Hsu HS, Wang ML, Tsai CM, Lu KH*, et al.* Cationic polyurethanes-short branch PEI-mediated delivery of Mir145 inhibited epithelial-mesenchymal transdifferentiation and cancer stem-like properties and in lung adenocarcinoma. *J Control Release* 2012 Apr 30; **159**(2)**:** 240-250.

158. Yang YP, Chien Y, Chiou GY, Cherng JY, Wang ML, Lo WL*, et al.* Inhibition of cancer stem cell-like properties and reduced chemoradioresistance of glioblastoma using microRNA145 with cationic polyurethane-short branch PEI. *Biomaterials* 2012 Feb; **33**(5)**:** 1462-1476.

159. Pramanik D, Campbell NR, Karikari C, Chivukula R, Kent OA, Mendell JT*, et al.* Restitution of tumor suppressor microRNAs using a systemic nanovector inhibits pancreatic cancer growth in mice. *Mol Cancer Ther* 2011 Aug; **10**(8)**:** 1470-1480.

160. Trang P, Wiggins JF, Daige CL, Cho C, Omotola M, Brown D*, et al.* Systemic delivery of tumor suppressor microRNA mimics using a neutral lipid emulsion inhibits lung tumors in mice. *Mol Ther* 2011 Jun; **19**(6)**:** 1116-1122.

161. Chen Y, Zhu X, Zhang X, Liu B, Huang L. Nanoparticles modified with tumor-targeting scFv deliver siRNA and miRNA for cancer therapy. *Mol Ther* 2010 Sep; **18**(9)**:** 1650-1656.

162. Piao L, Zhang M, Datta J, Xie X, Su T, Li H*, et al.* Lipid-based nanoparticle delivery of Pre-miR-107 inhibits the tumorigenicity of head and neck squamous cell carcinoma. *Mol Ther* 2012 Jun; **20**(6)**:** 1261-1269.

163. Wiggins JF, Ruffino L, Kelnar K, Omotola M, Patrawala L, Brown D*, et al.* Development of a lung cancer therapeutic based on the tumor suppressor microRNA-34. *Cancer Res* 2010 Jul 15; **70**(14)**:** 5923-5930.

164. Wu Y, Crawford M, Yu B, Mao Y, Nana-Sinkam SP, Lee LJ. MicroRNA delivery by cationic lipoplexes for lung cancer therapy. *Mol Pharm* 2011 Aug 1; **8**(4)**:** 1381-1389.

165. Liu C, Kelnar K, Liu B, Chen X, Calhoun-Davis T, Li H*, et al.* The microRNA miR-34a inhibits prostate cancer stem cells and metastasis by directly repressing CD44. *Nat Med* 2011 Feb; **17**(2)**:** 211-215.

166. Craig VJ, Tzankov A, Flori M, Schmid CA, Bader AG, Muller A. Systemic microRNA-34a delivery induces apoptosis and abrogates growth of diffuse large B-cell lymphoma in vivo. *Leukemia* 2012 Nov; **26**(11)**:** 2421-2424.

167. Ibrahim AF, Weirauch U, Thomas M, Grunweller A, Hartmann RK, Aigner A. MicroRNA replacement therapy for miR-145 and miR-33a is efficacious in a model of colon carcinoma. *Cancer Res* 2011 Aug 1; **71**(15)**:** 5214-5224.

168. Takeshita F, Patrawala L, Osaki M, Takahashi RU, Yamamoto Y, Kosaka N*, et al.* Systemic delivery of synthetic microRNA-16 inhibits the growth of metastatic prostate tumors via downregulation of multiple cell-cycle genes. *Mol Ther* 2010 Jan; **18**(1)**:** 181-187.

169. Babar IA, Cheng CJ, Booth CJ, Liang X, Weidhaas JB, Saltzman WM*, et al.* Nanoparticle-based therapy in an in vivo microRNA-155 (miR-155)-dependent mouse model of lymphoma. *Proc Natl Acad Sci U S A* 2012 Jun 26; **109**(26)**:** E1695-1704.

170. McCarty DM. Self-complementary AAV vectors; advances and applications. *Mol Ther* 2008 Oct; **16**(10)**:** 1648-1656.

171. Campbell RB, Fukumura D, Brown EB, Mazzola LM, Izumi Y, Jain RK*, et al.* Cationic charge determines the distribution of liposomes between the vascular and extravascular compartments of tumors. *Cancer Res* 2002 Dec 1; **62**(23)**:** 6831-6836.

172. Tanaka T, Legat A, Adam E, Steuve J, Gatot JS, Vandenbranden M*, et al.* DiC14-amidine cationic liposomes stimulate myeloid dendritic cells through Toll-like receptor 4. *Eur J Immunol* 2008 May; **38**(5)**:** 1351-1357.

173. Lonez C, Vandenbranden M, Ruysschaert JM. Cationic liposomal lipids: from gene carriers to cell signaling. *Prog Lipid Res* 2008 Sep; **47**(5)**:** 340-347.

174. Aliabadi HM, Landry B, Bahadur RK, Neamnark A, Suwantong O, Uludag H. Impact of lipid substitution on assembly and delivery of siRNA by cationic polymers. *Macromol Biosci* 2011 May 12; **11**(5)**:** 662-672.

175. Beduneau A, Saulnier P, Hindre F, Clavreul A, Leroux JC, Benoit JP. Design of targeted lipid nanocapsules by conjugation of whole antibodies and antibody Fab' fragments. *Biomaterials* 2007 Nov; **28**(33)**:** 4978-4990.

176. Li Z, Hassan MQ, Jafferji M, Aqeilan RI, Garzon R, Croce CM*, et al.* Biological functions of miR-29b contribute to positive regulation of osteoblast differentiation. *J Biol Chem* 2009 Jun 5; **284**(23)**:** 15676-15684.

177. Liu Y, Taylor NE, Lu L, Usa K, Cowley AW, Jr., Ferreri NR*, et al.* Renal medullary microRNAs in Dahl salt-sensitive rats: miR-29b regulates several collagens and related genes. *Hypertension* 2010 Apr; **55**(4)**:** 974-982.

178. Sengupta S, den Boon JA, Chen IH, Newton MA, Stanhope SA, Cheng YJ*, et al.* MicroRNA 29c is down-regulated in nasopharyngeal carcinomas, up-regulating mRNAs encoding extracellular matrix proteins. *Proc Natl Acad Sci U S A* 2008 Apr 15; **105**(15)**:** 5874-5878.

179. van Rooij E, Sutherland LB, Thatcher JE, DiMaio JM, Naseem RH, Marshall WS*, et al.* Dysregulation of microRNAs after myocardial infarction reveals a role of miR-29 in cardiac fibrosis. *Proc Natl Acad Sci U S A* 2008 Sep 2; **105**(35)**:** 13027-13032.

180. Flavin R, Smyth P, Barrett C, Russell S, Wen H, Wei J*, et al.* miR-29b expression is associated with disease-free survival in patients with ovarian serous carcinoma. *Int J Gynecol Cancer* 2009 May; **19**(4)**:** 641-647.

181. Dai F, Zhang Y, Chen Y. Involvement of miR-29b signaling in the sensitivity to chemotherapy in patients with ovarian carcinoma. *Hum Pathol* 2014 Jun; **45**(6)**:** 1285-1293.

182. Xiong Y, Fang JH, Yun JP, Yang J, Zhang Y, Jia WH*, et al.* Effects of microRNA-29 on apoptosis, tumorigenicity, and prognosis of hepatocellular carcinoma. *Hepatology* 2010 Mar; **51**(3)**:** 836-845.

183. Yanaihara N, Caplen N, Bowman E, Seike M, Kumamoto K, Yi M*, et al.* Unique microRNA molecular profiles in lung cancer diagnosis and prognosis. *Cancer Cell* 2006 Mar; **9**(3)**:** 189-198.

184. Zhao JJ, Lin J, Lwin T, Yang H, Guo J, Kong W*, et al.* microRNA expression profile and identification of miR-29 as a prognostic marker and pathogenetic factor by targeting CDK6 in mantle cell lymphoma. *Blood* 2010 Apr 1; **115**(13)**:** 2630-2639.

185. Xiong Y, Li Z, Ji M, Tan AC, Bemis J, Tse JV*, et al.* MIR29B regulates expression of MLLT11 (AF1Q), an MLL fusion partner, and low MIR29B expression associates with adverse cytogenetics and poor overall survival in AML. *Br J Haematol* 2011 Jun; **153**(6)**:** 753-757.

186. Amodio N, Di Martino MT, Foresta U, Leone E, Lionetti M, Leotta M*, et al.* miR-29b sensitizes multiple myeloma cells to bortezomib-induced apoptosis through the activation of a feedback loop with the transcription factor Sp1. *Cell Death Dis* 2012; **3:** e436.

187. Zhang YK, Wang H, Leng Y, Li ZL, Yang YF, Xiao FJ*, et al.* Overexpression of microRNA-29b induces apoptosis of multiple myeloma cells through down regulating Mcl-1. *Biochem Biophys Res Commun* 2011 Oct 14; **414**(1)**:** 233-239.

188. Steele R, Mott JL, Ray RB. MBP-1 upregulates miR-29b that represses Mcl-1, collagens, and matrix-metalloproteinase-2 in prostate cancer cells. *Genes Cancer* 2010 Apr 1; **1**(4)**:** 381-387.

189. Ru P, Steele R, Newhall P, Phillips NJ, Toth K, Ray RB. miRNA-29b suppresses prostate cancer metastasis by regulating epithelial-mesenchymal transition signaling. *Mol Cancer Ther* 2012 May; **11**(5)**:** 1166-1173.

190. Teng Y, Zhao L, Zhang Y, Chen W, Li X. Id-1, a Protein Repressed by miR-29b, Facilitates the TGFbeta1-Induced Epithelial-Mesenchymal Transition in Human Ovarian Cancer Cells. *Cell Physiol Biochem* 2014; **33**(3)**:** 717-730.

191. Grant JL, Fishbein MC, Hong LS, Krysan K, Minna JD, Shay JW*, et al.* A novel molecular pathway for snail-dependent, SPARC-mediated invasion in non-small cell lung cancer pathogenesis. *Cancer Prev Res (Phila)* 2014 Jan; **7**(1)**:** 150-160.

192. Rothschild SI, Tschan MP, Federzoni EA, Jaggi R, Fey MF, Gugger M*, et al.* MicroRNA-29b is involved in the Src-ID1 signaling pathway and is dysregulated in human lung adenocarcinoma. *Oncogene* 2012 Sep 20; **31**(38)**:** 4221-4232.

193. Mott JL, Kobayashi S, Bronk SF, Gores GJ. mir-29 regulates Mcl-1 protein expression and apoptosis. *Oncogene* 2007 Sep 13; **26**(42)**:** 6133-6140.

194. Garzon R, Heaphy CE, Havelange V, Fabbri M, Volinia S, Tsao T*, et al.* MicroRNA 29b functions in acute myeloid leukemia. *Blood* 2009 Dec 17; **114**(26)**:** 5331-5341.

195. Alachkar H, Santhanam R, Maharry K, Metzeler KH, Huang X, Kohlschmidt J*, et al.* SPARC promotes leukemic cell growth and predicts acute myeloid leukemia outcome. *J Clin Invest* 2014 Apr 1; **124**(4)**:** 1512-1524.

196. Amodio N, Leotta M, Bellizzi D, Di Martino MT, D'Aquila P, Lionetti M*, et al.* DNA-demethylating and anti-tumor activity of synthetic miR-29b mimics in multiple myeloma. *Oncotarget* 2012 Oct; **3**(10)**:** 1246-1258.

197. Amodio N, Bellizzi D, Leotta M, Raimondi L, Biamonte L, D'Aquila P*, et al.* miR-29b induces SOCS-1 expression by promoter demethylation and negatively regulates migration of multiple myeloma and endothelial cells. *Cell Cycle* 2013 Dec 1; **12**(23)**:** 3650-3662.

198. Garzon R, Liu S, Fabbri M, Liu Z, Heaphy CE, Callegari E*, et al.* MicroRNA-29b induces global DNA hypomethylation and tumor suppressor gene reexpression in acute myeloid leukemia by targeting directly DNMT3A and 3B and indirectly DNMT1. *Blood* 2009 Jun 18; **113**(25)**:** 6411-6418.

199. Fabbri M, Garzon R, Cimmino A, Liu Z, Zanesi N, Callegari E*, et al.* MicroRNA-29 family reverts aberrant methylation in lung cancer by targeting DNA methyltransferases 3A and 3B. *Proc Natl Acad Sci U S A* 2007 Oct 2; **104**(40)**:** 15805-15810.

200. Wang H, Garzon R, Sun H, Ladner KJ, Singh R, Dahlman J*, et al.* NF-kappaB-YY1-miR-29 regulatory circuitry in skeletal myogenesis and rhabdomyosarcoma. *Cancer Cell* 2008 Nov 4; **14**(5)**:** 369-381.

201. Xu H, Cheung IY, Guo HF, Cheung NK. MicroRNA miR-29 modulates expression of immunoinhibitory molecule B7-H3: potential implications for immune based therapy of human solid tumors. *Cancer Res* 2009 Aug 1; **69**(15)**:** 6275-6281.

202. Liu S, Wu LC, Pang J, Santhanam R, Schwind S, Wu YZ*, et al.* Sp1/NFkappaB/HDAC/miR-29b regulatory network in KIT-driven myeloid leukemia. *Cancer Cell* 2010 Apr 13; **17**(4)**:** 333-347.

203. Blum W, Schwind S, Tarighat SS, Geyer S, Eisfeld AK, Whitman S*, et al.* Clinical and pharmacodynamic activity of bortezomib and decitabine in acute myeloid leukemia. *Blood* 2012 Jun 21; **119**(25)**:** 6025-6031.

204. Ozeki K, Kiyoi H, Hirose Y, Iwai M, Ninomiya M, Kodera Y*, et al.* Biologic and clinical significance of the FLT3 transcript level in acute myeloid leukemia. *Blood* 2004 Mar 1; **103**(5)**:** 1901-1908.

205. Paschka P, Marcucci G, Ruppert AS, Mrozek K, Chen H, Kittles RA*, et al.* Adverse prognostic significance of KIT mutations in adult acute myeloid leukemia with inv(16) and t(8;21): a Cancer and Leukemia Group B Study. *J Clin Oncol* 2006 Aug 20; **24**(24)**:** 3904-3911.

206. Liu S, Liu Z, Xie Z, Pang J, Yu J, Lehmann E*, et al.* Bortezomib induces DNA hypomethylation and silenced gene transcription by interfering with Sp1/NF-kappaB-dependent DNA methyltransferase activity in acute myeloid leukemia. *Blood* 2008 Feb 15; **111**(4)**:** 2364-2373.

207. Liu Z, Liu S, Xie Z, Blum W, Perrotti D, Paschka P*, et al.* Characterization of in vitro and in vivo hypomethylating effects of decitabine in acute myeloid leukemia by a rapid, specific and sensitive LC-MS/MS method. *Nucleic Acids Res* 2007; **35**(5)**:** e31.

208. Neviani P, Santhanam R, Oaks JJ, Eiring AM, Notari M, Blaser BW*, et al.* FTY720, a new alternative for treating blast crisis chronic myelogenous leukemia and Philadelphia chromosome-positive acute lymphocytic leukemia. *J Clin Invest* 2007 Sep; **117**(9)**:** 2408-2421.

209. Ranganathan P, Yu X, Na C, Santhanam R, Shacham S, Kauffman M*, et al.* Preclinical activity of a novel CRM1 inhibitor in acute myeloid leukemia. *Blood* 2012 Aug 30; **120**(9)**:** 1765-1773.

210. Stapnes C, Ryningen A, Hatfield K, Oyan AM, Eide GE, Corbascio M*, et al.* Functional characteristics and gene expression profiles of primary acute myeloid leukaemia cells identify patient subgroups that differ in susceptibility to histone deacetylase inhibitors. *Int J Oncol* 2007 Dec; **31**(6)**:** 1529-1538.

211. Henao-Mejia J, Williams A, Goff LA, Staron M, Licona-Limon P, Kaech SM*, et al.* The microRNA miR-181 is a critical cellular metabolic rheostat essential for NKT cell ontogenesis and lymphocyte development and homeostasis. *Immunity* 2013 May 23; **38**(5)**:** 984-997.

212. Zietara N, Lyszkiewicz M, Witzlau K, Naumann R, Hurwitz R, Langemeier J*, et al.* Critical role for miR-181a/b-1 in agonist selection of invariant natural killer T cells. *Proc Natl Acad Sci U S A* 2013 Apr 30; **110**(18)**:** 7407-7412.

213. Pichler M, Winter E, Ress AL, Bauernhofer T, Gerger A, Kiesslich T*, et al.* miR-181a is associated with poor clinical outcome in patients with colorectal cancer treated with EGFR inhibitor. *J Clin Pathol* 2014 Mar; **67**(3)**:** 198-203.

214. Yang CC, Hung PS, Wang PW, Liu CJ, Chu TH, Cheng HW*, et al.* miR-181 as a putative biomarker for lymph-node metastasis of oral squamous cell carcinoma. *J Oral Pathol Med* 2011 May; **40**(5)**:** 397-404.

215. Shi L, Cheng Z, Zhang J, Li R, Zhao P, Fu Z*, et al.* hsa-mir-181a and hsa-mir-181b function as tumor suppressors in human glioma cells. *Brain Res* 2008 Oct 21; **1236:** 185-193.

216. Taylor MA, Sossey-Alaoui K, Thompson CL, Danielpour D, Schiemann WP. TGF-beta upregulates miR-181a expression to promote breast cancer metastasis. *J Clin Invest* 2013 Jan 2; **123**(1)**:** 150-163.

217. Zhu Y, Wu J, Li S, Ma R, Cao H, Ji M*, et al.* The function role of miR-181a in chemosensitivity to adriamycin by targeting Bcl-2 in low-invasive breast cancer cells. *Cell Physiol Biochem* 2013; **32**(5)**:** 1225-1237.

218. Jiao X, Zhao L, Ma M, Bai X, He M, Yan Y*, et al.* MiR-181a enhances drug sensitivity in mitoxantone-resistant breast cancer cells by targeting breast cancer resistance protein (BCRP/ABCG2). *Breast Cancer Res Treat* 2013 Jun; **139**(3)**:** 717-730.

219. Zhu DX, Zhu W, Fang C, Fan L, Zou ZJ, Wang YH*, et al.* miR-181a/b significantly enhances drug sensitivity in chronic lymphocytic leukemia cells via targeting multiple anti-apoptosis genes. *Carcinogenesis* 2012 Jul; **33**(7)**:** 1294-1301.

220. Lin S, Pan L, Guo S, Wu J, Jin L, Wang JC*, et al.* Prognostic role of microRNA-181a/b in hematological malignancies: a meta-analysis. *PLoS One* 2013; **8**(3)**:** e59532.

221. Li Z, Huang H, Li Y, Jiang X, Chen P, Arnovitz S*, et al.* Up-regulation of a HOXA-PBX3 homeobox-gene signature following down-regulation of miR-181 is associated with adverse prognosis in patients with cytogenetically abnormal AML. *Blood* 2012 Mar 8; **119**(10)**:** 2314-2324.

222. Chung E, Kondo M. Role of Ras/Raf/MEK/ERK signaling in physiological hematopoiesis and leukemia development. *Immunol Res* 2011 Apr; **49**(1-3)**:** 248-268.

223. Tyner JW, Erickson H, Deininger MW, Willis SG, Eide CA, Levine RL*, et al.* High-throughput sequencing screen reveals novel, transforming RAS mutations in myeloid leukemia patients. *Blood* 2009 Feb 19; **113**(8)**:** 1749-1755.

224. Illmer T, Thiede C, Fredersdorf A, Stadler S, Neubauer A, Ehninger G*, et al.* Activation of the RAS pathway is predictive for a chemosensitive phenotype of acute myelogenous leukemia blasts. *Clin Cancer Res* 2005 May 1; **11**(9)**:** 3217-3224.

225. Kim WI, Matise I, Diers MD, Largaespada DA. RAS oncogene suppression induces apoptosis followed by more differentiated and less myelosuppressive disease upon relapse of acute myeloid leukemia. *Blood* 2009 Jan 29; **113**(5)**:** 1086-1096.

226. Parikh C, Subrahmanyam R, Ren R. Oncogenic NRAS rapidly and efficiently induces CMML- and AML-like diseases in mice. *Blood* 2006 Oct 1; **108**(7)**:** 2349-2357.

227. Towatari M, Iida H, Tanimoto M, Iwata H, Hamaguchi M, Saito H. Constitutive activation of mitogen-activated protein kinase pathway in acute leukemia cells. *Leukemia* 1997 Apr; **11**(4)**:** 479-484.

228. Wu J, Wong WW, Khosravi F, Minden MD, Penn LZ. Blocking the Raf/MEK/ERK pathway sensitizes acute myelogenous leukemia cells to lovastatin-induced apoptosis. *Cancer Res* 2004 Sep 15; **64**(18)**:** 6461-6468.

229. Grandage VL, Gale RE, Linch DC, Khwaja A. PI3-kinase/Akt is constitutively active in primary acute myeloid leukaemia cells and regulates survival and chemoresistance via NF-kappaB, Mapkinase and p53 pathways. *Leukemia* 2005 Apr; **19**(4)**:** 586-594.

230. Min YH, Eom JI, Cheong JW, Maeng HO, Kim JY, Jeung HK*, et al.* Constitutive phosphorylation of Akt/PKB protein in acute myeloid leukemia: its significance as a prognostic variable. *Leukemia* 2003 May; **17**(5)**:** 995-997.

231. Xu Q, Simpson SE, Scialla TJ, Bagg A, Carroll M. Survival of acute myeloid leukemia cells requires PI3 kinase activation. *Blood* 2003 Aug 1; **102**(3)**:** 972-980.

232. Kornblau SM, Womble M, Qiu YH, Jackson CE, Chen W, Konopleva M*, et al.* Simultaneous activation of multiple signal transduction pathways

confers poor prognosis in acute myelogenous leukemia. *Blood* 2006 Oct 1; **108**(7)**:** 2358-2365.

233. Min YH, Cheong JW, Kim JY, Eom JI, Lee ST, Hahn JS*, et al.* Cytoplasmic mislocalization of p27Kip1 protein is associated with constitutive phosphorylation of Akt or protein kinase B and poor prognosis in acute myelogenous leukemia. *Cancer Res* 2004 Aug 1; **64**(15)**:** 5225-5231.

234. Brandwein JM, Hedley DW, Chow S, Schimmer AD, Yee KW, Schuh AC*, et al.* A phase I/II study of imatinib plus reinduction therapy for c-kit-positive relapsed/refractory acute myeloid leukemia: inhibition of Akt activation correlates with complete response. *Leukemia* 2011 Jun; **25**(6)**:** 945-952.

235. Martelli AM, Nyakern M, Tabellini G, Bortul R, Tazzari PL, Evangelisti C*, et al.* Phosphoinositide 3-kinase/Akt signaling pathway and its therapeutical implications for human acute myeloid leukemia. *Leukemia* 2006 Jun; **20**(6)**:** 911-928.

236. Schubbert S, Shannon K, Bollag G. Hyperactive Ras in developmental disorders and cancer. *Nat Rev Cancer* 2007 Apr; **7**(4)**:** 295-308.

237. Shin KH, Bae SD, Hong HS, Kim RH, Kang MK, Park NH. miR-181a shows tumor suppressive effect against oral squamous cell carcinoma cells by downregulating K-ras. *Biochem Biophys Res Commun* 2011 Jan 28; **404**(4)**:** 896-902.

238. Huang X, Schwind S, Yu B, Santhanam R, Wang H, Hoellerbauer P*, et al.* Targeted delivery of microRNA-29b by transferrin-conjugated anionic lipopolyplex nanoparticles: a novel therapeutic strategy in acute myeloid leukemia. *Clin Cancer Res* 2013 May 1; **19**(9)**:** 2355-2367.

239. Bai H, Cao Z, Deng C, Zhou L, Wang C. miR-181a sensitizes resistant leukaemia HL-60/Ara-C cells to Ara-C by inducing apoptosis. *J Cancer Res Clin Oncol* 2012 Apr; **138**(4)**:** 595-602.

240. Sears R, Nuckolls F, Haura E, Taya Y, Tamai K, Nevins JR. Multiple Ras-dependent phosphorylation pathways regulate Myc protein stability. *Genes Dev* 2000 Oct 1; **14**(19)**:** 2501-2514.

241. Marcucci G, Mrozek K, Radmacher MD, Garzon R, Bloomfield CD. The prognostic and functional role of microRNAs in acute myeloid leukemia. *Blood* 2011 Jan 27; **117**(4)**:** 1121-1129.

242. Jiang X, Huang H, Li Z, He C, Li Y, Chen P*, et al.* MiR-495 is a tumor-suppressor microRNA down-regulated in MLL-rearranged leukemia. *Proc Natl Acad Sci U S A* 2012 Nov 20; **109**(47)**:** 19397-19402.

243. Mims A, Walker AR, Huang X, Sun J, Wang H, Santhanam R*, et al.* Increased anti-leukemic activity of decitabine via AR-42-induced upregulation of miR-29b: a novel epigenetic-targeting approach in acute myeloid leukemia. *Leukemia* 2013 Apr; **27**(4)**:** 871-878.

244. Chen G, Zhu W, Shi D, Lv L, Zhang C, Liu P*, et al.* MicroRNA-181a sensitizes human malignant glioma U87MG cells to radiation by targeting Bcl-2. *Oncol Rep* 2010 Apr; **23**(4)**:** 997-1003.

245. Ouyang YB, Lu Y, Yue S, Giffard RG. miR-181 targets multiple Bcl-2 family members and influences apoptosis and mitochondrial function in astrocytes. *Mitochondrion* 2012 Mar; **12**(2)**:** 213-219.

246. Hutchison ER, Kawamoto EM, Taub DD, Lal A, Abdelmohsen K, Zhang Y*, et al.* Evidence for miR-181 involvement in neuroinflammatory responses of astrocytes. *Glia* 2013 Jul; **61**(7)**:** 1018-1028.

247. Cichocki F, Felices M, McCullar V, Presnell SR, Al-Attar A, Lutz CT*, et al.* Cutting edge: microRNA-181 promotes human NK cell development by regulating Notch signaling. *J Immunol* 2011 Dec 15; **187**(12)**:** 6171-6175.

248. Chen CZ, Schaffert S, Fragoso R, Loh C. Regulation of immune responses and tolerance: the microRNA perspective. *Immunol Rev* 2013 May; **253**(1)**:** 112-128.

249. Ward AF, Braun BS, Shannon KM. Targeting oncogenic Ras signaling in hematologic malignancies. *Blood* 2012 Oct 25; **120**(17)**:** 3397-3406.

250. Borthakur G, Kantarjian H, Ravandi F, Zhang W, Konopleva M, Wright JJ*, et al.* Phase I study of sorafenib in patients with refractory or relapsed acute leukemias. *Haematologica* 2011 Jan; **96**(1)**:** 62-68.

251. Zhao S, Zhang Y, Sha K, Tang Q, Yang X, Yu C*, et al.* KRAS (G12D) Cooperates with AML1/ETO to Initiate a Mouse Model Mimicking Human Acute Myeloid Leukemia. *Cell Physiol Biochem* 2014; **33**(1)**:** 78-87.

252. Gritsman K, Yuzugullu H, Von T, Yan H, Clayton L, Fritsch C*, et al.* Hematopoiesis and RAS-driven myeloid leukemia differentially require PI3K isoform p110alpha. *J Clin Invest* 2014 Apr 1; **124**(4)**:** 1794-1809.

253. Kothe S, Muller JP, Bohmer SA, Tschongov T, Fricke M, Koch S*, et al.* Features of Ras activation by a mislocalized oncogenic tyrosine kinase: FLT3 ITD signals through K-Ras at the plasma membrane of acute myeloid leukemia cells. *J Cell Sci* 2013 Oct 15; **126**(Pt 20)**:** 4746-4755.

254. Stephen AG, Esposito D, Bagni RK, McCormick F. Dragging ras back in the ring. *Cancer Cell* 2014 Mar 17; **25**(3)**:** 272-281.

Appendix: Detailed Protocols

1. Empty nanoparticle preparation
    a. Dissolve lipids in ethanol solutions at the concentration of:

        DOPE: 25 mg/ml (Avanti Polar Lipids; 850725E or 850725P)

        Linoleic acid: 100 mg/ml (Sigma-Aldrich; L1376-500MG)

        DMG-PEG: 20 mg/ml (NOF America Corporation; SUNBRIGHT® GM-020)

    b. Mix three lipids ethanol solutions at the molar ratio of DOPE:linoleic acid:DMG-PEG=50:48:2. Mix 1069.3 µl DOPE, 96.7 µl linoleic acid, 179.7 µl DMG-PEG and 654.3 µl ethanol up to total 2 ml. Lipids mixture concentration is 20 mg/ml.
    c. Put 300 µl lipids mixture from above step into 1.5 ml ependorf.
    d. Draw 300 µl lipids mixture into U100 Insulin syringe with $29_G½″$ gauge (Becton Dickinson; 309311). Put 2.7 ml 20 mM HEPES buffer (Fisher; BP299-500; 1M) into BD 5 ml polyprogylene Round-Bottom flow tube (BD Falcon; 352063). Put needle tip under the HEPES buffer surface and inject lipids solution as fast as possible into buffer to form empty nanoparticles.

e. Vortex. And sonicate empty nanoparticle solution in water bath sonicator (VWR International; Model No. 50HT; Serial No. 01HS 38 184; 120 Volts 2 Amps 50/60Hz) for 3-5 minutes. The final concentration of empty nanoparticles is 2 mg/ml.

f. Store empty nanoparticles at 4°C.

2. Transferrin-PEG-DSPE synthesis

a. Dissolve Traut's reagent (Thermo Scientific; PI-26101; No.26101) in PBS buffer (pH=8.0) at 1 mg/ml. Dissolve holo-Tf (Tf, Sigma-Aldrich; T4132-500MG) in PBS buffer (pH=8.0) at 5 mg/ml.

b. Mixed 5 mg Tf solution with 0.086 mg Traut's reagent at molar ratio of 10:1 at room temperature for 2 hours to yield Tf-SH

c. Remove extra Traut's reagent by PD10 column (GE Health). Wash the column with PBS buffer (pH=6.5) three times. Load Tf and Traut's mixture solution into PD10 column. Add 500 µl PBS buffer (pH=6.5) twice. At the third time, start to collect elution solution. Collect 8 tubes of elution solution.

d. Dilute Bio-Rad protein assay dye reagent (Bio-Rad; #500-0006) 1:4 with water. Put 300 µl of diluted dye reagent into ependorf tube and mixted with 10 µl Tf elution buffer from each collected tubes. Combined all Tf-SH in collected tubes which corresponding dye reagent turn blue.

e. Dissolve 1.83 mg Mal-PEG-DSPE (Avanti Polar Lipids; 880126P) in 183 µl PBS buffer (pH=6.5). The molar ratio of Tf to Mal-PEG-DSPE is 10:1. Mix

Tf-SH with Mal-PEG-DSPE for overnight at room temperature to yield micelles of Tf-PEG-DSPE.

f. Filter Tf-PEG-DSPE with 0.22 μm filter (Fisher; 09-720-3). Measure the Tf concentration by Nanodrop A280.

g. Store Tf-PEG-ESPE at 4°C.

3. Antibody-PEG-DSPE synthesis

a. Load Ab solution (without BSA and other proteins; usually 500 μg) in Centrifugal Filter Unit (Millipore; Microcon®-10; MRCPRT010). Concentrate Ab by centrifugation at 13,200 rpm for 20 minutes. Wash with PBS buffer (pH=8.0) twice. Dilute Ab with PBS buffer (pH=8.0) by adding ~400 μl.

b. Mix Ab solution in PBS buffer (pH=8.0) with 4.6 μl (4.6 μg) Traut's reagent at room temperature for 2 hours.

c. Remove extra Traut's by loading the mixture solution into Centrifugal Filter Unit and centrifuging at 13,200 rpm for 25 minutes. Wash with PBS buffer (pH=6.5) for three times. Refill filter cartridge with ~400 μl PBS buffer (pH=6.5).

d. Mix Ab-SH with 98 μl (98 μg) Mal-PEG-DSPE PBS (pH=6.5) solution.

e. Measure Ab concentration by Nanodrop (choosing IgG category).

f. Store Ab-PEG-DSPE at 4°C.

Note: Final Ab recovery rate is around 60-70%. Since there is no filtering step at the end, try to keep every step as sterilizing as possible.

4. Targeted lipopolyplex nanoparticle preparation

a. Prepare miR stock solution by adding sterilized Nuclease-free water to miR powder. For *in vitro* study, miR duplex mimic (MW ~14,000) stock concentration is 100 µM (50 µl water is added to 5 nmol miR powder). For *in vivo* study, miR duplex mimic stock concentration is 7 µg/µl (500 µl water is added to 250 nmol miR powder). For *in vivo* study, miR single strand or ODN (MW ~7,000) stock concentration is 5 µg/µl. Prepare PEI (Sigma Aldrich; 408700; low mol. Wt., 50 wt. % soln. in water; MW ~2000; density ~1.08 g/ml at 25°C) stock solution. Weight PEI 1 g (~ 926 µl) in 50 ml tube and add HEPES buffer up to 50 ml to have PEI concentration of 10 mg/ml. Then further dilute to 1 mg/ml working solution.
b. Calculate how much miR/siRNA/antagomiR/ODN will be used in the treatment determined by cell numbers and miR final concentration. Calculate how much PEI and empty nanoparticle will be used. The weight ratio of miR:PEI is 1:1.25 and miR:lipid is 1:10. For example, if I want to treat 4 ml cells at 100 nM miR, I will need 5.6 µg miR which is 4 µl of 100 µM miR stock. Then 7 µg of PEI and 56 µg empty nanoparticles are need.
c. Dilute miR stock solution and PEI with HEPES buffer (20 mM) to desired volume (4 µl miR + 18 µl HEPES; 7 µl PEI + 15 µl HEPES). Add miR solution to PEI solution and mix them by vortex. Incubate mixture at room temperature for 3-5 minutes.
d. Dilute empty nanoparticle with HEPES buffer to 1 mg/ml. Add 56 µl empty nanoparticles to PEI/miR mixture. Vortex and then sonicate for 3-5 minutes. Incubate at room temperature for another 10 minutes.

e. Add Tf-PEG-DSPE or Ab-PEG-DSPE to miR-loaded nanoparticles and mix by vortex. The molar ratio of Tf to lipid is 1:2000. The optimal molar ratio of Ab to lipid can be determined by cellular uptake assay. Incubate the mixture solution at 37°C for ~1 hour.

f. Better to use the final product in 24 hours, otherwise store at 4°C. During the storage time, if the conjugations of nanoparticles occur, break the conjugations by vortex.

5. Concentrate nanoparticles

   a. Load prepared nanoparticles in Centrifual Filter Tube (Millipore; Amicon® Ultra Centrifual Filters; Ultracel® -3K; UFC800324).

   b. Centrifuge Tube at 3000 rpm for 30 min. The volume can be reduced half.

6. RNA extraction by TRIzol (modified from TRIzol® manufacture's protocol)

   a. Lyse ~1 million cells with TRIzol Reagent (Life Technology; 15596-018). Incubate the sample for 5 minutes at room temperature.

   b. Add 200 µl chloroform per 1 ml TRIzol and shake tube vigorously for 15 second.

   c. Incubate for 2-3 minutes at room temperature.

   d. Centrifuge the sample at 13,200 rpm for 20 minutes at 4°C.

   e. Transfer the aqueous phase of the sample to a new tube (~150 µl, 3 times).

   f. Add 500 µl 100% isopropanol the aqueous phase. Incubate at room temperature for 10 minutes on a shaker.

   g. Centrifuge at 13,200 rpm for 15 minutes at 4°C.

h. Remove the supernatant from the tube.

i. Wash the pellet with 1 ml of 75% ethanol. Vortex the sample briefly.

j. Centrifuge the tube at 12,000 rpm for 5 minutes at 4°C. Discard the wash and centrifuge the tube again.

k. Carefully remove the remaining ethanol.

l. Resuspend the RNA pellet in RNAase-free water.

m. Store RNA sample at -80°C.

7. Quantitative RT-PCR for mRNA expression

a. Measure RNA concentration by NanoDrop. Make 50 ng/µl RNA solution for each sample.

b. CDNA synthesis (modified from SuperScript® III First-Strand Synthesis (Life Technology; 18080-051) protocol)

c. 50 ng/µl random hexamers	1 µl	
d. 10 mM dNTP mix	1 µl	
e. 50 ng/µl RNA sample	8 µl	

f. Incubate the tube at 65°C for 5 minutes, then place on ice for 5 minutes.

g. cDNA Synthesis Mix

10X RT buffer	2 µl	
25 mM $MgCl_2$	4 µl	
0.1 M DTT	2 µl	
RNaseOUT™ (40 U/ µl)	1 µl	(10777-019)
SuperScript® III RT (200 U/ µl)	1 µl	(18080-044)

h. Add 10 µl cDNA Synthesis Mix to each RNA/primer mixture.

i. Incubate 10 minutes at 25°C, 50 minutes at 50°C, then 5 minutes at 85°C. Chill on ice.

j. Real-time PCR (modified from TaqMan® Fast Universal PCR Master (2x) (Life Technology; 4352042) protocol)

Each well (10 µl) add Mater Mix	5 µl
TaqMan® Gene Expression Assay Mix	0.5 µl
RNase-free water	2.5 µl
cDNA sample	2 µl

Note: TaqMan® Gene Expression Assay Mix (20X) containing:

Forward PCR primer (18 µM)

Reverse PCR primer (18 µM)

Taqman® probe (5 µM)

8. Quantitative RT-PCR for miRNA expression

a. Measure RNA concentration by NanoDrop. Make 50 ng/µl RNA solution for each sample.

b. miR reverse-transcription reaction (modified from Taqman® Small RNA Assay protocol)

c. RT reaction master mix (15 µl including three sets of different 5X RT primers)

d. Taqman MicroRNA Reverse Transcription Kit (Life Technology; 4366597)

Water	4.51 µl
10X RT Buffer	1.5 µl
MultiScribe™ Reverse Transcriptase, 50 U/ µl	0.75 µl

RNase Inhibitor, 20 U/ µl	0.07 µl
100mM dNTPs	0.17 µl
5X RT primers #1	2 µl
5X RT primers #2	2 µl
5X RT primers #3	2 µl
50 ng/ µl RNA	2 µl

e. Incubate 30 minutes at 16°C, 30 minutes at 42°C and 5 minutes at 85°C. Chill on ice.

f. Real-time PCR is the same as above.

9. Western blotting

a. Prepare lysis buffer.

Blank lysis buffer	Stock	Volume
20mM HEPES pH=7.4	1 M	1 ml
150mM NaCl	5 M	1.5 ml
0.1% NP40	10% (w/v)(Roche Diagnostics; 11332473001)	500 µl
		+ water up to 50 ml

10 ml Blank lysis buffer Substitute with	Stock	Volume
Protease Inhibitor (Calbiochem; 539134)	100X	100 µl
Phosphatase Inhibitor Cocktail 2 (Sigma; P5726)	100X	100 µl
Phosphatase Inhibitor Cocktail 3 (Sigma; P0044)	100X	100 µl

b. Lyse ~4 million cells with ~200 µl lysis buffer. Maintain constant agitation for 30 minutes on ice.

c. Sonicate lysis samples for 5 seconds. Centrifuge the sample at 12,000 rpm for 10 minutes at 4°C. Transfer supernatant to a new tube.

d. Measure the protein concentration. Dilute Bio-Rad Protein Assay Reagent with water (2 ml reagent+8 ml water). Put 1 ml diluted reagent in disposable plastic cuvette (Fisher; 14-955-127). Add 2 µl protein sample to each cuvette. Votex and measure absorbance under wavelength of 590 nm in NanoDrop.

e. Make each sample have the same amount of protein by adding lysis buffer. (40 µl protein samples for 12-well 4-20% Criterion™ TGX™ gel; 30 µl protein samples for 18-well gel).

f. Mix protein samples with 6X SDS loading buffer.

   4X Tris-HCl/SDS (pH=6.8): Dissolve 6.05 g Tris base (121.14 g/mol) in 40 ml water. Adjust pH to 6.8 with 1 N HCl. Add 0.4 g SDS (or 4 ml 10% SDS). Add water to 100 ml total volume (0.5 M Tris). Filter solution through a 0.45 µm filter. Store at 4°C up to 1 month.

   6X SDS loading buffer:

   7 ml 4X Tris-HCl/SDS (pH=6.8)

   1 g SDS

   3 ml Glycerol

   0.938 g DDT

   1.2 mg bromophenol blue

g. Boil samples at 100°C for 10 minutes. Cool the samples' temperature to room temperature and votex.

h. Set up electrophoresis equipment. Load 12+2-well 4-20% Criterion™ TGX™ gel (Bio-Rad; 567-1093) or 18-well 4-20% Criterion™ TGX™ gel (Bio-Rad; 567-1094) into electrophoresis Criterion™ Cell (Bio-Rad; 165-6020).

i. Fill the chamber with 1X running buffer.

   Running buffer: 10X

Tris Base	60.4 g
Glycine	288 g
SDS	20 g
Water	up to 2000 ml

j. Load protein samples and 10 µl protein marker (Precision Plus Protein All Blue Standards: Bio-Rad, 161-0373; BenchMark Prestained Protein Ladder: Invitrogen, 10748-010) with Gel-Loading tips (Fisher; 05-408-151).

k. Cap the chamber and connect to power. Run electrophoresis at 215 mV for ~40 minutes.

l. Transfer protein from gel to PVDF membrane (Trans-Blot® Turbo™ Midi PVDF Transfer Packs; 170-4157) by using Trans-Blot Turbo Transfer Starter System (Bio-Rad; 170-4155).

m. Block the membrane with 5% (w/v) milk or BSA for an hour. Milk or BSA is dissolved with 1X washing buffer.

   Washing buffer: 10X

Tris Base 48.4 g

NaCl 160 g

Water up to 2000 ml

Adjust pH to 7.6 with HCl.

Washing buffer: 1X

Dilute 10X washing buffer with water to 2000 ml and add 2 ml Tween 20 (Sigma; P7949-500ML)

n. Dilute the primary antibody with 5% milk or BSA in the ratio range of 1:300-1:2000 depending on different antibodies. Incubate the membrane in the primary antibody at 4°C overnight.
o. Wash the membrane with 1X washing buffer for four times and each time for 10 minutes.
p. Dilute the secondary antibody with 5% milk or BSA with 1:5000. Incubate the membrane in the secondary antibody at room temperature for 1 hours.
q. Wash the membrane with 1X washing buffer for four times and each time for 10 minutes.
r. Prepare developing Working Solution by mixing equal parts of the Stable Peroxide Solution and the Luminol/Enhancer Solution (Thermo; SuperSignal® West Dura Extended Duration Substrate, 34075). Use 0.1 ml Working Solution per cm^2 of memberane. (Note: if signal is too strong, dilute Working Solution by water). Incubate blot with Working Solution for ~2 minutes.

s. Place the membrane in a plastic membrane protector. And place the protected blot in a film cassette.

t. Exposure films (Denville Scientific; HyBlot CL® Autoradiography Film; E3018) in dark room.